2006-01-01

Fuel Cell Design for Gas Hydrates Exploration and Research

Gerhard Sauer
Technological University Dublin

FUEL CELL DESIGN FOR GAS HYDRATES EXPLORATION AND RESEARCH

Gerhard Sauer

Dipl.-Ing. Maschinenbau (FH)

Master of Philosophy (MPhil)

School of Control Systems and Electrical Engineering

Faculty of Engineering

Dublin Institute of Technology

Supervisors:

Dr. Eugene Coyle

Dr. David Kennedy

Professor Dr. James P. Hamilton

Professor Dr.-Ing. Heinz Schmidt-Walter

January 2006

I certify that this thesis, which I now submit for examination for the award of MPhil, is entirely my own work and has not been taken from the work of others save and to the extent that such work has been cited and acknowledged within the text of my work.

This thesis was prepared according to the regulations for postgraduate studies by research of the Dublin Institute of Technology and has not been submitted in whole or in part for an award in any other Institute or University.

The Institute has permission to keep, to lend or to copy this thesis in whole or in part, on condition that any such use of the material of the thesis be duly acknowledged.

Signature Gerard Sam Date 26th January 2006

Candidate

Acknowledgements

I would like to thank Dr. Eugene Coyle, Dr. David Kennedy, Dr. James Hamilton, Dr. Michael Conlon and Prof. Heinz Schmidt-Walter for their advice during this research. Furthermore, I want to express my gratitude to Elmar for his effort with the translation, Margareta for looking after my health, and my friends and family for their friendship and continuous support during the progress of the work.

Great thanks to Steffen for being an excellent colleague and fellow researcher. I also wish to express my gratitude to the colleagues at Gaskatel who gave me a helping hand during the experimental work of this research and for their academic support.

Abstract

In this thesis the design, manufacture and testing of an Alkaline Fuel Cell (AFC) that provide electrical power to a deep sea measurement probe is described. The fuel cell was designed to operate in a long-term mode at low temperatures. The power required for the measurement probe was in the order of 5 Watts. The measurement probe was designed to operate at a depth of 3000 m in sea water at a temperature of approximately 5 °C and at 300 bar pressure.

The main design issues included;

The design of a Fuel Cell to operate at these conditions and produce enough energy for at least one full year without maintenance or repair. The flow of the ions, electrolyte and water were also critical for this project and the analysis and understanding of how they interact with each other was of particular importance for the Fuel Cell. Attempting to emit the waste water from the chemical reactions was also a difficult task to achieve. This component of the fuel cell had to be designed and tested also. One other key element of the design was to remove the pumping system for the electrolyte as this was not feasible for the operating conditions specified.

Testing was carried out in a simulated environment at a Fuel Cell and Membrane Research and Development company in Germany*. Testing consisted of low temperature tests. A number of tests without the use of a pumping system were also undertaken. An analysis and investigation of the transport of ions and water within the fuel cell was undertaken. One of the main outcomes was to determine which electrode the reaction water leaves the fuel cell. As the Fuel cell will be incorporated in a specially designed pressurised container, the 300 bar operating pressure was not tested as the fuel cell will operate at room pressure.

Testing and results showed that the Alkaline Fuel Cell has the ability to operate in this environment as reported in the thesis.

List of Publications

23 June 2005	Electrical Engineering Colloquium, University of Applied Sciences, Darmstadt, Germany; Presentation: Alkaline Fuel Cells
4-6 October 2005	Ninth Grove Fuel Cell Symposium, London, United Kingdom; Poster presentation: Water and KOH Transport in an Alkaline Fuel Cell
3-5 November 2005	XII Symposium "Nutzung Regenerativer Energiequellen und Wasserstofftechnik" ("Utilisation of Renewable Energy Resources and Hydrogen Technology"), University of Applied Sciences, Stralsund, Germany; Presentation: Alkaline Electrolyser Systems for Generating Small Amount of Pressurised Hydrogen and Oxygen.

List of Contents

List of Symbols and Abbreviations

A	cross-section of the conductor in cm²
A	Area in cm²
c_E	End concentration in M
c_S	Start concentration in M
D	Diffusion coefficient
d_x	Pore diameter in m
E_{el}	Electrical energy
e	Elementary charge
F	Faraday constant
I	Current in A (mA)
I	Current density in A/cm² (mA/cm²)
J	Mass flux
l	total length of the conductor in cm
M	Molar mass in kg/kmol
m	Mass in kg
N	Avogadro constant
n	Number of electrons
p	Pressure in bar
p^{atm}	Atmospheric pressure in bar
R	Gas constant
T	Temperature in °C
T_1	Inlet Temperature in °C
T_2	Outlet Temperature in °C
t	Time in s
V	Voltage in V (mV)
V_0	No-load voltage in V
$\dot{V}$	Gas flow in l/min

α	Wetting angle
η_C	Efficiency of the Carnot process
η_{ideal}	Ideal efficiency of a fuel cell
σ	Surface tension
Δp	Pressure difference in bar
ΔG	Gibbs free energy
ΔH	Heat of reaction
ΔH_{LCV}	Lower calorific value
ΔS	Reaction entropy
AFC	Alkaline Fuel Cell
Ag_2O	Silver oxide
CE	Counter electrode
c	Concentration
C	Carbon
CO	Carbon monoxide
CO_2	Carbon dioxide
CO	Carbon monoxide
DMFC	Direct Methanol Fuel Cell
EMF	Electromotive force
EPDM	Ethylene propylene diene monomer
EOF	Electroosmotic flow
e^-	Electron
G 1/8"	Pipe thread
GC	Gas Chromatograph
GDE	Gas Diffusion Electrode
GP	Gas permeation
H^+	Hydrogen ion
H_2	Hydrogen
H_2O	Water
H_2O g	Water gaseous

H_2O l	Water liquid
K^+	Potassium ion
KOH	Potassium hydroxide
MCFC	Molten Carbonate Fuel Cell
OH^-	Hydroxide ion
O_2	Oxygen
OSCAR	Ocean Sediment Carbon Aerobic Reactor
Oxag	Gaskatel name for electrodes with Ag_2O-catalyst
PA	Polyamide
PAFC	Phosphoric Acid Fuel Cell
PEMFC	Polymer Membrane Fuel Cell
PESU	Polyether sulphone
PP	Polypropylene
PTFE	Polytetrafluorethylene
PVC	Polyvinylchloride
RE	Reference electrode
SEM	Scanning electron microscope
Silflon	Name of a catalyst (Company Krupp Uhde, Germany)
SOFC	Solid Oxide Fuel Cell
WE	Working electrode

1 Introduction

1.1 Fuel Cell Engineering

The main objectives of this research work were to design, develop and test a fuel cell that operates at low temperature conditions in a hostile environment. The fuel cell developed is to be used as an energy source for a deep sea measurement probe, used for investigating the properties and conditions of deep sea gas hydrate deposits. The probe is currently been developed by a research team in Germany.

The fuel cell was designed to have an operating life of at least one year without any maintenance or inspection.

The research was funded by the TTZ-Umweltinstitut (Technology Transfer Centre – Environmental Department) in Bremerhaven, Germany.

The measurement instruments are to be supplied with energy from the fuel cell.

The fuel cell is rated with 5 V at 1 A. The operating time is one year during which the fuel cell can neither be serviced nor be refuelled. Due to the high water pressure at an operational depth of up to 3000 metres the measurement probe cannot release exhaust gases into the water. At those depths the ambient water temperature is approximately 5 °C. After completion of the operation the measurement probe will remain in the ocean.

The optimal operational temperatures of so-called "low temperature" fuel cells are between 50 °C and 100 °C. The required power delivery of 5 W in this application is relatively low. In conjunction with the usually high efficiency, the heat dissipation of the cell will be too low to reach the optimal operational temperature of the cell. Even with good thermal insulation the fuel cell temperature will only marginally differ from the ambient temperature. This is a key design parameter of the fuel cell to be addressed.

Firstly, various types of fuel cell systems were analysed with regards to their suitability for the deep sea application. Due to its high efficiency and the ability to operate at low temperature the alkaline fuel cell (AFC) was chosen for this project.

1.2 Research Areas Investigated and Outcomes for this Thesis

As part of this research work, the following main topics were investigated:

i) Various fuel cells were examined with regards to their suitability for a run-time of one year at an ambient temperature of 5 °C.

ii) The electrolyte dilution was investigated and the necessary supply of potassium hydroxide solution was calculated.

iii) Possibilities for storing the reaction gases are discussed and the storage of pressurised gas is described in detail.

iv) The potassium hydroxide supply cycle for the cell was investigated and a gas pump developed during the project is outlined and described.

v) A system for solely employing diffusion for the electrolyte transport was considered. For this research work the aim was to eliminate the pump.

vi) During the experiments on diffusion it was found that the reaction product water of the fuel cell did not leave the cell via the hydrogen electrode but via the oxygen electrode. For this, various electrodes and separators were examined with respect to their diffusion properties.

1.3 Structure of the Thesis

This section describes the structure of this thesis and the contents of the individual chapters. Chapter 2 describes the aims of the TIGER project. It provides information about gas hydrates and their situation at the continental shelf. Furthermore the theoretical fundamentals of fuel cells are described. There an overview is given about the different types of alkaline fuel cells. The construction and function of the EloFlux-AFC is described in detail. A variety of different mass transport mechanisms in an AFC are presented. Finally different types of fuel cells and primary energy storages are compared. Chapter 3 describes the experimental set-up. A variety of different pump mechanisms for circulating the electrolyte are described and compared. Further on different test methods for measuring characteristic parameters of electrodes and separators are described. In the end the test rig for the tests with the EloFlux-AFC is described. Chapter 4 shows the results of the experiments. For each test some short information is given. In Chapter 5 the results of chapter 4 are discussed. These are the results on the test on electrodes and separators. Furthermore the results of the increase of volume and the transport of substances are discussed. Finally the results of a calculation about the transport of water and KOH solution in an EloFlux-AFC are shown.

1.4 Fuel Cell Systems

Typical fuel cells consume hydrogen and oxygen producing water, electrical energy and heat. The different types of fuel cells are distinguished by the operating temperature, by the electrolyte used and in some cases by the fuel used. All fuel cells need a somewhat complicated supply system that can be divided into a fuel and an oxidant system. Furthermore it is necessary to control the temperature of the fuel cell and to get rid of the water formed during the reaction.

In the following section, some different types of fuel cells are described.

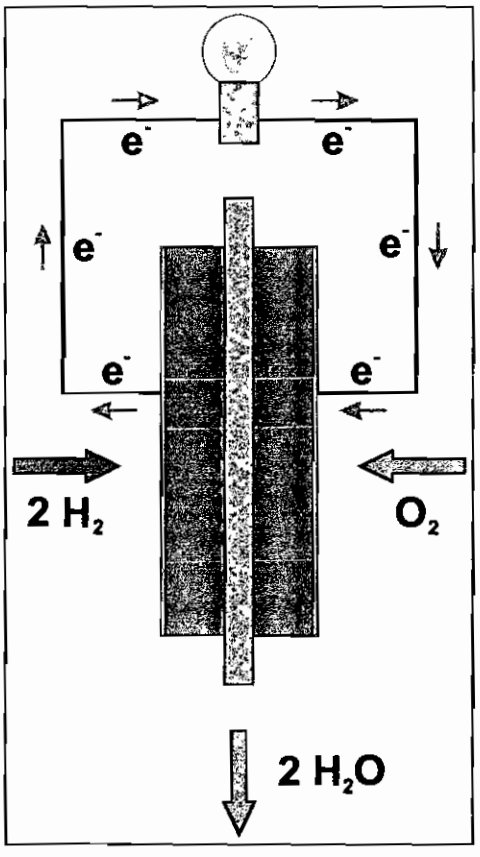

Figure 1.1: Schematic representation of a fuel cell Hydrogen reacts with oxygen and forms water. The electrons have to move from the hydrogen electrode (anode) to the oxygen electrode (cathode). They take the way over an external circuit. There they can power an electrical consumer (load)

1.4.1 Alkaline Fuel Cell (AFC)

The AFC is a low temperature fuel cell with a typical operating temperature of 50 °C to 100 °C. Some AFC run at higher temperature, up to 200 °C. The electrolyte is a liquid potassium hydroxide solution (KOH) with a typical concentration of about 7 M. Potassium hydroxide solution has one of the best conductivities of all hydroxide solutions. In some cases, it is possible to use sodium hydroxide for the electrolyte. The conductivity of sodium hydroxide solution is not as well as the conductivity of potassium hydroxide solution but it is cheaper. The transport of charge inside the AFC is done by OH^- ions. The AFC uses hydrogen and oxygen. It is also possible to use methanol for fuel instead of hydrogen.

1.4.2 Polymer Electrolyte Membrane Fuel Cell (PEMFC)

The PEMFC is also a low temperature fuel cell. The typical operating temperature is about 50 °C to 100 °C. The electrolyte is an ion-selective polymer membrane. In comparison to the separator of an AFC the polymer membrane is much more expensive. The membrane is able to transport H^+ ions but no hydrogen molecules. So the transport of charge is done by the H^+ ions. The catalyst used in an PEMFC is platinum. The PEMFC uses hydrogen and oxygen. Air can be used as a source for the oxygen.

1.4.3 Direct Methanol Fuel Cell (DMFC)

The DMFC is similar to the PEMFC. The only difference is that it uses a mixture of methanol and water for fuel instead of hydrogen.

1.4.4 Phosphoric Acid Fuel Cell (PAFC)

The PAFC is a high temperature fuel cell. The normal operating temperature is about 160 °C to 200 °C. The electrolyte of a PAFC is high concentrated phosphoric acid. It

is fixed in a membrane between the anode and the cathode. The charge is transported by H^+ ions. It uses hydrogen and oxygen. Oxygen also can be used from the air.

1.4.5 Molten Carbonate Fuel Cell (MCFC)

The MCFC is a high temperature fuel cell. Its operating temperature is about 500 °C to 650 °C. The electrolyte is a molten mass of potassium carbonate (K_2CO_3). The charge is transported by the CO_3^{2-} ions. The fuel for the MCFC is hydrogen, biogas or natural gas.

1.4.6 Solid Oxide Fuel Cell (SOFC)

The SOFC is a high temperature fuel cell. The operating temperature is about 750 °C to 1000 °C. The electrolyte is solid zirconium dioxide (ZrO_2). The charge is transported by O^{2-} ions. The fuel for the SOFC is hydrogen, biogas or natural gas.

1.5 Different Storage Systems for Hydrogen and Oxygen

Hydrogen and oxygen are the primary energy sources.
Hydrogen can be stored as a compressed gas, as a liquid, in a metal hydrate storage or in combination with other chemical substances.
Oxygen can only be stored as a compressed gas or as a liquid.

1.6 Design of the EloFlux-AFC and its System

The hydrogen electrode (anode) of an AFC consists of Raney-nickel and the oxygen electrode (cathode) consists of silver. The anode and the cathode are separated by a porous plastic foil called separator. The housing of the AFC consists of epoxy. In general an AFC consists of one to six single cells, perhaps more. The single cells can be connected in series or parallel. This belongs to the application.
The electrolyte in an AFC is an aqueous potassium hydroxide (KOH) solution. The reaction water is absorbed in the electrolyte and dilutes the latter. The convective

water extraction is carried out with an electrical pump. The KOH is stored in a reservoir. The pump circulates the KOH from the tank to the fuel cell and back.
The pressurised reactant gases hydrogen and oxygen are carried in high-pressure gas cylinders. The pressure has to be reduced on the operating pressure of the fuel cell.

1.7 Aims and Objectives

In this project, the fuel cells described in the section above were compared concerning use in the deep sea project. The AFC seemed to be the most suitable for the deep sea application. Several tests were started to see what has to be done to run the AFC under the conditions in a deep sea probe. The most important questions were if it is possible to run an AFC at a temperature of 5 °C and without a convective electrolyte circulation. The hitherto used electric pumps had relatively high energy consumption. It was necessary to find another process to take out the reaction water of the fuel cell. The transport of water caused by diffusion seemed to be an alternative in comparison to the convective KOH flow.
During the test of reaction water extraction by diffusion it was figured out, that the increase of volume caused by the reaction water happens on the electrolyte distributor at the oxygen electrode. Because of the chemical reactions at the electrodes it was guessed that the reaction water leaves the AFC over the hydrogen electrode. A number of tests and calculations were made about the transport of K^+ ions, OH^- ions and water molecules.
The size of the fuel cell system is affected by the storage system for the reactant gases. The required amounts of reactant gases were calculated and the most suitable storage system was figured out.
The reaction water of an AFC dilutes the potassium hydroxide solution. An AFC can only operate within a certain electrolyte concentration range. It was necessary to extract the reaction water or to have enough KOH solution so that the KOH solution can carry the reaction water. Therefore the supply of potassium hydroxide has to be determined.

1.8 Results

It was demonstrated that an AFC can operate at low temperature. The inherent exothermic of the AFC are big enough to heat up the cell from 5 °C to 10 °C.

The demand of KOH solution, hydrogen and oxygen were calculated.

It was figured out that hydrogen and oxygen can be stored in high pressure gas cylinders best.

The electrical pump was replaced by a gas-driven pump first. So the energy consumption was reduced. Later a system was tested without a pump. The water transport was done by diffusion.

For the diffusive variation it could be shown that the transport of molecules and ions at a temperature of 5 °C is sufficient for the operation of a fuel cell. This solution was preferred since it can operate without an external energy supply and does not require additional mechanical or electrical components.

As part of the tests the transport of molecules and ions inside the fuel cell was examined closely. In order to maintain the chemical reaction a balanced transport cycle of K^+ ions, OH^- ions and water molecules has to take place.

A part of the water produced at the hydrogen electrode dilutes the electrolyte as reaction water. This lead to the assumption, that the reaction water leaves the cell via the hydrogen electrode. However, it became apparent that for the most part the reaction water leaves the cell via the oxygen electrode. To explore this unexpected behaviour in greater detail the electrodes and separators were examined with regards to their diffusion properties. This resulted in very different behaviours; some components behaved like semipermeable membranes. Such properties can strongly influence the transport of molecules and ions in the fuel cell which can also influence the cell performance. In order to explain this behaviour the composition of the electrodes and separators as well as pressure-related permeability, wetting and pore size were considered. The diffusion properties of the utilised components constitute one of the most important parameter characterising electrodes and separators. It will be the aim to adapt the diffusion properties of the electrodes and the separators with regards to their application in the fuel cell.

Furthermore tests were made with an alkaline electrolyser to get more information about the transport of KOH solution inside the cell. It was found that the liquid electrolyte moves in direction of the cathode.

2 Background

This chapter provides a background to the research undertaken in this project. It also provides further information about gas hydrate and about deep sea probes. Furthermore, a retrospect of the development of the alkaline fuel cell (AFC) is presented. The theoretical fundamentals and the construction of the EloFlux-AFC are explained. This is followed by a discussion on the suitability of other fuel cell systems for deep sea applications. Finally, various storage systems for hydrogen and oxygen are compared and the problem of electrolyte dilution is elaborated.

2.1 Introductory Considerations

The available reserves of fossil fuels are being depleted an ever increasing rates. As a consequence of this, obtaining energy from fossil sources will become increasingly expensive.

In recent years, massive quantities of gas hydrates have discovered along the continental shelves. This substance could become major energy source for the future, however, the mining of this substance is not only difficult due to its location. On the other hand it also involves some risks. They are discussed below.

Gas hydrate is a crystalline form of methane and water that exists only at higher pressure. The gas molecules are enclosed in a cage-like structure formed by water molecules (as seen in Figure 2-2). This particular molecular arrangement that only exists in a frozen state has an outer appearance that can be compared with snow (see Figure 2-1). Gas hydrate can only exist at a lower temperature such as 0 °C and at a pressure of at least 30 bar [2-1]. Such conditions are found in the ocean depth, especially at the continental slopes, deeper than 2000 m.

Some of the risks associated with mining hydrate materials include inducing under water landslides, sinking ships and increasing global warming.

Gas hydrates are very unstable and small changes or perturbations in pressure or temperature cause a release of the methane gas. Such a release might cause an increase in volume (dependent on the ambient pressure, i.e. water depth) of up to three times of the original volume [2-1].

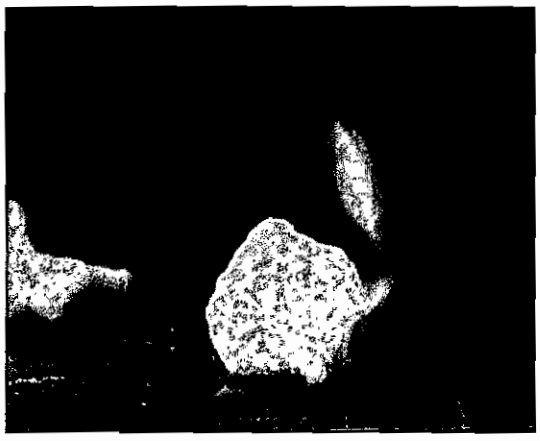

Figure 2-1: Burning gas hydrate

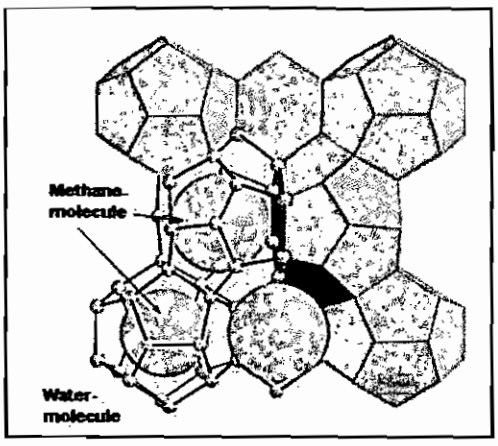

Figure 2-2: Schematic representation of gas hydrate

Researchers found out that the frozen gas hydrate stabilises the ocean ground and the continental slopes [2-1]. If gas hydrate were mined some slope regions could become unstable with the danger of underwater landslides. This could cause flood waves such as tsunamis which could in return cause severe damage in case they reach costal areas.

If large amounts of gas are released from gas hydrate, large gas bubbles can form which rise to the surface all at once. These gas bubbles present a danger for all kinds of floating objects such as ships drilling rigs. They can dramatically reduce the buoyancy of the objects, so that they sink.

Additionally, when the gas reaches the ocean surface, it can mix with air and can form an explosive mixture of methane and air. The explosion limit of methane in air is between 4.4 % and 16.5 % (volume) [2-15]. (The explosion limit is the specific range of concentration where the gas mixture can ignite)

Like CO_2, methane is known to amplify global warming due to the greenhouse effect. However, for methane this effect is approximately 30 times stronger than for CO_2 [2-1].

2.2 Why Fuel Cells? -The TIGER Project

To begin to address the potential of using these gas hydrates as a source of energy the TTZ-Umweltinstitut (Technology Transfer Centre – Environmental Department) in Bremerhaven, Germany, initiated a research project.

The TIGER project which is the abbreviation for

Techniques and **I**nstruments for **G**as hydrates **E**xploration and **R**esearch

The project has as its aim the construction of a deep sea probe. The main focus is the gathering of long-term data about the release and the behaviour of methane at the continental shelves under natural environmental conditions.

Several partners co-operate in the project:

- Capsum company, methane sensor
- JHK, construction of a pressure proof housing
- iSiTec company, data acquisition
- ttz Umweltinstitut, project management

The task of the Gaskatel Company was to assess the possibility of using a fuel cell system as an electricity supply for the measurement and data storage systems of the probe. In addition to theoretical development and analysis practical laboratory tests were to be carried out as well.

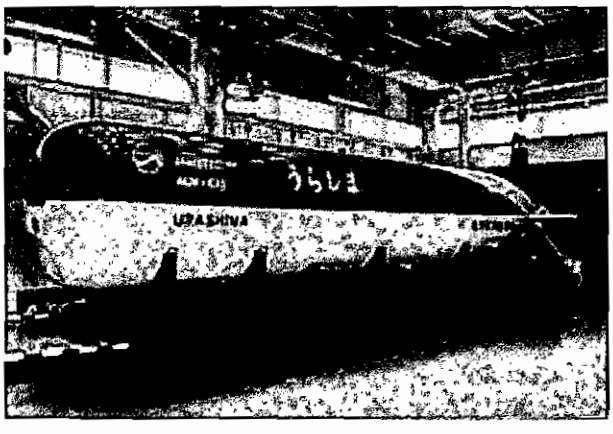

Figure 2-3: Deep sea probe "Urashima", JAMSTEC

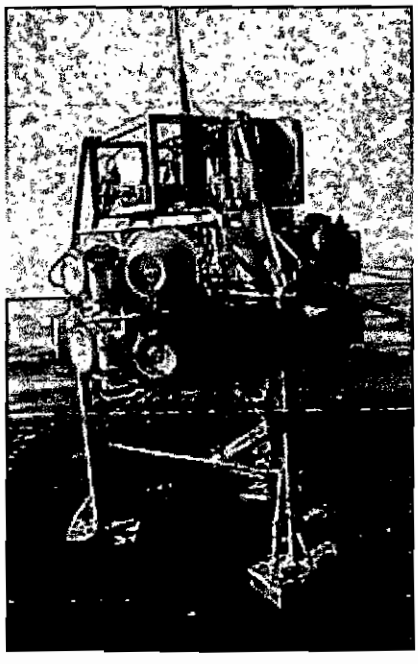

Figure 2-4: Deep sea probe, IFM Geomar

The specifications set by TTZ-Umweltinstitut for the power supply of the deep sea probe are that it run at 5 V and 1 A with a run-time of one year and an operational temperature of approximately 5 °C.

Figure 2-3 shows an autonomous deep sea probe of the research institute JAMSTEC (Japan Agency for Marine-Earth Science and Technology). Figure 2-4 shows a deep sea probe of IFM-Geomar from Kiel, Germany. This device is connected to a ship via a cable for energy supply and data transmission.

2.3 The Fuel Cell

The phenomenon of electro-chemical energy conversion in a fuel cell was first observed in 1839 by Sir William Robert Grove [2-2].

In a fuel cell, the reaction of hydrogen and oxygen produces water while generating electric energy and, to a small extent, heat. Contrary to thermal engines (e.g. internal combustion engines, gas turbines) a fuel cell converts the energy directly into electric energy and not via thermal energy (e.g. steam) into electric or mechanical energy.

The main components of a H_2/O_2 fuel cell are the hydrogen electrode, the oxygen electrode, a membrane or a separator and the electrolyte.

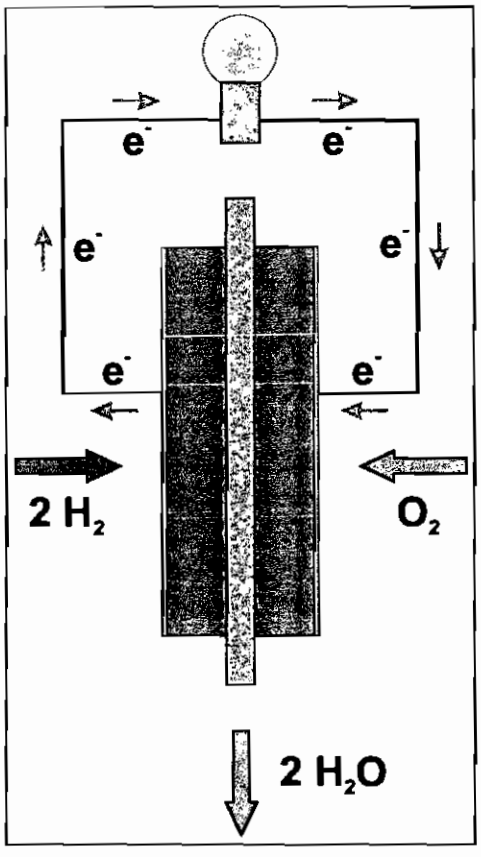

Figure 2-5: Schematic representation of a fuel cell
Hydrogen reacts with oxygen and forms water. The electrons have to move from the hydrogen electrode (anode) to the oxygen electrode (cathode). They take the way over an external circuit. There they can power an electrical consumer (load)

2.3.1 Efficiency Comparison

When comparing energy sources like fossil and nuclear fuels as well as fuel cells, it is important to have a measure of energy conversion efficiency. However, the thermodynamic considerations discussed below must be balanced by consideration of the transport properties within a fuel cell. Transport properties are also discussed below.

The most commonly used energy conversion systems are steam turbines, gas turbines or internal combustion engines. They convert chemical energy (usually from fossil sources) or nuclear energy into mechanical or electrical energy using a cyclic thermodynamic process. The energy conversion into mechanical or electrical energy is not direct and thermal energy is always necessary as an interim step. This additional conversion step results in significant energy losses and process engineering plays an important role in controlling these losses.

Of all cyclic thermodynamic processes the Carnot process [2-3] has the highest efficiency. The efficiency is only determined by the temperature difference between the inlet temperature (T_1) and the outlet temperature (T_2).

$$\eta_C = \frac{T_1 - T_2}{T_1} \qquad \textbf{(Eq.: 2-1)}$$

The efficiency of a Carnot process (η_C) can only be equal to 1 if $T_2 = 0$ K. Since it is impossible to operate at 0 K, the aim is to maximise the value of T_1. T_1 is limited by the properties of the utilised materials in the thermal engine such as metals and ceramics.

The efficiency of a fuel cell is not limited by the Carnot efficiency as it does not convert the chemical energy via thermal energy into electrical energy. Since the reaction already takes place at relatively low temperatures, fuel cell operation is often referred as cold combustion.

The maximum work that can be gained from a chemical reaction is given by Gibbs free energy, ΔG [2-4]. It is determined from the enthalpy or heat of reaction, ΔH and the reaction entropy, ΔS.

$$\Delta G = \Delta H - T \cdot \Delta S \qquad \textbf{(Eq.: 2-2)}$$

Because of the chemical reaction and the number of moles from the reactant and the product, it holds that in a H_2/O_2-cell $\Delta S<0$.

$$H_2 + \frac{1}{2} O_2 \rightarrow H_2O \qquad \textbf{(Eq.: 2-2)}$$

One mole of hydrogen gas reacts with half a mole of oxygen gas and forms one mole of water. The number of moles are reduced from 1.5 moles to one mole and so $\Delta S<0$. The water can be liquid (ΔS = -163.29 J/mol/K) or gaseous (ΔS = -44.38 J/mol/K). It follows that $\Delta G<\Delta H$.

For the partial reaction of carbon to carbon monoxide the number of moles decrease and further more the phase change from solid to gaseous (ΔS = 89.6 J/mol/K).

$$C + \frac{1}{2} O_2 \rightarrow CO \qquad \textbf{(Eq.: 2-2)}$$

It holds that $\Delta S>0$ and hence $\Delta G>\Delta H$.

When calculating the ideal efficiency η_{ideal} of a fuel cell using Equation: 2-3, it follows that the efficiency is larger than one (only for the reaction C + ½ O_2 → CO). It has to be noted that the sign of ΔH is negative (since energy is released).

$$\eta_{ideal} = \frac{\Delta G}{\Delta H} = 1 - T\left(\frac{\Delta S}{\Delta H}\right) \qquad \textbf{(Eq.: 2-3)}$$

According to the first law of thermodynamics this is not possible. The equation to calculate the efficiency of a fuel cell is, nevertheless, correct. In fact, the fuel cell can

absorb ambient thermal energy during the reaction of C to CO and convert the thermal energy into electric energy on top of the free reaction enthalpy.

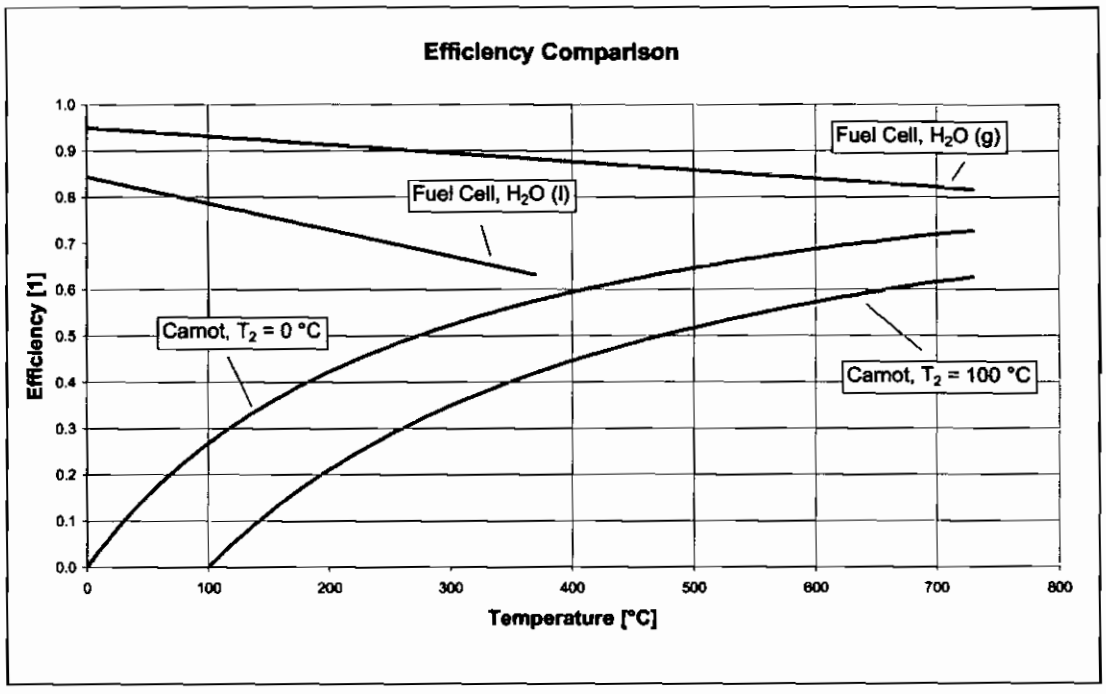

Diagram 2-1: Efficiency comparison, fuel cell – Carnot process

Diagram 2-1 shows an efficiency comparison of a H_2/O_2-fuel cell and a cyclic Carnot process. For the fuel cell it is clearly visible that, from a thermodynamic viewpoint, a H_2/O_2-element should be operated at low temperatures. In practice, it is found that the reaction kinetics of a fuel cell also has an influence on the operation and improves with increasing temperature. As a consequence the optimal operating temperature—taking both factors into consideration—has to be found. The two characteristic curves differ in whether the reaction water is generated as a gas or as a liquid.

The characteristic curve for liquid reaction water ends at 374 °C which is the critical point of water. Above this temperature water cannot exist as a liquid.

The two characteristic curves of the Carnot process differ in that the outlet temperature is 0 °C in one case and 100 °C in the other case. It can be clearly seen that the efficiency of the Carnot process increases with increasing ΔT.

2.3.2 Electromotive Force (EMF)

The EMF or no-load voltage V_0 is the electric voltage between the anode and cathode provided that no current is drawn from the cell.

The electric energy of a fuel cell can be calculated as follows [2-5]:

$$E_{el} = -N \cdot e \cdot n \cdot V_0 = -F \cdot n \cdot V_0 = \Delta G \qquad \textbf{(Eq.: 2-4)}$$

n is the number of electrons transferred per reaction step. $N = 6\times10^{23}$ is the number of n-valued molecules of one mole fuel. Each electron carries an electric charge of $e = 1.6\times10^{-19}$ As (As, Ampere second is convenient instead of Coulomb because it is a SI-unit). Multiplying these three factors with the no-load voltage V_0 yields the total transferable energy. The product of the number of molecules N and the elementary charge e is also known as Faraday-constant (F = 96485 As) [2-5].

Equating the electric energy E_{el} with the free reaction enthalpy ΔG according to Equation 2-4 and solving the equation for V_0 yields:

$$V_0 = \frac{T \cdot \Delta S - \Delta H}{F \cdot n} = \frac{-\Delta G}{F \cdot n} \qquad \textbf{(Eq.: 2-5)}$$

From Equation 2-2 can be seen that ΔG is temperature dependent. In a H_2/O_2-cell the change of entropy has a negative sign. From this, using

$\Delta G = \Delta H - T \cdot \Delta S$ follows that the EMF of the cell decreases with increasing temperature.

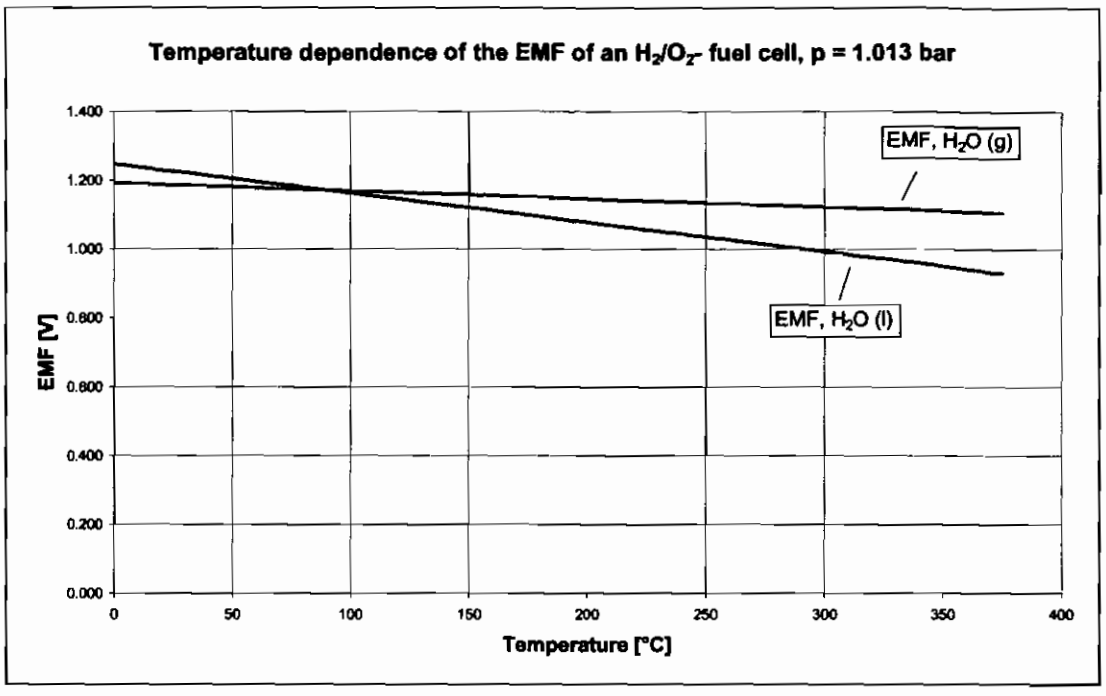

Diagram 2-2: Temperature dependence of the EMF of a H_2/O_2 fuel cell

Diagram 2-2 shows the temperature dependence of a H_2/O_2-cell at atmospheric pressure (p = 1.013 bar) for the two cases that the reaction water is generated as a gas and as a liquid respectively.

The different EMFs at 0 °C result from the different enthalpies for liquid and gaseous reaction water (ΔH_{liquid} = 285.29 kJ/mol and $\Delta H_{gaseous}$ = 242.16 kJ/mol) [2-6]. The different gradients can be explained with the different rates of change of the entropy of liquid and gaseous reaction water (ΔS_{liquid} = 163.29 J/mol/K and $\Delta S_{gaseous}$ = 44.38 J/mol/K) [2-6].

Some fuel cells operate at high temperatures and above a temperature of approximately 374 °C (i.e. the critical point of water) [2-7] water can under no circumstances exist in a liquid form.

In addition to the temperature the free energy ΔG also depends on the gas pressure according to Equation 2-6 that is plotted below

$$\Delta G(p) = \Delta G(p^{atm}) + R \cdot T \cdot \ln\left(\frac{p}{p^{atm}}\right) \qquad \textbf{(Eq.: 2-6)}$$

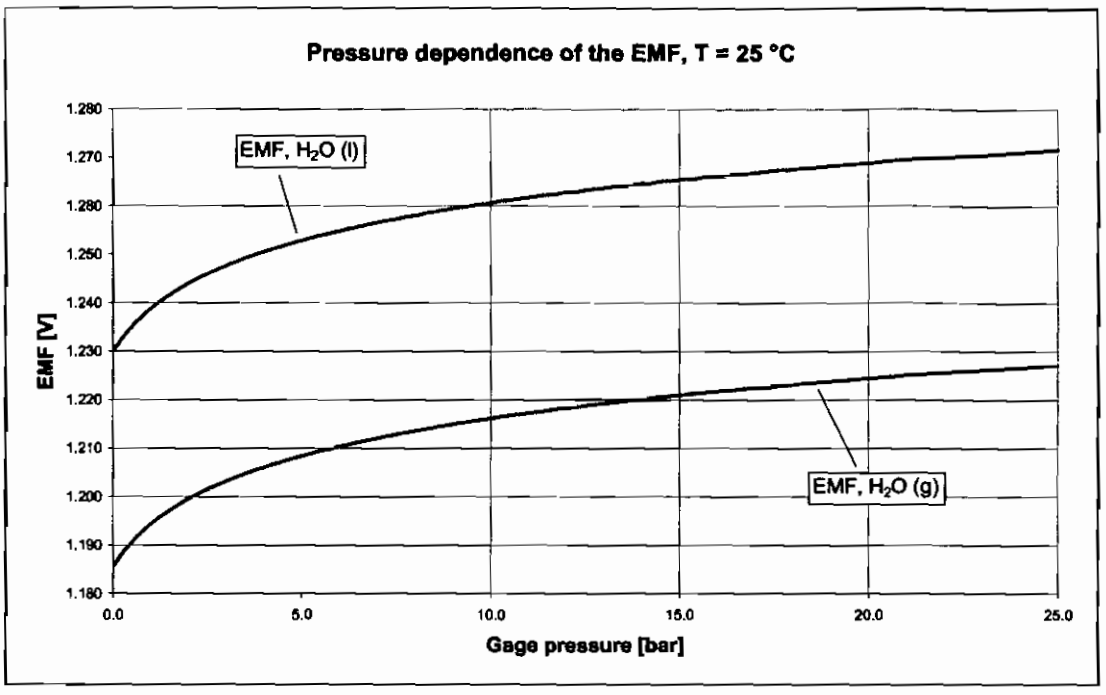

Diagram 2-3: Pressure dependence of the EMF of a H_2/O_2 fuel cell

As can be seen in Diagram 2-3, the EMF is pressure dependent. However, in the operating range of the EloFlux-AFC ($pH_2 \approx pO_2 \approx 0.5$ bar) the changes are very small and in this work we can neglect this pressure dependence.

To a good approximation, the EMF (V_0) can also be determined using the lower calorific value ΔH_{LCV} of the used fuel. However, this procedure neglects the fact that not the entire reaction heat ΔH can be converted into electric energy [2-5].

In the limit of small entropy change, equation 2-5 becomes:

$$V_0 \approx \frac{\Delta H_{LCV}}{F \cdot n} \qquad \textbf{(Eq.: 2-7)}$$

ΔH_{LCV} is called the lower calorific value.

$$\Delta G = \Delta H - T \cdot \overset{0}{\cancel{\Delta S}} = -n \cdot F \cdot V_0 \qquad \textbf{(Eq.: 2-7)}$$

2.4 Construction and Function of an AFC

The electrolyte in an alkaline fuel cell is a potassium hydroxide solution, hence the name "alkaline". The reactant gases used are hydrogen and oxygen. The use of air oxygen is limited due to the CO_2 contained in the air [2-14]. Alkaline fuel cells are mainly low-temperature fuel cells. With operational temperatures normally between 50 °C and 80 °C. Some cells have been operated at 200 °C (Bacon-cell) and more.
For alkaline H_2/O_2-fuel cells three construction types are possible. These are the conventional AFC, the matrix AFC and the EloFlux-AFC. They are distinguished individually below. The main distinguishing feature is the position of the electrolyte within the cell.

- **Conventional AFC**

  In a conventional AFC the liquid electrolyte is located in a separate electrolyte compartment between the two electrodes and is moved by a pump [2-8].

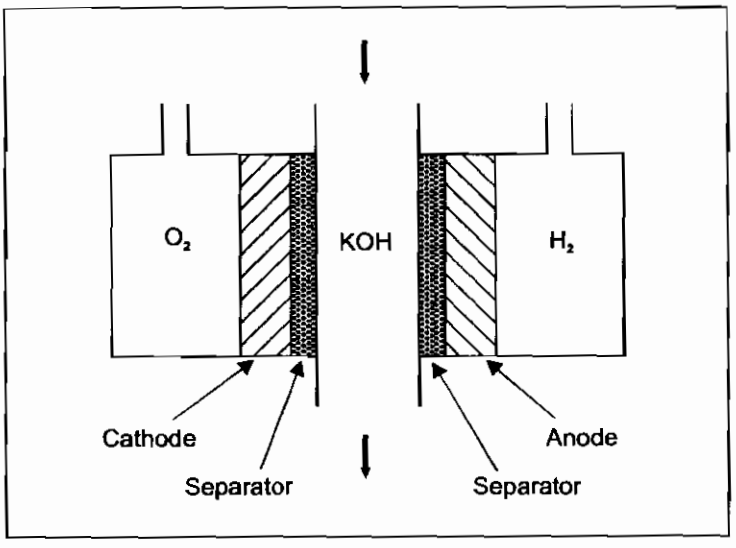

Figure 2-6: Construction of a conventional AFC

- **Matrix-AFC**

  In a matrix-AFC the electrolyte is positioned in a solid, non circulating matrix between the two electrodes [2-9].

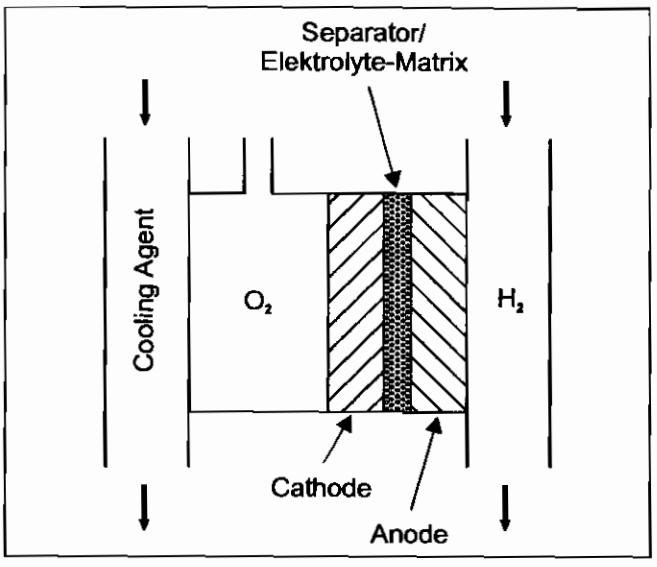

Figure 2-7: Construction of a matrix-AFC

- **EloFlux-AFC**

  In the EloFlux-AFC a pressure-dependent cross-flow is generated through the electrode package. The electrodes have two pore systems. The electrolyte moves through the lyophilic pore system while the gases use the lyophobic pore system.

All experiments, tests and developments of this research work were carried out using the EloFlux-fuel cell. Therefore, the following description of the construction and functionality is focused on this type of AFC.

The development of this type of alkaline fuel cell began around 1960 by A. Winsel and R. Wendtland at the University of Braunschweig, Germany [2-16]. In the 1970s the research and development was carried further by the Varta Battery Company

(Varta Batterien AG) in Kelkheim, Germany. Following this, the University of Kassel, Germany, worked in co-operation with Varta on further developments.
Since 1997, the Gaskatel Company has continued work on further developments and enhancements of the EloFlux-AFC and alkaline EloFlux-electrolyser system.

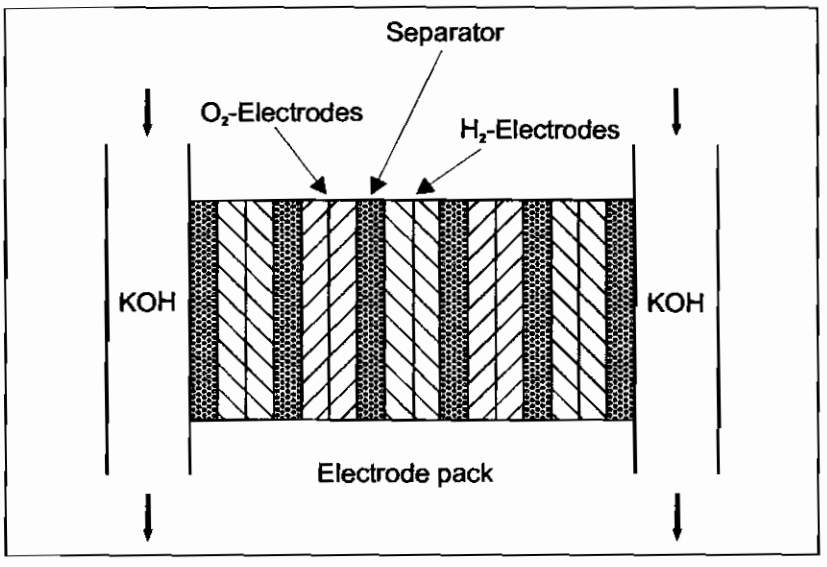

Figure 2-8: Construction of an EloFlux-AFC

2.4.1 Components of an EloFlux- Alkaline Fuel Cell (AFC)

An EloFlux-AFC consists of the following components:

- an electrode for the fuel (hydrogen),
- an electrode for the oxidant (oxygen),
- an electrolyte (aqueous potassium hydroxide solution),
- a separator (porous plastic film),
- a housing (epoxy resin).

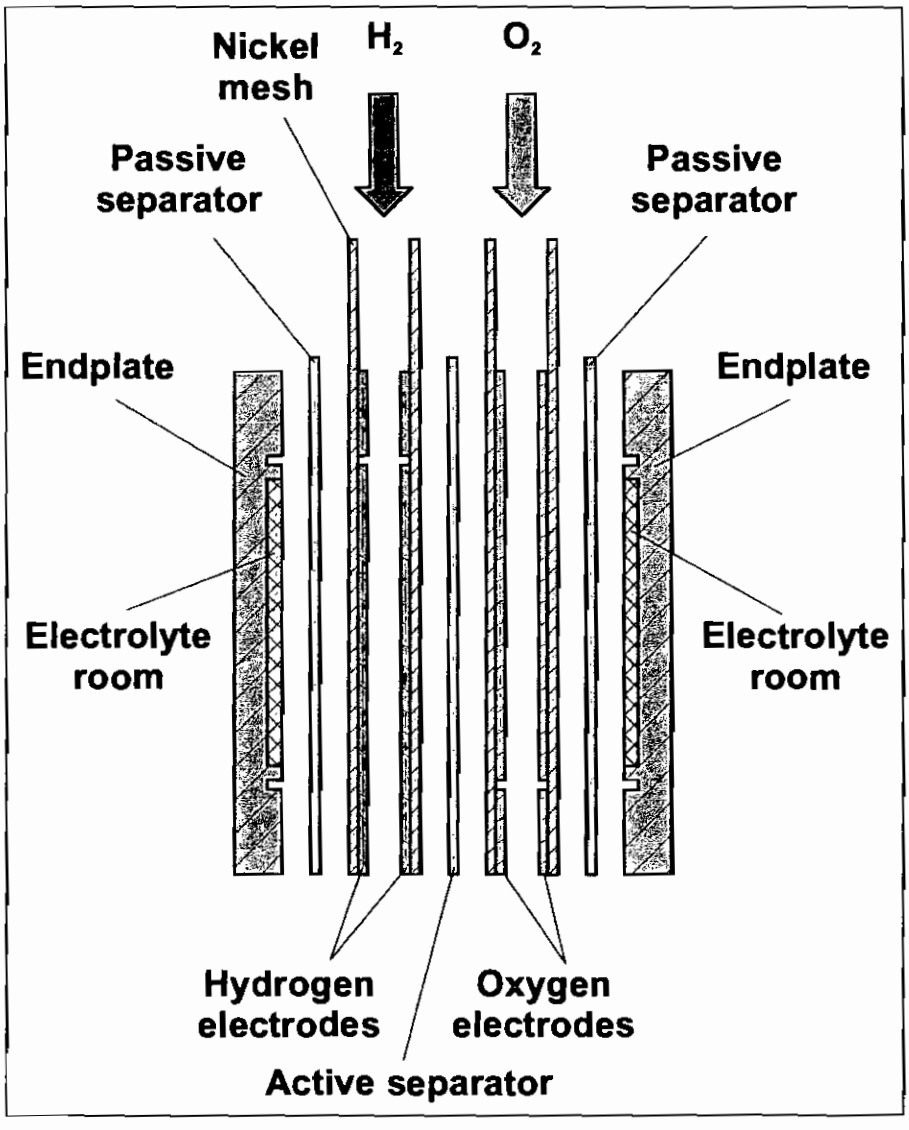

Figure 2-9: Component arrangement of an EloFlux-AFC (one cell unit)

Gas Diffusion Electrode (GDE)

The electrodes are the most important components of an EloFlux-AFC. They mainly consist of a catalytic material. At the hydrogen electrode, Raney nickel is used while silver is used for the oxygen electrode.

The deactivated (passivated) catalyst powder is mixed with a certain weight percentage PTFE. This mixture is ground and then rolled out to a 10 cm wide band using a roller mill (pair of rollers). In a second step, the band is rolled into a 10 cm wide nickel lattice.

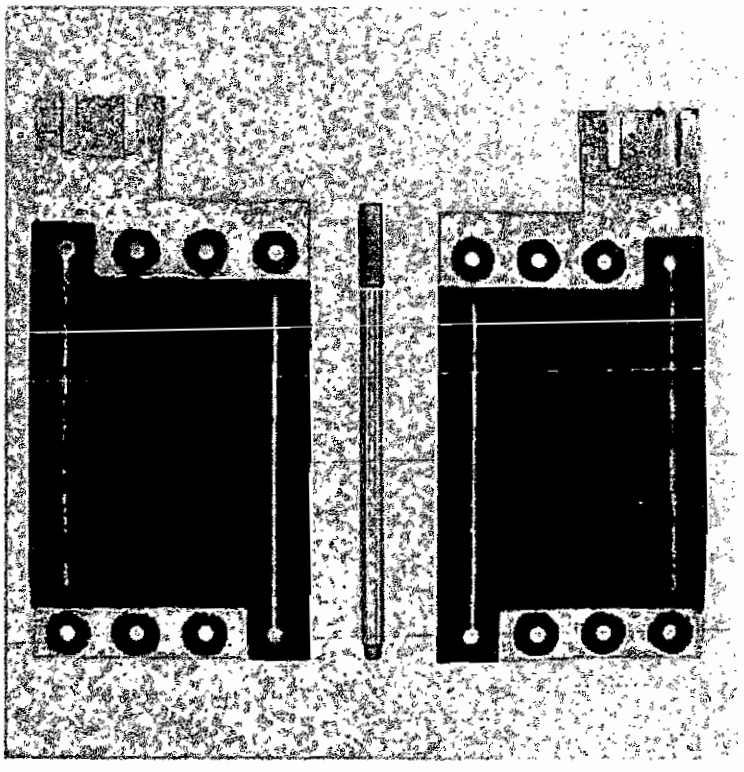

Figure 2-10: Electrode pair, nickel grid with Raney-nickel layer

The Raney-nickel catalyst consists of porous grains. The catalyst has therefore a fine pore system which is lyophilic (has an affinity to KOH). During the mixing process the PTFE forms a fine PTFE web (as can be seen in Figure 2-11) between the nickel grains and thus creates the lyophobic pore system. For the electrode, this means the existence of two intersecting pore systems with different properties.

Figure 2-10 shows a pair of hydrogen electrodes. The black material is the nickel layer. In this stadium the electrodes are ready for assembly. The two electrodes are mounted nickel layer facing nickel layer.

The electro-chemical reactions occur at the phase boundaries of the reaction partners inside the electrode. In case of the anodic hydrogen consumption this is a triple phase boundary between the hydrogen, the electrolyte and the nickel as catalyst. Hereby, the electrolyte is transported through the lyophilic pore system and the hydrogen is transported through the lyophobic pore system.

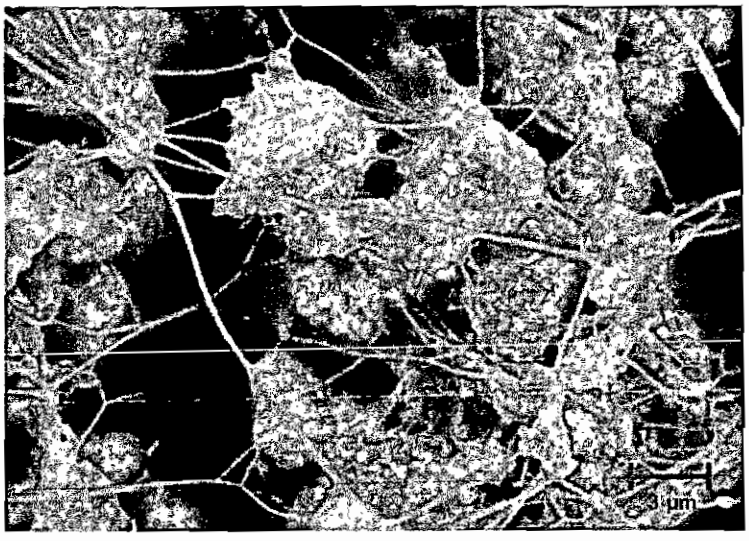

Figure 2-11: SEM-picture of a Raney nickel layer

Figure 2-11 shows a SEM-picture of a Raney nickel layer. The PTFE web is clearly visible. The large spaces in between the catalyst grains are the gas pores. The pores filled with liquid are located inside the catalyst grains. The construction and manufacturing of the oxygen electrode is similar to the hydrogen electrode [2-10].

The Separator

The separator consists of a porous plastic film. In case of an EloFlux-AFC, a distinction is made between active and passive separators. The active separator is placed in between the anode and the cathode. It is denoted active because it facilitates the electric charge transport between the electrodes. The passive separator only isolates the gas compartment from the electrolyte compartment.

The purpose of the separator is:

- to isolate the hydrogen and the oxygen electrode against each other
- to facilitate ionic conduction
- to enable the transport of hydroxide solution and water
- to separate the reaction gases
- to separate the reaction gases from the electrolyte (only the passive separator)

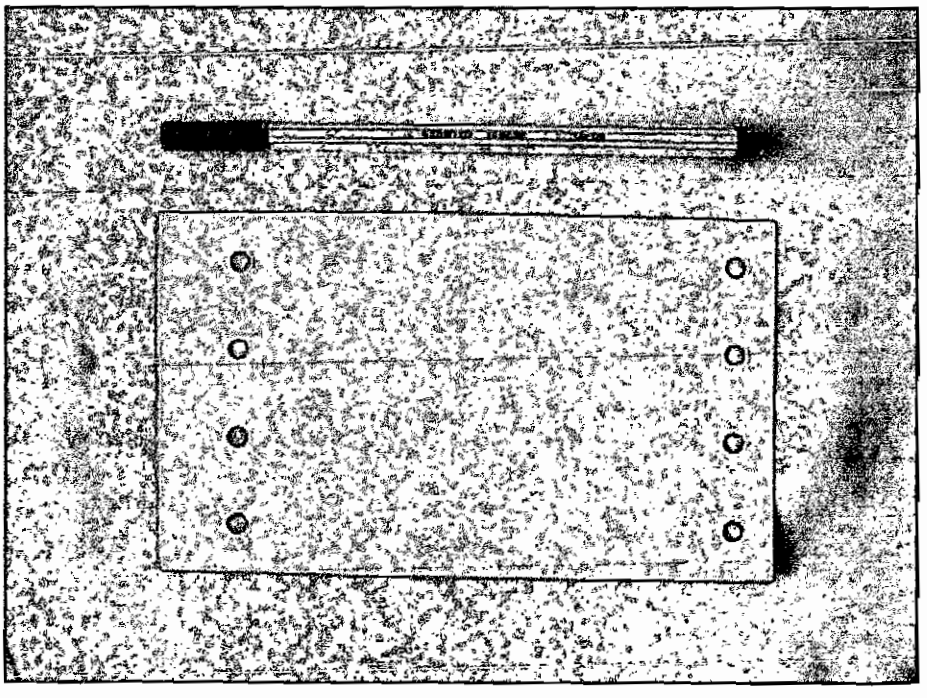

Figure 2-12: Separator of an EloFlux-AFC

When the AFC is filled with potassium hydroxide for the first time the pores of the separator have to be filled with liquid potassium hydroxide to make the separator gas-tight. The completely filled pores enable the transport of ions through the separator. With a pressure difference a liquid flow through the pores can be achieved. In order to prevent the pores from letting bubbles pass, the pore radius and the wetting properties have to be matched. To quantify this, the so-called "bubble point" is used. For this, the differential gas pressure necessary to press a bubble through the first pore is determined via the separator. In order to be certain to prevent a mixing of the reaction gases, the bubble point should always be higher than the highest possible pressure difference of the reaction gases. Figure 2-12 shows a separator ready for assembly (0.25 mm thickness). The cuttings are to allow an unobstructed gas and hydroxide solution transport through the supply channels. Furthermore, the separator is positioned with the individual components of an EloFlux-AFC using the holes on the top and bottom. They are used in all components.

The Electrolyte

The function of the electrolyte is to transport the OH^--ions and the water molecules respectively between the electrodes and to absorb the reaction water. Since potassium hydroxide solution has one of the best conductivities of all hydroxide solutions it is preferentially used as electrolyte. Depending on the kind of application it is also possible to use other hydroxide solutions, e.g. sodium hydroxide.

The conductivity of a hydroxide solution changes with the concentration (see Diagram 2-4). Potassium hydroxide has the highest conductivity at a concentration of approximately 7 M and therefore it is used in EloFlux-AFCs with this concentration. Apart from these purposes the liquid electrolyte is also used to maintain the cell temperature and to extract the reaction water from the cell.

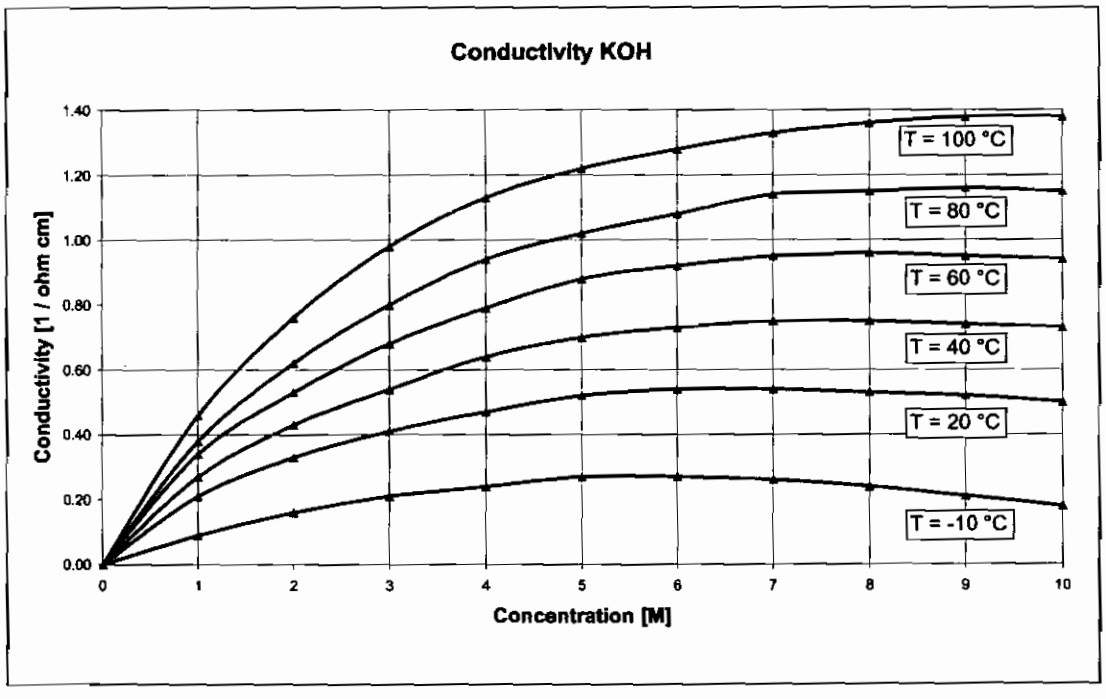

Diagram 2-4: Conductivity of KOH solution, following Varta [2-19]

The Housing

The housing of an EloFlux-AFC consists of two end plates which are epoxy resin castings. The fluid tubing fittings are integrated into the cell (G 1/8 inch) and the Nickel foam electrolyte distributor and also provide the necessary stability to the cell. In order to improve the mechanical stability, the end plates are enforced with a fibre glass fleece and a fibre glass mat.

Figure 2-13 shows the inward side of an end plate. The areas marked in black are circa 1 mm higher than the remaining area. They form a frame which accommodates the electrolyte distributor. The latter consists of nickel foam of circa 1.2 mm thickness (grey rectangle). The electrolyte distributor is connected to the KOH supply threads (left: third thread from the top, right: second thread from the top).

The remaining housing is formed by the epoxy resin which is used to seal the components and to glue the individual parts together.

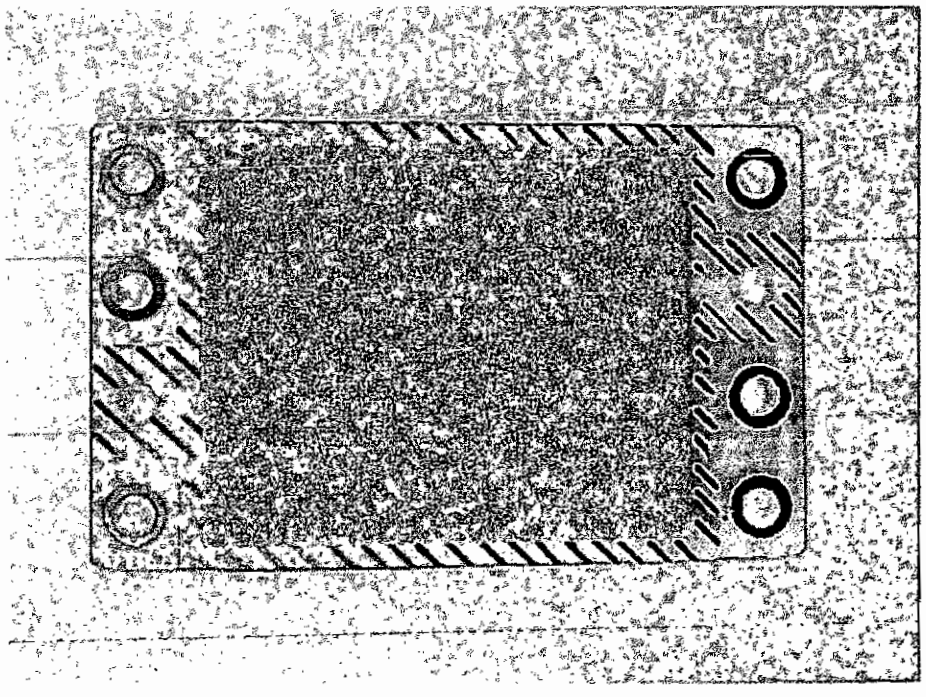

Figure 2-13: End plate of an EloFlux-AFC

2.4.2 Component Arrangement in an EloFlux-AFC

The simplest EloFlux-AFC, a so-called mono cell, consists of nine components (see Figure 2-14). These are:

- a pair of hydrogen electrodes,
- a pair of oxygen electrodes,
- three separators (one active, two passive),
- two end plates

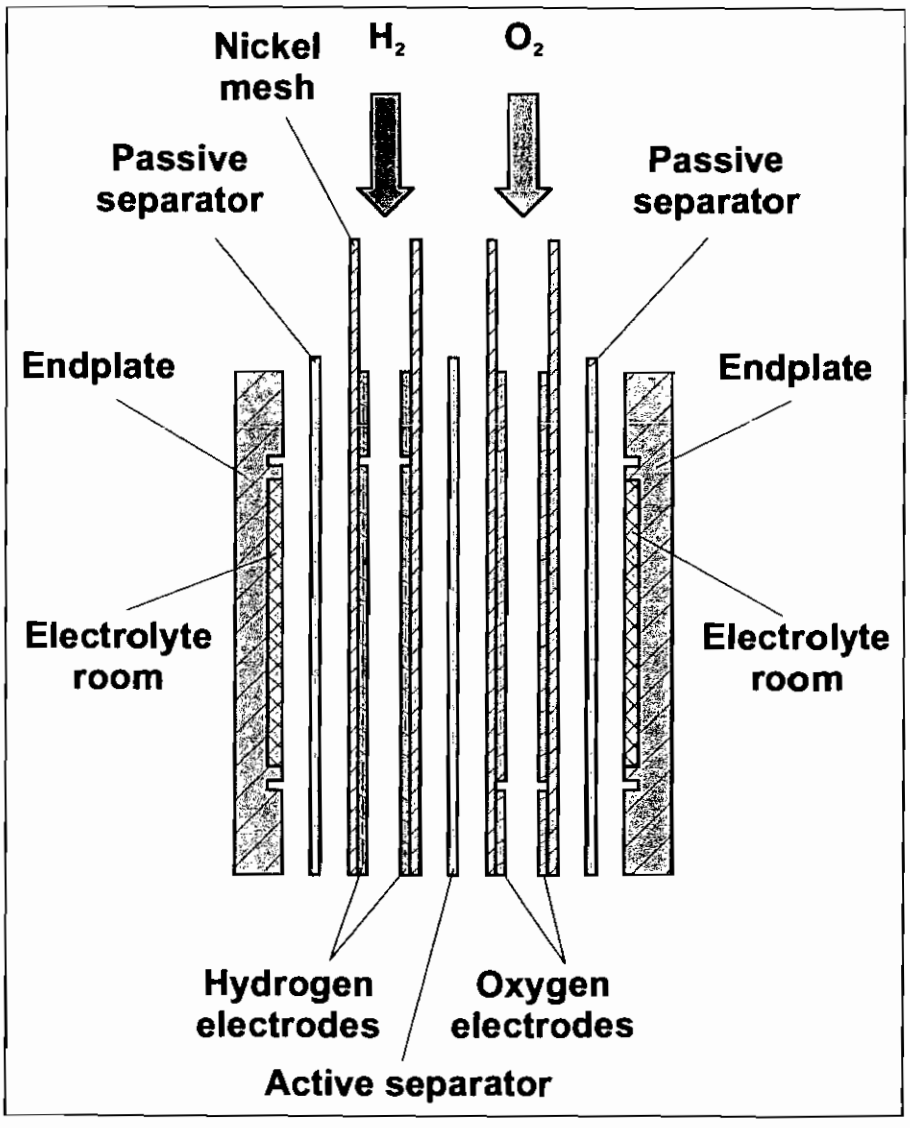

Figure 2-14: Component arrangement of an EloFlux-AFC

2.4.3 The electro-chemical Reactions in an AFC

The overall reaction in a H_2/O_2 fuel cell is as follows:

$$H_2 + 1/2\ O_2 \rightarrow H_2O \qquad \textbf{(Eq.: 2-8)}$$

Hydrogen and oxygen react to form water while releasing energy. The overall reaction can now be split into the two half reactions taking place at the anode and the cathode.

The electrode reaction of an AFC at the hydrogen side (anode) is:

$$H_2 + 2OH^- \rightarrow 2H_2O + 2e^- \qquad \textbf{(Eq.: 2-9)}$$

During the reaction, the hydrogen molecule is oxidised. Each H atom releases its electron and reacts with an OH^--ion to form a water molecule. The electrons are conducted out of the cell via the electrode. In the event that an electric load is present, the electrons can perform electric work before being conducted back to the cathode. Since the electrons are released here, an electron excess results and the hydrogen electrode of the fuel cell is the negative pole.

The electrode reaction of an AFC at the oxygen side (cathode) is:

$$1/2\ O_2 + H_2O + 2e^- \rightarrow 2OH^- \qquad \textbf{(Eq.: 2-10)}$$

At the oxygen electrode the oxygen is reduced and reacts with a water molecule to form two OH^--ions. For this, the two electrons of the anode are required. This causes a lack of electrons at the oxygen side. Consequently, the cathode is the positive pole of the fuel cell.

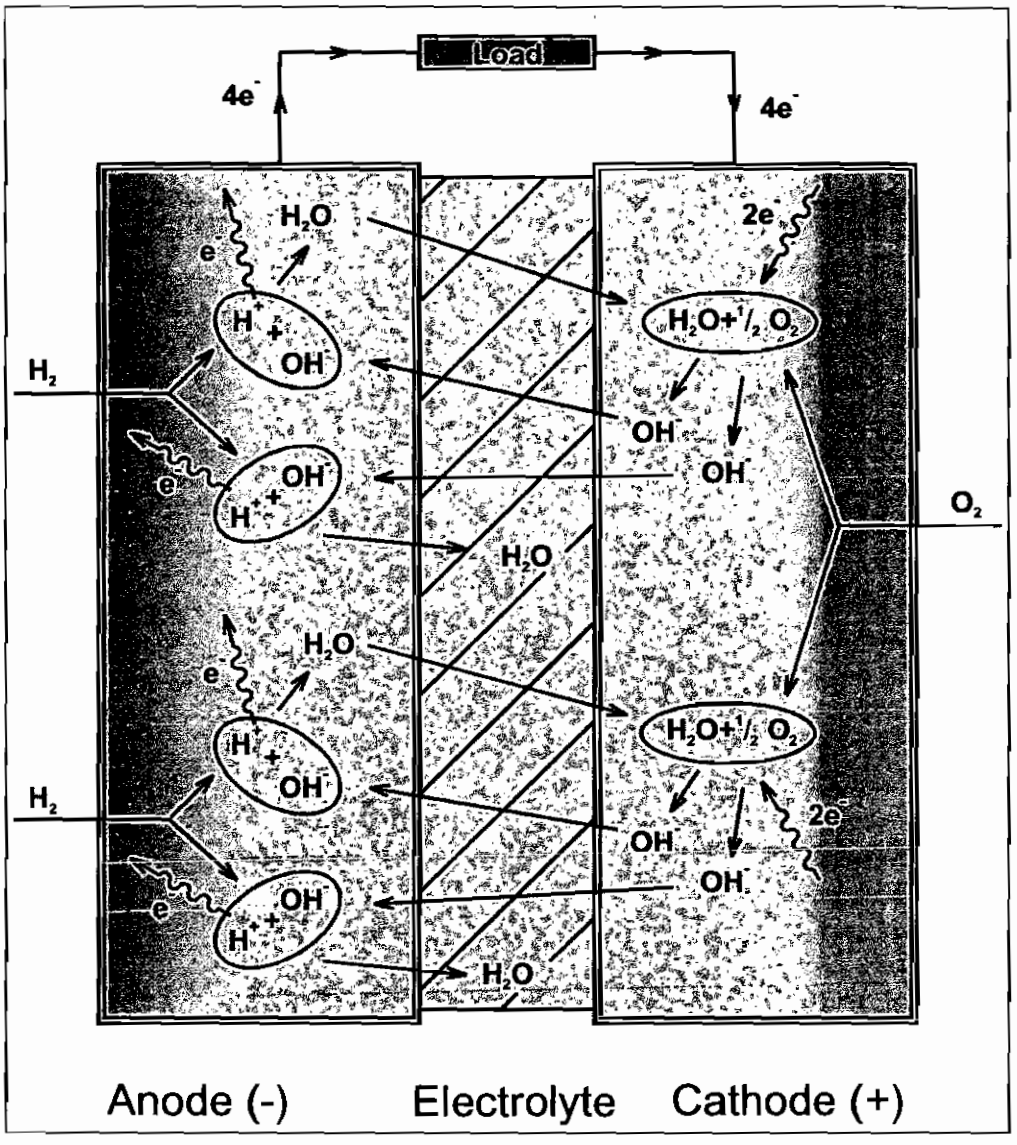

Figure 2-15: Mass transport in an AFC [2-20]

From a mass transport standpoint in an AFC, this means that OH^--ions have to get from the cathode to the anode while water molecules have to migrate in the opposite direction. These transport processes occur mainly through diffusion or are, in case of an EloFlux-AFC, supported by a pressure-dependent flow. Figure 2-15 shows the mass transport cycle inside an alkaline fuel cell.

2.4.4 Reaction Kinetics in the Electrode

The chemical reactions of a fuel cell take place at the triple phase boundary (reaction gas, catalyst grain and electrolyte) in the pores. The reaction gas moves into the pores by diffusion and convection. The molecular connection of the hydrogen molecule is broken at the triple phase boundary. Then the actual reactions take place. Each hydrogen atom looses one electron. The electrons leave the fuel cell via the electrodes. The hydrogen reacts with the OH^--ions to form water. The reactions can only take place, if there is gas electrolyte and catalyst. If one of the three participating reaction partners is missing the reaction stops [2-11]. Figure 2-16 shows the situation in the pores of the hydrogen electrodes.

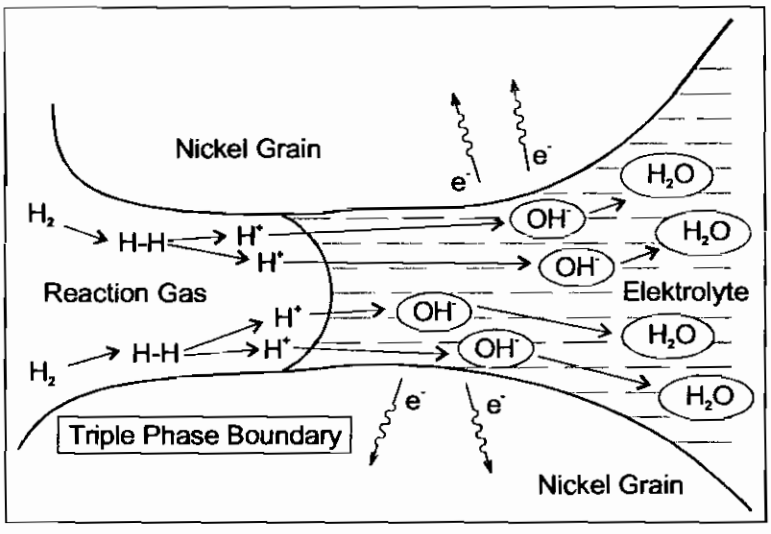

Figure 2-16: Reaction kinetics in a pore (hydrogen electrode)

The situation on the oxygen electrode is similar to the situation at the hydrogen electrode. The reaction gas moves into the pore. The oxygen molecule is divided into two oxygen atoms. For each oxygen atom are two electrons needed. They enter the cell via the oxygen electrode. The oxygen atom reacts with a water molecule and forms two OH^--ions. Figure 2-17 shows the situation in the pores of the oxygen electrode.

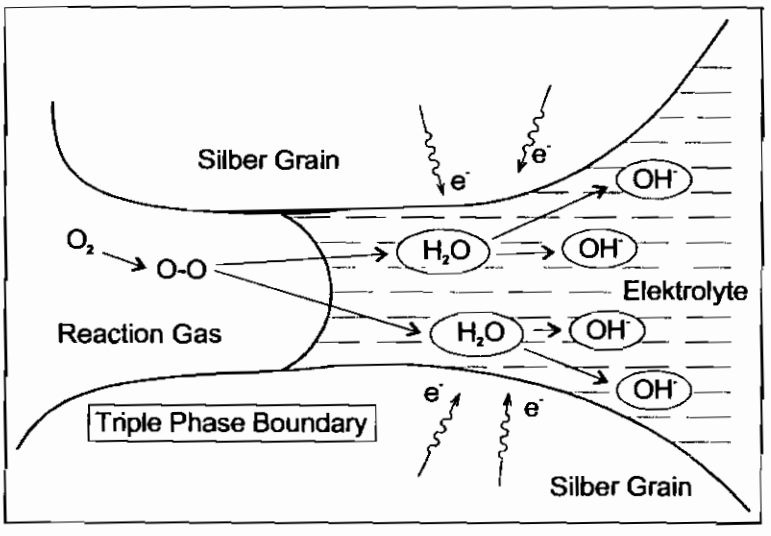

Figure 2-17: Reaction kinetics in a pore (oxygen electrode)

2.5 Mass Transport Mechanisms in an AFC

The transport of K^+, OH^- and water can take place through different mechanisms which are:

- diffusion,
- a pressure-dependent flow
- electroosmotic flow
- osmotic flow
- proton transfer reactions (Grotthus mechanism).

In the following, these mechanisms are explained in more detail.

2.5.1 Diffusion

Diffusion is an equalisation process between two different concentrations. Ions or particles migrate from a location with a higher concentration to a location with a lower concentration. If considered from a macroscopic point of view, the concentration gradient is a driving force for particle transport and is suitable to describe and calculate this behaviour. Microscopically it is Brownian motion that is actually responsible for the mass transport, a fact that also explains the temperature dependence of diffusion. The particle movement is inhibited by the friction between the ions and the solvent. This property is expressed by the diffusion coefficient. In case of the alkaline fuel cell this is the mobility of K^+-ions, OH^--ions and water molecules in potassium hydroxide solution. In addition to these parameters the mass transport is also influenced by the components through which the particles have to pass.

For all these considerations it is essential to become familiar with the characteristics of the electrolyte. The simple consideration that a particle migrates from one electrode to another cannot sufficiently describe the observations. There are strong interactions between the ions and the water and the electrodes respectively which necessarily have to be included in the considerations. The interactions are of an

electrostatic nature. Since water exhibits dipole properties this causes the ions to surround themselves with water molecules; they form so-called hydrate shells.
The dimension of the hydrate shell and the number of water molecules around an ion respectively does not only depend on the ion's electrostatic attraction, but also depends on the concentration of the electrolyte. The concentration determines how many water molecules are actually available to form hydrate shells.

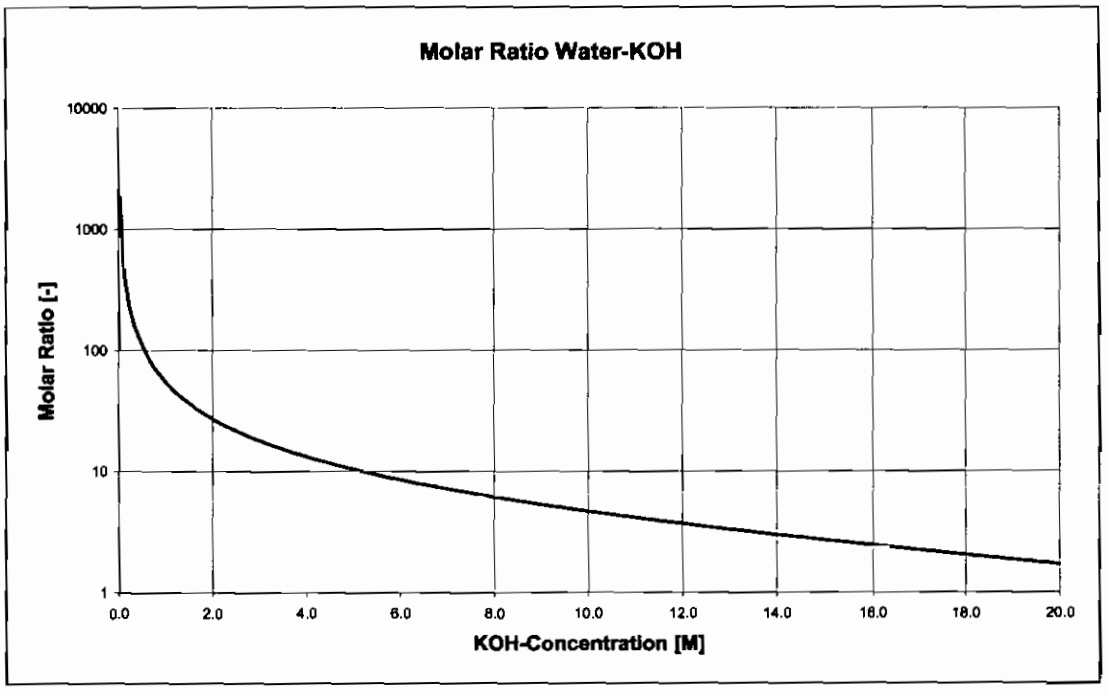

Diagram 2-5: Ratio of water and KOH molecules as a function of the concentration

The water molecules also interact with each other. This becomes apparent when considering the formation of the so-called secondary hydrate shell. Here, a second hydrate shell is formed around the first one.
Diagram 2.5 shows the calculated ratio of water and KOH molecules as a function of the concentration. The number of available water molecules quickly decreases with increasing concentration. At a concentration of 7.0 M the ratio is 7. Then only 7 water molecules are available for 1 KOH unit. Since KOH consists of one K^+-ion and one OH^--ion only 3.5 molecules are available for each ion.

These conditions indicate that a simple particle migration is not possible. The water molecules and the ions are interacting very intensive because of there charge and the dipole character of water. Here, the model of mass transport through a permanent transfer of molecules, the ongoing disintegration and new formation of hydrate shells or parts thereof, appears more plausible.

In a fuel cell the motion of water and ions is influenced by the electrodes and the separators. In case of the ions it is apparent that the electrical field between the electrodes has an influence on the motion of the ions.
In case of fuel cells the following possibilities of transport behaviour of the electrodes and separators can be considered:

1. the mass transport is not influenced by the component,
2. water can pass through the component, but KOH cannot pass,
3. KOH can pass through the component, but water cannot pass.

Points 2. and 3. are not to be seen as absolute statements. Interim stages are possible, for instance, if more water is transported than KOH, or vice versa.

2.5.2 Pressure-Dependent Cross-flow, EloFlux

Another possibility to provide the mass transport is the so-called EloFlux-principle. Here, a forced flow through the entire cell is generated. This convective flow supports the already existing flow caused by the volume increase through the formation of OH^--ions at the oxygen side. This non-directional flow is converted to a directed flow with the aid of a pressure difference. The EloFlux-flow is generated by a pressure difference of the electrolyte between the two electrolyte distributors. The flow moves from the high pressure to the low pressure and causes a flow through the electrolyte-filled pore system and the porous separators. The flow dimension depends on the extent of the pressure difference and the pressure loss and the permeability of the components respectively.

The EloFlux-flow offers various advantages over the mass transport caused by diffusion. The diffusion properties of the components do not have a significant influence any more since they are superseded by the EloFlux flow. In this, it is assumed that diffusive mass transport is important at the various pores at the triple phase boundary.

2.5.3 Electroosmotic Flow (EOF)

Electroosmosis is a flow of ions through a pore caused by an electrical field and the interaction of the ions and the walls of the pores. The liquid must be an electrolyte solution like KOH solution. The type of ions who are adsorbed at the wall or what type of ions are free to move depends on the material properties of the wall of the pores.

Figure 2-18 shows the situation in a pore. The positive charged ions are adsorbed at the wall of the pores. The negative charged ions are free to move. At the beginning and at the end of the pores are the electrodes. They can produce the electrical field. The negative ions move in direction of the positive charged electrode. The ions are surrounded by a hydrate shell. The hydrate shell also moves with the ions. [2-17]

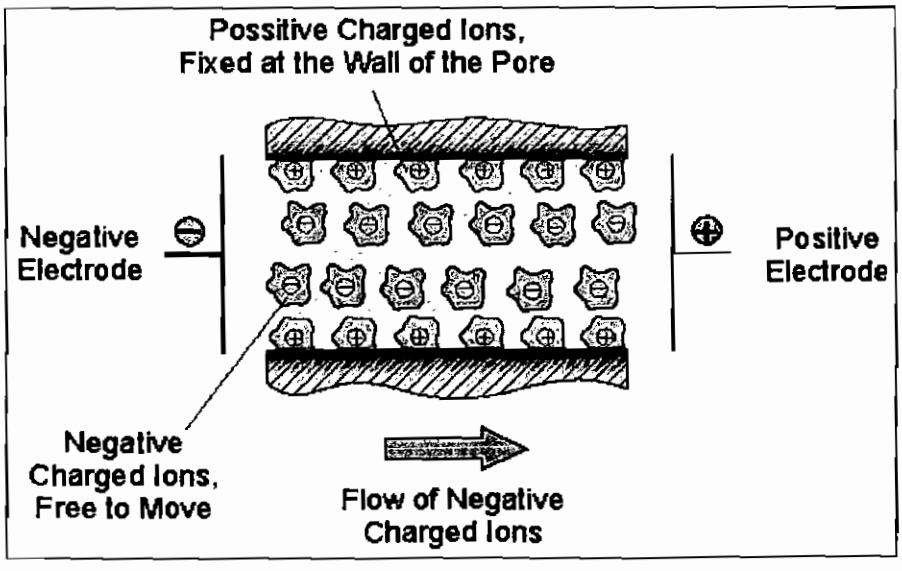

Figure 2-18: Electroosmotic flow through a pore caused by an electrical field

2.5.4 Osmotic Flow

Osmosis is the passage of water from a region of high water concentration through a semi-permeable membrane to a region of low water concentration. In Figure 2-19 the concentration of water is higher at the right side of the membrane than at the left side of the membrane. The semipermeable membrane is permeable for water but not for the solved substance. The water molecules move from the right side of the membrane to the left side.

If the solution can not leave the compartment on the left side the flow of water molecules will cause an increase of pressure. That pressure is called osmotic pressure. It can calculated by the following equation.

$$p = c \cdot R \cdot T \qquad \textbf{(Eq.: 2-11)}$$

Where c is the molar solute concentration, R is the gas constant, and T is the absolute temperature. [2-18]

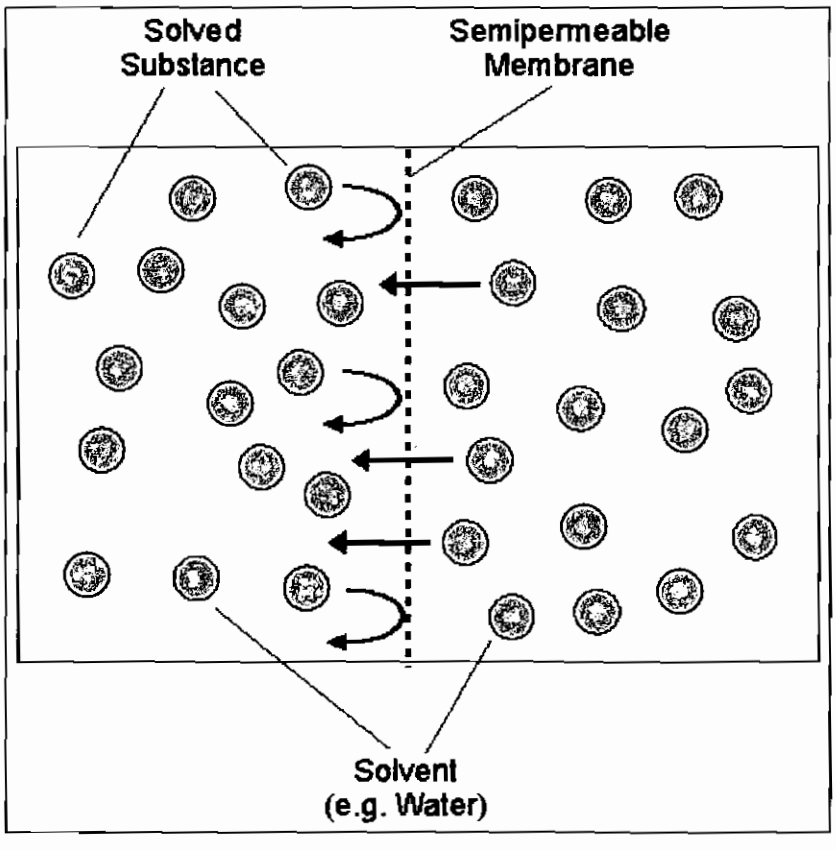

Figure 2-19: Osmotic flow through a semipermeable membrane.

2.5.5 Grotthus-Mechanism

As is shown in Diagram 2.4, in alkaline fuel cells potassium hydroxide is used as electrolyte because of its high conductivity. Compared to other ions the conductivity of H^+ and OH^--ions is significantly higher. This property is commonly attributed to a different transport mechanism of these ions. While all other ions actually have to migrate to the other electrode in order to transport electric charges, H^+ and OH^--ions use a different mechanism. In the presence of water molecules only the hydrogen binding connections "hop and turn". Figure 2-20 shows a schematic representation of this process. While on one side an OH^--ion becomes a water molecule the opposite process occurs at the other side. While there is a net transport of water molecules from left to right the OH^--ions move in the opposite direction. Since the ion does not move from one electrode to the other but probably only assumes another orientation the effort necessary for transporting a charge is considerably lower. This can result in a high conductivity.

Applying this mechanism to a fuel cell would mean that the reaction water is formed at the hydrogen electrode, but that it is transported to the oxygen electrode due to this mechanism. Reciprocally, the same holds for OH^--ions. [2-21]

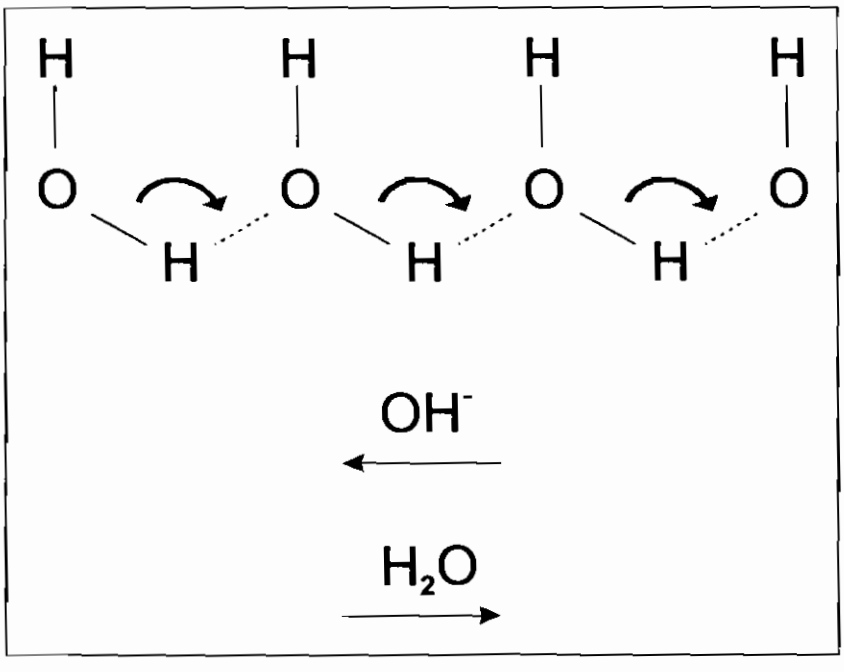

Figure 2-20: Schematic representation of the Grotthus-mechanism

2.6 Comparison of Various Fuel Cell Systems

A large variety of different fuel cells is available on the market. Unfortunately, all fuel cells are still more or less prototypes. They are usually distinguished by the electrolyte, the operating temperature and the used fuel.

For this project only the low temperature fuel cells were considered.

The so-called high-temperature fuel cell with operating temperatures of 400 °C to 1000 °C will not be included in the considerations. At a low power rating of only 5 W it is not possible to heat up those cells to their operational temperature using their own heat dissipation. The reactions in high temperature fuel cells only happen at the operating temperature. So it is not possible to use them at 5 °C.

Additionally, systems not using pure hydrogen as fuel are also not considered here. If hydrogen is bound to other chemical substances the latter will remain in the fuel cell after the reaction. Since they cannot be conducted outside the cell they would cause an undesired pressure increase inside the probe and they would clog the electrode surface respectively.

For this effort (Deep Sea Probe) the fuel cell types SOFC, MCFC and DMFC were deemed unsuitable. The SOFC and MCFC are only running at high temperature. The DMFC uses methanol for fuel. The latter of this fuel is CO_2. It is not possible for the CO_2 to leave the deep sea probe because of the high water pressure outside the probe and the fuel electrode will clog.

Three fuel cells remain, to be considered: These are the PEMFC, the PAFC and the AFC. The suitability of these fuel cells is discussed in the following.

2.6.1 Polymer Exchange Membrane Fuel Cell (PEMFC)

In a PEMFC the electrolyte is replaced by proton-conducting membrane. In order to work properly the membrane has to be moistened with water. The more hydration there is the better the ion conductivity and the gas impermeability of the membrane. Since a PEMFC does not contain a liquid electrolyte the reaction water cannot be transported off in this way. It would have to be extracted via the gas compartments of

the cell and is often removed through gravitational dripping. There are strong doubts that the water extraction can be achieved in this manner.

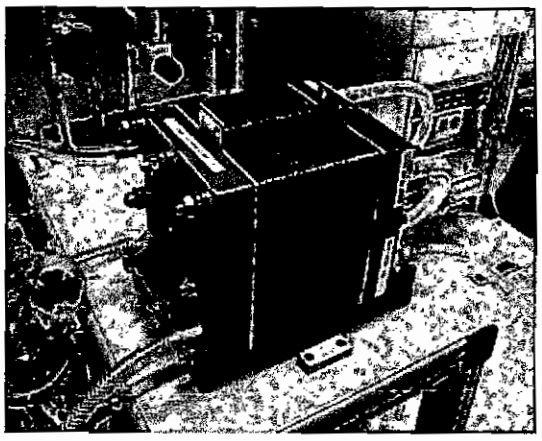

Figure 2-21: PEMFC by ZSW

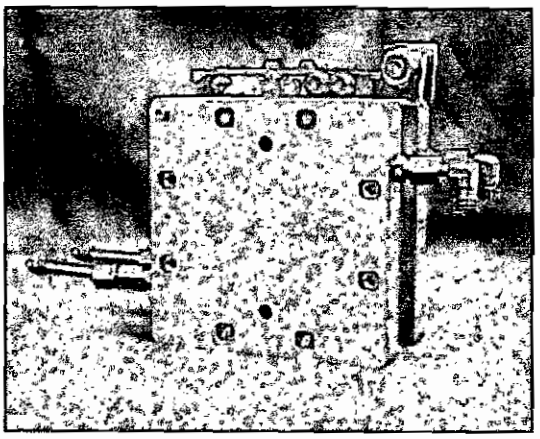

Figure 2-22: PAFC by Sartorius

The normal operating temperature of a PEMFC is 60 to 80 °C. The cell would have to be largely over-dimensioned in order to supply the required electric power at a temperature of 5 °C.

2.6.2 Phosphoric Acid Fuel Cell (PAFC)

The electrolyte of a PAFC is highly concentrated phosphoric acid. To achieve acceptable reaction kinetics these cells are usually operated at 160 °C to 200 °C. In the deep ocean it is not possible to heat the cell also the power density of the cell is not sufficient to heat the cell with its generated heat. The PAFC is therefore also not suitable for a deep sea application.

2.6.3 Alkaline Fuel Cell (AFC)

The electrolyte of an AFC is, as already mentioned, a potassium hydroxide solution of approximately 30 % concentration (equivalent to 7 M). The reaction water is absorbed by the electrolyte thus diluting the latter. The water extraction would in this case happen by diffusion. This process could be supported through the concentration dependency of the hydroxide solution density. With increasing concentration the density increases as well.

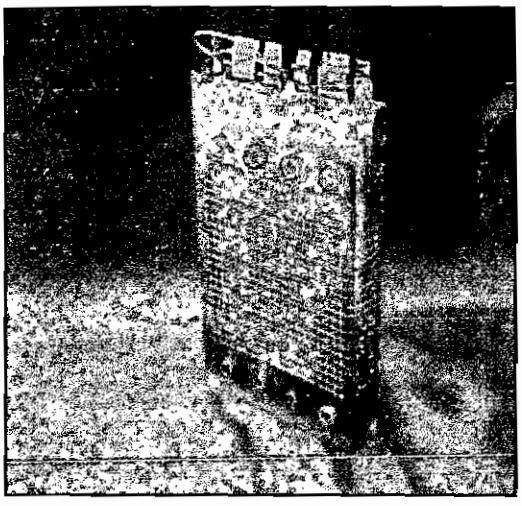

Figure 2-23: EloFlux-AFC by Gaskatel

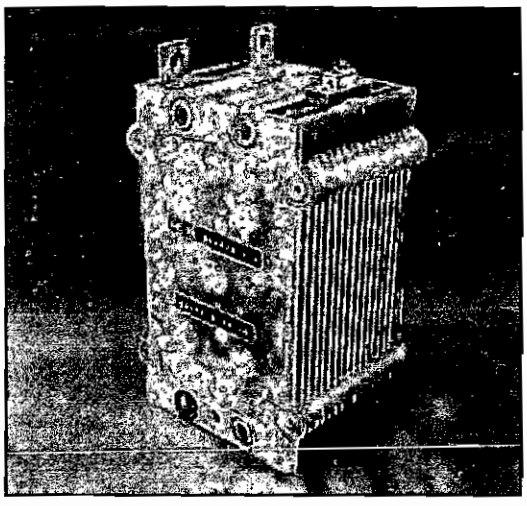

Figure 2-24: AFC by Siemens

Positioning the hydroxide storage container above the fuel cell effects an exchange of the hydroxide caused by the different densities in conjunction with gravity. The usual operating temperature of an AFC is between 50 °C and 80 °C. At a potassium hydroxide concentration of approximately 30 % it can also be operated well below the freezing point of water.

At an operating temperature of 5 °C the AFC would also have to be largely over-dimensioned because the chemical reactions also become slower.

2.7 Primary Energy Storage

To provide electric energy, an alkaline fuel cell requires hydrogen and oxygen gas as a primary energy source. The electric energy is calculated as:

$$E_{el} = V \cdot I \cdot t \qquad \textbf{(Eq.: 2-12)}$$

This yields an electric energy of 43.8 kWh. The required amount of primary energy and the size of the measurement probe (see below) depend on the efficiency of the fuel cell and on the kind of storage for the primary energy.

In the following, the amount of hydrogen and oxygen are calculated and various storage possibilities are discussed.

2.7.1 Primary Energy Amount

The amount of required reaction gases results from the electrical energy to be supplied while considering the efficiency of the fuel cell. The efficiency of a fuel cell becomes apparent when the cell voltage is at the operating point.

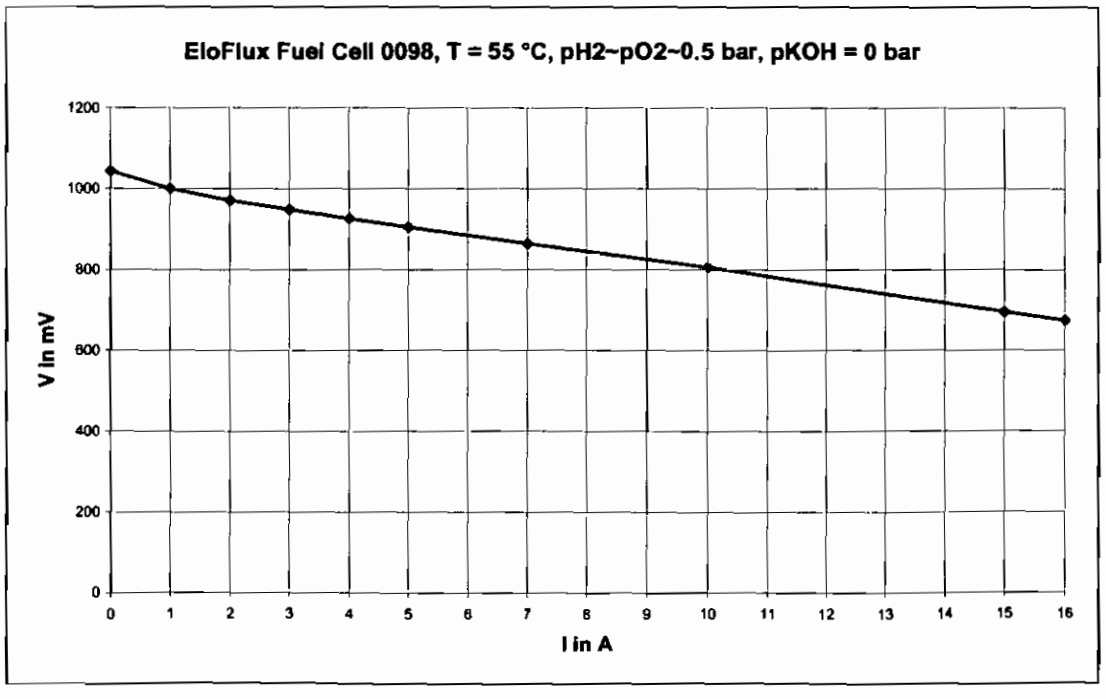

Diagram 2-6: Characteristic of an EloFlux-AFC at standard conditions

Based on the characteristic curve of an EloFlux-AFC (see Diagram 2-6) at normal operating temperature five cells would be sufficient to achieve a stack voltage of 5 V (at 1 A).

Due to the low operating temperature and the resulting lower power capacity the number of cells is increased by two to seven cells. This yields a minimum individual cell voltage of 720 mV.

Using Faraday's law the hydrogen volume required to convert the electrical energy can be calculated:

$$V_{H_2} = \frac{n \cdot I \cdot t}{z \cdot F} \cdot V_{mol} \qquad \textbf{(Eq.: 2-12)}$$

(where n is the number of individual cells, I is the current, t is the time, z is the number of electrons, F is the Faraday constant and V_{mol} is the volume of one mol H_2)

$$V_{H_2} = \frac{7 \cdot 1A \cdot 31536000s}{2 \cdot 96485 \frac{C}{mol}} \cdot 22.41 \frac{l}{mol} \approx 25640\,l \qquad \textbf{(Eq.: 2-13)}$$

Applying the corresponding figures yields:

The oxygen volume is accordingly calculated (with z=4) and is 12820 l. Considering the safety reserves 30000 l hydrogen and 15000 l oxygen have to be supplied.

Converted to weight this corresponds to approximately 2.7 kg hydrogen and approximately 21.4 kg oxygen.

2.7.2 High Pressure Gas (300 bar)

The storage of the reaction gases as high pressure gas is an established method for terrestrial applications. High pressure steel containers are available with 10 l, 20 l and 50 l volume and they can be filled at a pressure of 200 bar or 300 bar (see Figure 2-17). An empty 50 l cylinder weighs approximately 70 kg. For the storage of the hydrogen two 50 l cylinders (300 bar) are required. For the oxygen one cylinder is sufficient (300 bar). The total weight is then approximately 210 kg. Another 2.7 kg

of hydrogen and 21.4 kg of oxygen have to be added to that. It became apparent that the gas storage system has the highest weight and the largest dimensions in relation to the remaining fuel cell system. As an alternative, high pressure containers made from composite materials are currently being tested. They are designed for a pressure of up to 1000 bar and have a lower weight. Unfortunately, these containers are not yet commercially available. A statement about the costs and the durability is not yet possible.

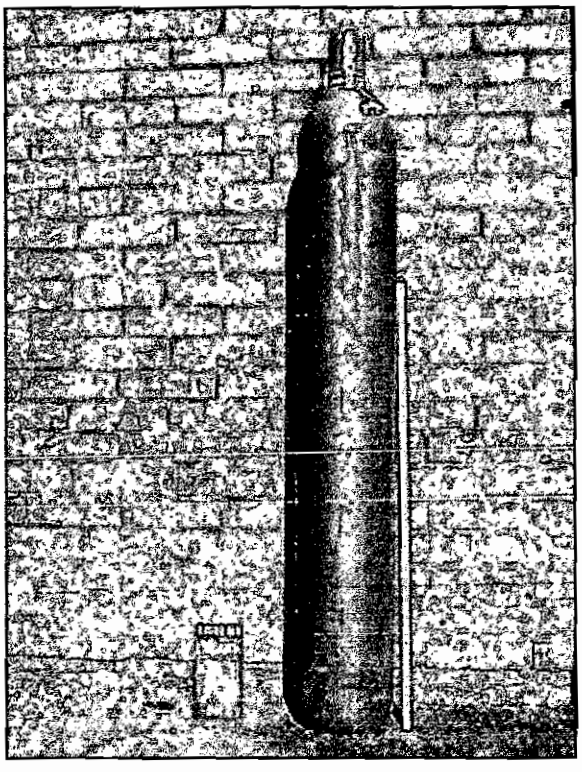

Figure 2-25: High pressure gas cylinder, steel, 50 l, 200 bar

Figure 2-26: 50 l Cryo-tank by AIR LIQUIDE

2.7.3 Chemical Storage

Hydrogen can also be stored with other substances as a chemical compound which could be, for example, hydrocarbons, methanol or hydrazine. In order to make the hydrogen usable for a fuel cell these compounds have to be broken up. Thereby the carrier substances remain as carbon dioxide or nitrogen. Since these substances cannot be released into the environment the pressure inside the probe would increase. Furthermore, it has to be ensured that the CO_2 or the nitrogen do not clog the electrode surface which would prevent the hydrogen from reacting.

With this method only the hydrogen could be stored, oxygen cannot be stored in this manner.

Chemical storage is hence unsuitable for the application.

2.7.4 Metal Hydride Storage

Another possibility of storing hydrogen is the use of metal hydrides. For this, the hydrogen can be stored within the crystal lattice of various metal alloys. The charging process is an exothermic reaction while the discharging process is endothermic. The storage capacity for hydrogen is approximately 1.3 to 3.6 % of weight. Table 2-1 shows an overview of various metal alloys, their storage capacity as well as pressures and temperatures.

Typical alloy	% of weight	Pressure (bar)	Temp. (°C)
$LaNi_5$	1.38	4.0	50
$TiMn_2$	2.0	9.0	20
TiFe	1.8	10.0	50
Mg_2Ni	3.6	1.0	250

Table 2-1: Comparison of various metal hydride storage alloys [2-22]

This kind of hydrogen storage is still in a prototype state. A definitive statement about the costs and the durability is not yet possible. Since this storage method can

only be applied to hydrogen and not to oxygen it is not suited for a deep sea application. Figure 2-21 shows a metal hydride storage device for 20 Nl hydrogen.

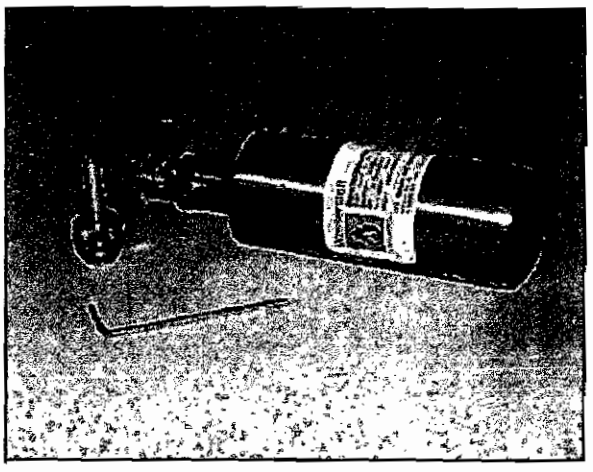

Figure 2-27: Metal hydride storage device by H_2-Interpower

2.7.5 Liquid Gas

At low temperatures, hydrogen and oxygen can also be stored as liquids. Hydrogen only turns liquid below –253 °C while oxygen is already liquid below –183 °C. For the storage of liquid gases so-called cryo tanks are used (see Figure 2-20). They are characterised by their good thermal insulation. The absorption of heat from the ambient environment is minimal. However, the warming of the tank cannot be totally eliminated and hence, over time, the tank will indeed warm up. Through the evaporation of parts of the liquid gas the temperature inside the tank can be stabilised. The evaporation enthalpy is 454 kJ/kg for hydrogen and 213 kJ/kg for oxygen [2-7]. Provided the hydrogen consumption of a fuel cell system is equal to the evaporated gas required to stabilise the tank temperature then the system could be operated without a loss of reaction gas. If the hydrogen consumption is lower then a part of the evaporated hydrogen would have to be released into the environment and would thus be lost. Liquid hydrogen has a density of 70.79 g/l. In relation to high pressure gas a density equilibrium would be achieved at 788 bar. Above this pressure the use of liquid gas does not yield an advantage with respect to the storage volume.

The question arises which method is more energetically advantageous or rather better manageable.

It can be stated that the storage as liquid gas is not suitable for a deep sea application since the gas consumption of the fuel cell is too low.

2.7.6 Energy Generation from Methane

Another possibility to generate energy is the use of bacteria which convert methane in several oxidation steps to CO_2 and H_2O. If it were possible to directly intervene in these oxidation steps, to tap into the electron flow and conduct it to an external circuit without affecting the work of the bacteria, then they could be used for direct energy generation. However, that is exactly where the problem lies. The hydrogen is always bound to other elements and is hence initially not available. In order to prove the feasibility of this method corresponding investigations would have to be initiated. Suitable bacteria genus's are methylomonas, methylococcus and methylosinus. However, they still require oxygen. Furthermore, it needs to be clarified if bacteria can be used at 5 °C and how it can be achieved to make the gas hydrate available to the bacteria. In case adequate bacteria are available they need to be in contact with an electrode to catch the electrons [2-12]. It is not possible to give a statement here if and in which timeframe this could be realised.

2.7.7 Energy Generation from Plankton

The plankton of the oceans could also be used as an energy carrier. According to reports of U.S. scientists dead plankton which accumulates at the ocean ground can be used in conjunction with the oxygen solved in the sea water to generate energy in a fuel cell. The sea water would act as the electrolyte. The first experimental fuel cells of the OSCAR project (Ocean Sediment Carbon Aerobic Reactor) achieved a power density of approximately 50 mW/m^2 at a voltage of 0.7 V. The electrode area required for the supply of the Tiger probe would hence be approximately 100 m^2 [2-13].

2.8 Electrolyte Dilution

The reaction water produced during the operation of the fuel cell dilutes the electrolyte. The ionic conductivity depends on the concentration of the potassium hydroxide (see Diagram 2-4).

Diagram 2-5: KOH-requirement when adding 24.1 kg of water to 7 M KOH

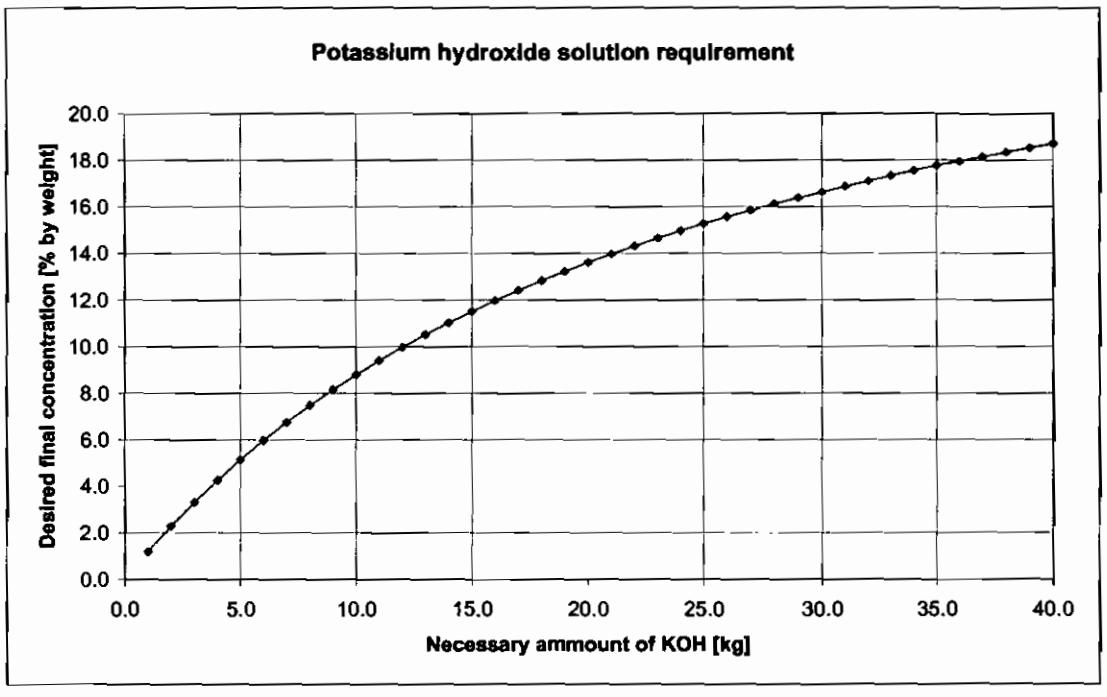

To ensure that, at the end of the run-time, the capacity of the fuel cell is still sufficient to supply the measurement system with electricity the amount of potassium hydroxide has to be calculated which is required to prevent the hydroxide concentration from decreasing below 3.5 M (16.78 % by weight).

The initial concentration is specified with 7.0 M (30.68 % by weight). As calculated in Section 2.5.1, approximately 2.7 kg of hydrogen and 21.4 kg of oxygen are required. This means that, in total, the potassium hydroxide has to absorb 24.1 kg of water. With an initial amount of substance of approximately 30 kg 7.0 M KOH the specified final concentration can be met (see Diagram 2-7).

3 Experimental Set-Up

In this section the different experimental set-ups are illustrated. Firstly, the electrolyte circulation of an EloFlux-AFC is described. A special focus is put on the pump. Following the description of electrically operated pumps the functionality of a self-developed gas pump is elaborated. Eventually, a system is presented where the mass transport takes place through diffusion.

The experimental set-ups for testing the fuel cell as well as characterising the electrodes are described. This includes the pressure-dependent flow rate measurement as well as the mass transport through diffusion. The measurements of the gas permeability (permeation) and the construction of a half cell is also described.

Furthermore, the concentration measurement probe Densoflex as used in the fuel cell is elaborated in detail.

3.1 KOH Circulation in an Alkaline Fuel Cell

The hydroxide circulation through an alkaline fuel cell has several functions. It has to regulate the temperature, transport the produced reaction water from the cell and supply fresh hydrate solution to the cell respectively. Consequently, the flow rate (circa 5 l/h) has to be controlled. Additionally, the hydroxide pressure has to be adjustable. Depending on the used electrodes and separators pressures differences of merely 50 mbar to 500 mbar with respect to the gas pressures can be permitted. In order to facilitate the required potassium hydroxide flow a pump is necessary.

The majority of pumps can be divided into positive displacement pumps and flow pumps. They are distinguished by their operating principle.

In a positive displacement pump the fluid to be pumped is displaced by e.g. a diaphragm or a piston. The pump cycle consists of a suction stroke and a discharge stroke, which normally causes a pulsating flow. In order to prevent the fluid from re-entering the pump from the discharge side during the suction stroke, and to prevent the fluid from re-entering the suction side during the discharge stroke respectively, this type of pump requires some sort of check valve. Figure 3-1 shows the schematic

construction of a positive displacement pump. When the piston moves up the check valve at the discharge side is closed. The fluid is drawn into the chamber through the check valve at the suction side. When the piston moves down the check valve at the suction side is closed and the fluid leaves the chamber through the check valve at the discharge side.

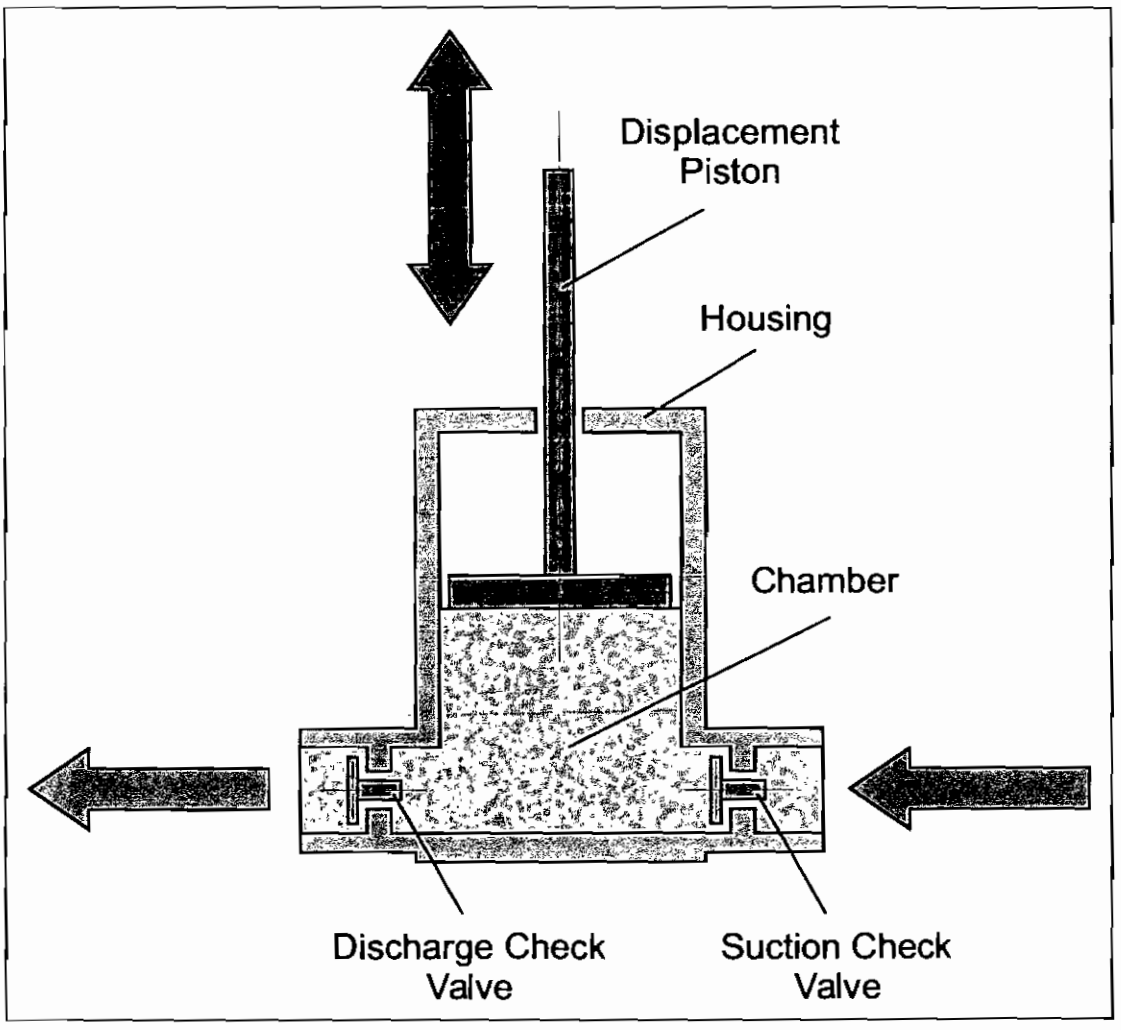

Figure 3-1: Schematic cross-section of a positive displacement pump (piston pump)

Flow pumps have a different working principle than positive displacement pumps. Here, the fluid to be pumped is accelerated by a rotating impeller. Inside the pump the fluid velocity energy is converted into pressure energy using a suitable changing profile. This is a continuous process.

Figure 3-2 shows the schematic construction of a flow pump. Via the intake socket the fluid reaches the impeller and is accelerated by the blades of the rotating impeller. The intake socket is not shown in the drawing. The direction of the inlet is perpendicular to the plane of the drawing. From the impeller the fluid gets into the pump housing and leaves the pump via the pressure socket.

The volume flow is steady. The achievable pressure depends on the circumferential velocity of the impeller wheel. The circumferential velocity depends on the rotation speed and the diameter / radius respectively. With an increase of these two parameters the volume flow increases as well.

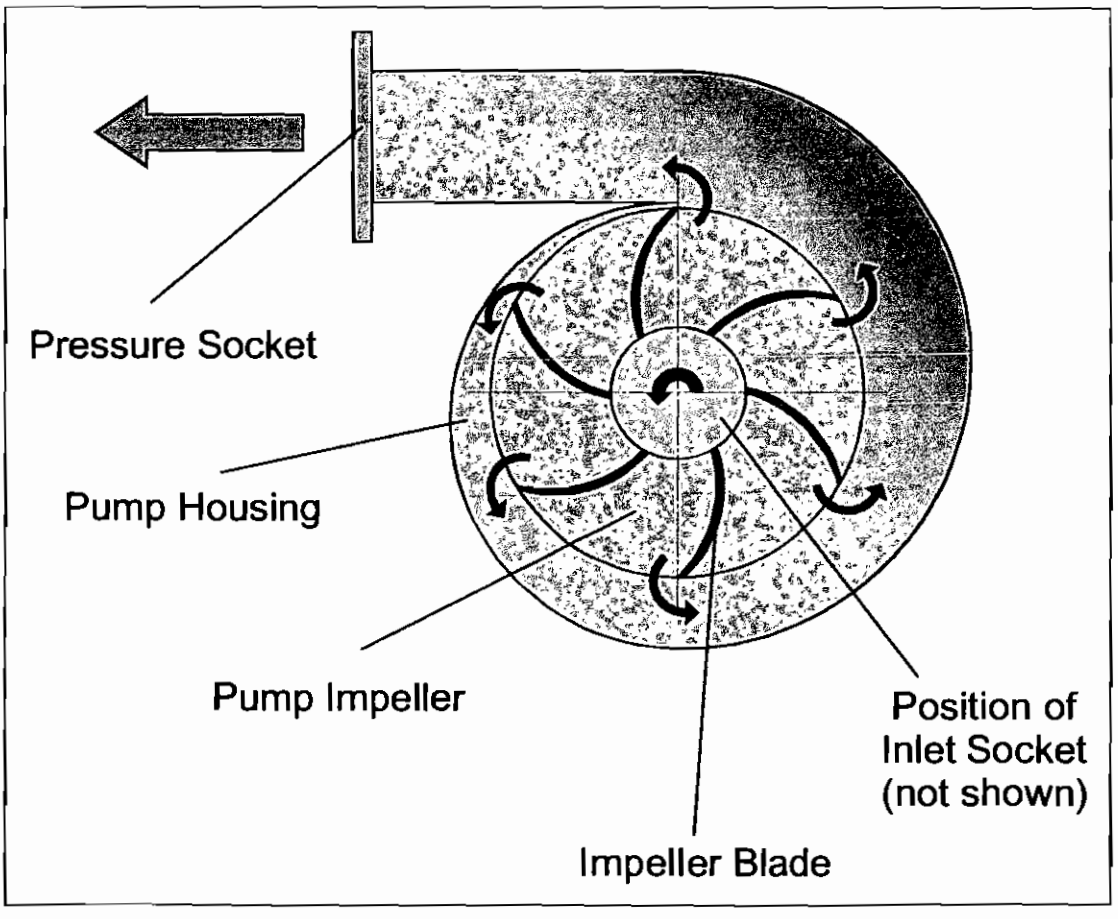

Figure 3-2: Schematic cross-section of a flow pump (radial flow pump)

For a fuel cell, the ratio of volume flow rate (5 l/h) and pressure (0.5 bar) is so disadvantageous, that a flow pump cannot be used for it. With a diameter of circa

20 mm the impeller wheel would have to be very small resulting in a required rotation speed of several ten thousand rounds per minute.

Consequently, only positive displacement pumps can be used for the supply of an AFC. They can pump small volumes at relatively high pressures.

In the following section a previously used solution is presented, followed by a description of a newly developed pump. Concluding, a concept is presented that works without a pump. The mass transport takes place through diffusion and does not require any additional energy. This is the system to be used for the deep sea probe.

3.1.1 Previous KOH Solution Circulation System

The hydroxide was taken from an unpressurised storage tank and led to an electric gear pump (by Ismatec) or an electric diaphragm pump (by Prominent). It delivered the hydroxide through the fuel cell and, through a choke valve, back to the storage tank. The build-up of the pressure was achieved with a pump and a choke valve.

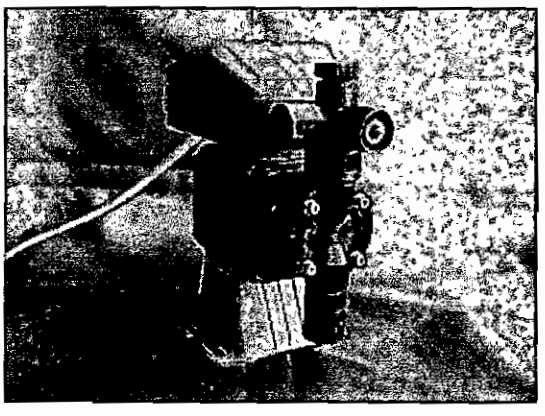

Figure 3-3: Diaphragm pump (IWAKI)

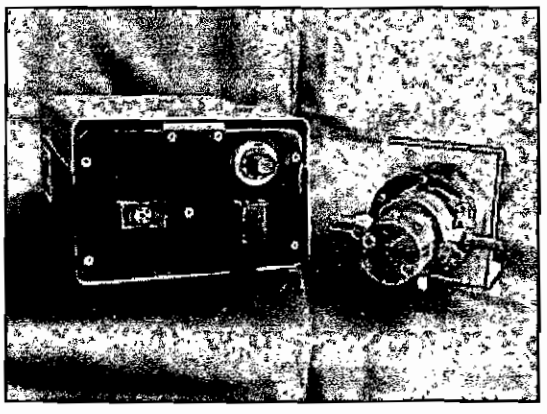

Figure 3-4: Gear pump (Ismatec)

This set-up had various disadvantages. These were:

- Blockage of the needle valve / the pump
  Due to the small flow volume of circa 0.5 to 5 l/h at relatively high pressures, the occurring diameters are very small. The valve and the pump are prone to contaminations or gas bubbles. In particular gear pumps with their small clearance could also be damaged by crystallising KOH.

- Power consumption
  The pumps available by Ismatec, IWAKI or Prominent are mostly oversized for this application and hence require an electric power of up to 20 W and a DC supply voltage of 12 V or 24 V. For a practical fuel cell application this energy would have to be supplied by the fuel cell. In particular in the low-power range of up to 500 W, the system's efficiency is strongly reduced as a consequence.
  With regards to the deep sea application, this means that such a pump cannot be used since the fuel cell can neither supply the required power nor the appropriate voltage (the fuel cell for TIGER is rated for 5 W at 5 V).

- Pressure regulation
  The above set-up requires a pressure-dependent pressure regulation for the gas. This component makes the system more complicated, causes additional costs and also requires extra energy. Furthermore, the operational reliability is further reduced by the added component.

Figure 3-5 shows the schematic construction of a gear pump. Gear pumps are positive displacement pumps. The pump mainly consists of two gears and a housing. The gears are meshing, making it sufficient to drive one of the two gears. The fluid flows from the suction side into the pump housing where it is moved by the gears. The fluid is transported to the discharge side in the gaps between the housing wall

and the gear. Due to the meshing of the gears the fluid is displaced from the gaps of the gears thus enabling the fluid transport.

In order to minimise a reflow between gear and housing wall from the discharge side to the suction side due to the pressure difference the mechanical clearances have to be kept small.

This holds similarly for the meshing of the gears. This should preferably be free of clearance, because too large gaps could result in a reflow.

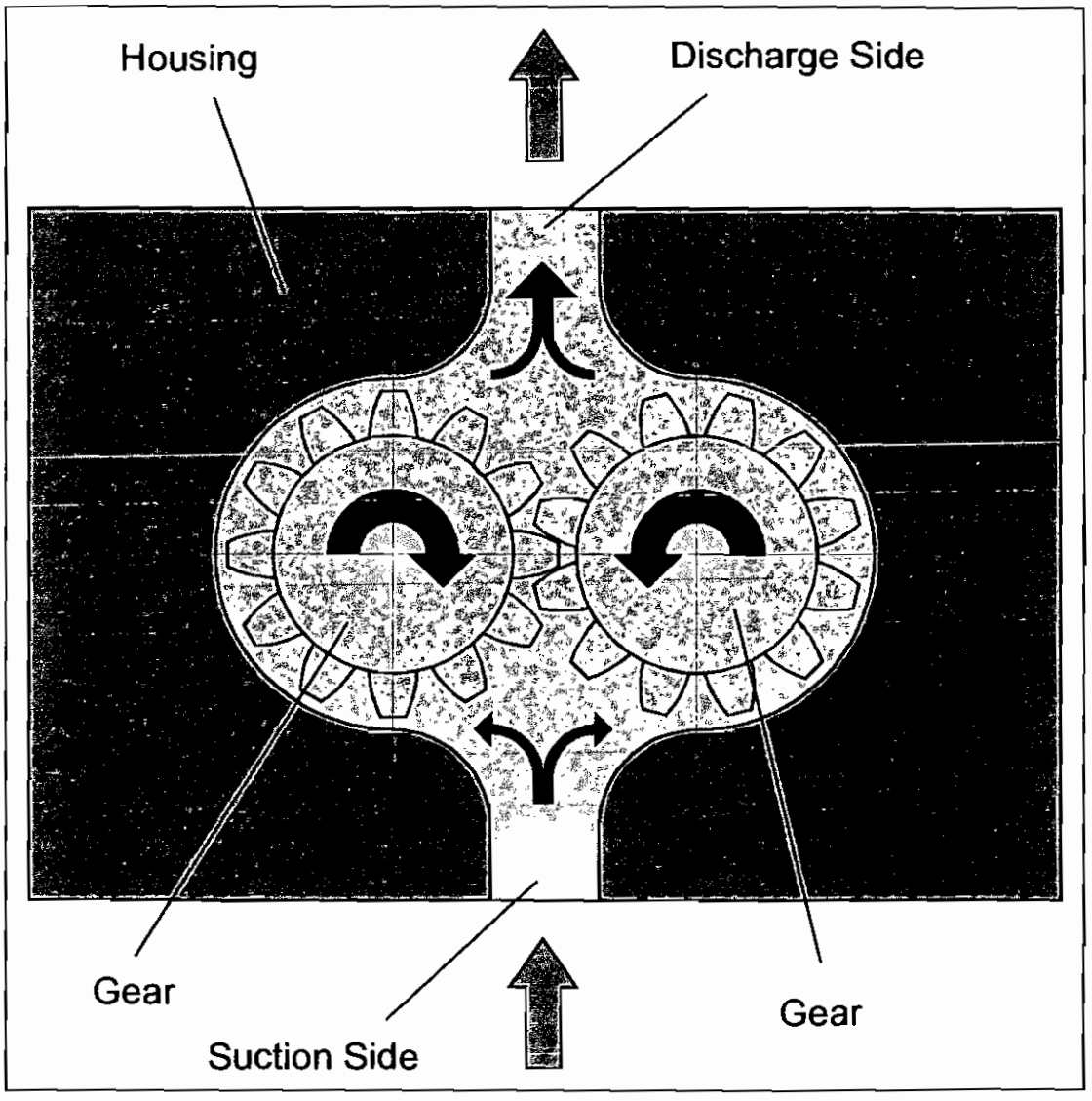

Figure 3-5: Schematic cross-section of a gear pump

3.1.2 Compressed Gas-driven Diaphragm Pump

When compressed gas storage systems are used, the pressure energy released when the gas is relaxed to operating pressure can be used to pump the hydroxide solution. For this, a gas-driven diaphragm pump type CX 10 by Almatec was tested (see Figure 3-6). It became clear, that this type of pump is in principle suitable, but could not be used in this specific application. The pump was enormously over-dimensioned with regards to its flow rate, even though it was the smallest model available.

Figure 3-8 shows the schematic construction of a gas diaphragm pump by Almatec.

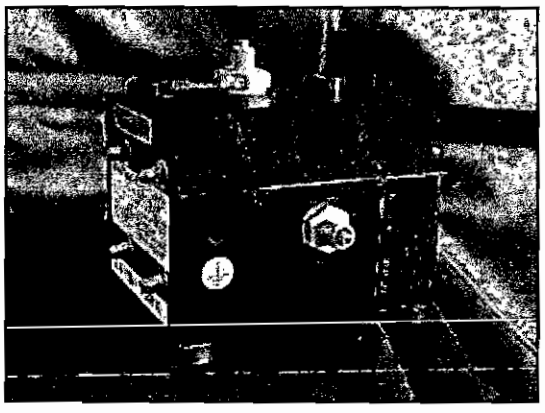

Figure 3-6: Gas diaphragm pump (Almatec)

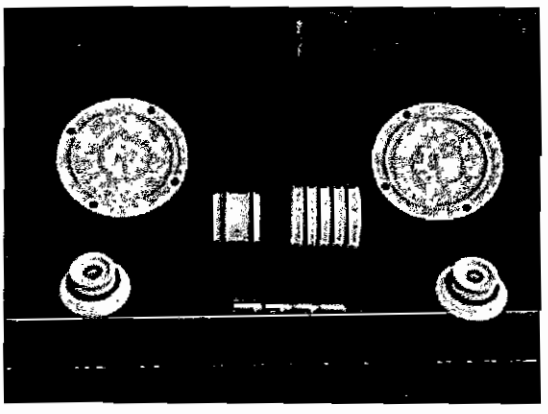

Fig. 3-7: Diaphragms and control unit

The function is identical to the above described piston pump. Instead of a displacement piston here flexible diaphragms are used. The two diaphragms are connected via the control piston. When both diaphragms reach their maximum amplitude (dead point) then one diaphragm has completely filled the fluid space and the other one has completely filled the gas volume. In this case, the pressure of the compressed gas works on the diaphragm that has just displaced the fluid. The gas volume of the other diaphragm is meanwhile discharged into the surroundings. Since both diaphragms are fast connected to each other the diaphragm just displacing fluid moves the other diaphragm as well, so the latter can draw fluid in. When both diaphragms reach their dead points, the control unit toggles the direction. The pressurised gas behind the diaphragm that had just pumped is discharged into the

surroundings and fresh compressed gas is conducted behind the diaphragm which had just drawn in fluid. When both diaphragms reach their dead points, the control unit reverses again and the cycle starts over. The control unit works completely mechanical.

Figure 3-7 shows the diaphragms, the control piston as well as the control unit for the compressed gas.

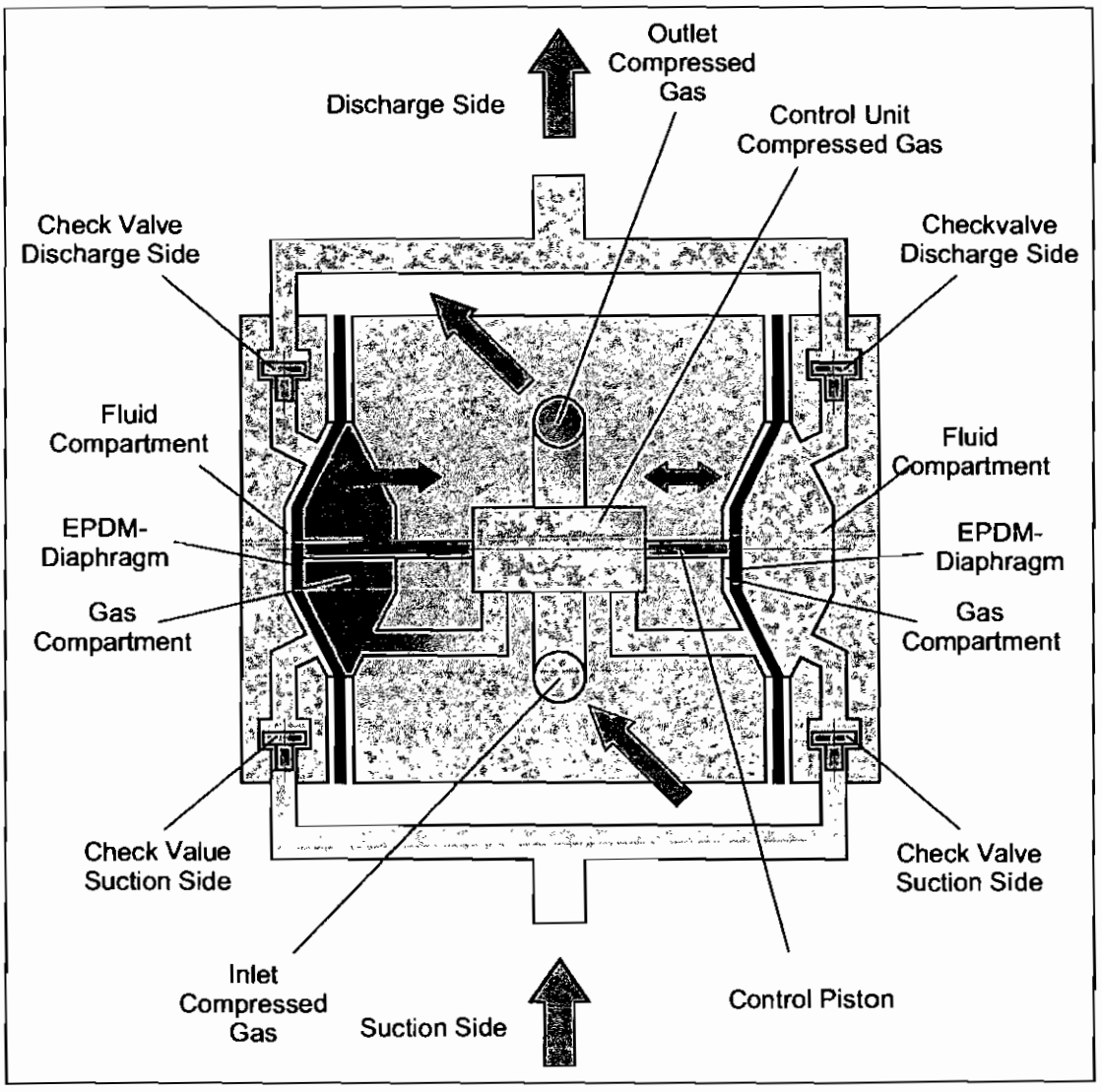

Figure 3-8: Schematic cross-section of a gas diaphragm pump by Almatec

During the first tests, soon different problems arose with regards to the application for supplying a fuel cell. The large pressure difference ($\Delta p \approx 1.0$ bar) between the gas inlet and the gas outlet, which was necessary in order to operate the pump, was a problem. This was caused by the friction between the control piston and the seals, as well as the force necessary to flex the EPDM diaphragm. It was tried to reduce the friction by modifying the fit between control piston and seals. The control piston was modified and its diameter reduced. The required pressure difference could be slightly reduced ($\Delta p \approx 0.8$ bar). However, the alteration of the control piston resulted in a degradation of the seal function and leakages in the area of the compressed gas.

Furthermore, it became apparent that the ball check valves used in the pump were not completely tight, thus causing a reflow. Exchanging the steel balls for EPDM balls clearly reduced the reflow, but could not totally eliminate it. For a nominal flow rate of 10 l/min a reflow rate of 0.0008 l/min is quite small. However, for the low volume flow rate of a fuel cell with 0.5 to 5 l/h, the reflow rate is in a similar range.

Smaller pumps that were operated with compressed gas could not be sourced. For a fuel cell application such a pump would have to be adapted to the small volume flow and to be newly built. However, since the TIGER project is a singular application the effort seemed too large and other solutions were investigated.

3.1.3 Compressed Gas-Operated Tank Pump (Own Development)

This pump is self-regulating and has a low power consumption. The energy required for pumping is obtained by relaxing one of the reaction gases.

Based upon the insights obtained above it appeared sensible to develop and build a pump for a fuel cell system. Initially, a system working with two tanks was developed. This was then further developed into a system with one pump tank and one storage tank.

The principle of the pump is based on the effect that a gas pressure displaces a fluid, against a lower pressure, from the tank. While displacing the fluid, the gas becomes relaxed thus delivering the energy required for pumping.

For the pump system the following general specifications resulted:

1. The hydroxide flow has to be depended on the drained current and the gas consumption of the cell respectively; this allows to also regulate the temperature more easily.
2. The compressed gas relaxed during the pumping process has to be supplied to the fuel cell in order to lower the energy consumption.
3. The compressed gas has to be relaxed through the pumping process to the level of the supply pressure of the fuel cell. The pressure difference during the relaxation has to be smaller than the bubble point of the electrodes in order to prevent an overflowing of the pores (magnitude of 50 mbar to 100 mbar).
4. The hydroxide pressure has to be dependent on the gas pressure; the advantage of this is that the hydroxide pressure follows any changes of the gas pressure automatically.

The following additional detailed specifications were made:

a) The energy required to pump the hydrogen solution has to be generated through the relaxation of one of the reaction gases, preferably oxygen.
b) The system has to consume significantly less than 20 W external electric energy, if possible none at all.
c) No moving parts are to be used whose performance could suffer through contaminations or crystallisation of the potassium hydroxide.
d) If possible, a storage tank for the hydroxide is to be integrated.
e) The system has to be constructed as simple as possible and the components have to be easy to manufacture.

3.1.3.1 System with two Pump Tanks

The first approach was a pump system working with two pressure tanks made of plastic and one magnetic valve. To pilot the magnetic valve a float switch was used, which was mounted in one of the two tanks. The two tanks were connected to each other via the electrolyte distributors of the fuel cell. The gas pressure is adjusted to the operating pressure level of the fuel cell using a pressure reducer. Furthermore, the gas is led into either one or the other tank via a 5/2 valve, depending on the current state of the float switch. The tank not currently being pressurised supplies its pressure gas to the fuel cell. The potassium hydroxide is hence pumped alternately from one tank to the other. Hereby, the tanks function alternately as pressure and return tanks respectively. The flow direction of the hydroxide alternates between two pump cycles. This means that the cell flow is alternately forwards and then backwards. The hydroxide is only pumped when the fuel cell consumes gas.

The tanks were made of polypropylene and are welded or assembled with screws. The position of the tanks can be chosen almost completely arbitrarily. It has to be ensured that the float switch is mounted in its specified position, that the gas connectors are in touch with the gas and the hydroxide connectors are in touch with hydroxide in order to prevent the mixing of hydroxide and gas. The two tanks can also be combined to one tank. They have to be specified to match the operating pressure of the fuel cell and hold the produced reaction water.

Since it is difficult to obtain hydroxide-resistant 5/2 valves, the latter was replaced with two 3/2 valves. With 1.5 W and 0.65 W respectively per valve the power consumption of the magnetic valves was very low. Furthermore, the valves do not work continuously like an electric pump. To further reduce the power consumption so-called piezo valves could be used, which have a power consumption of 0.007 W.

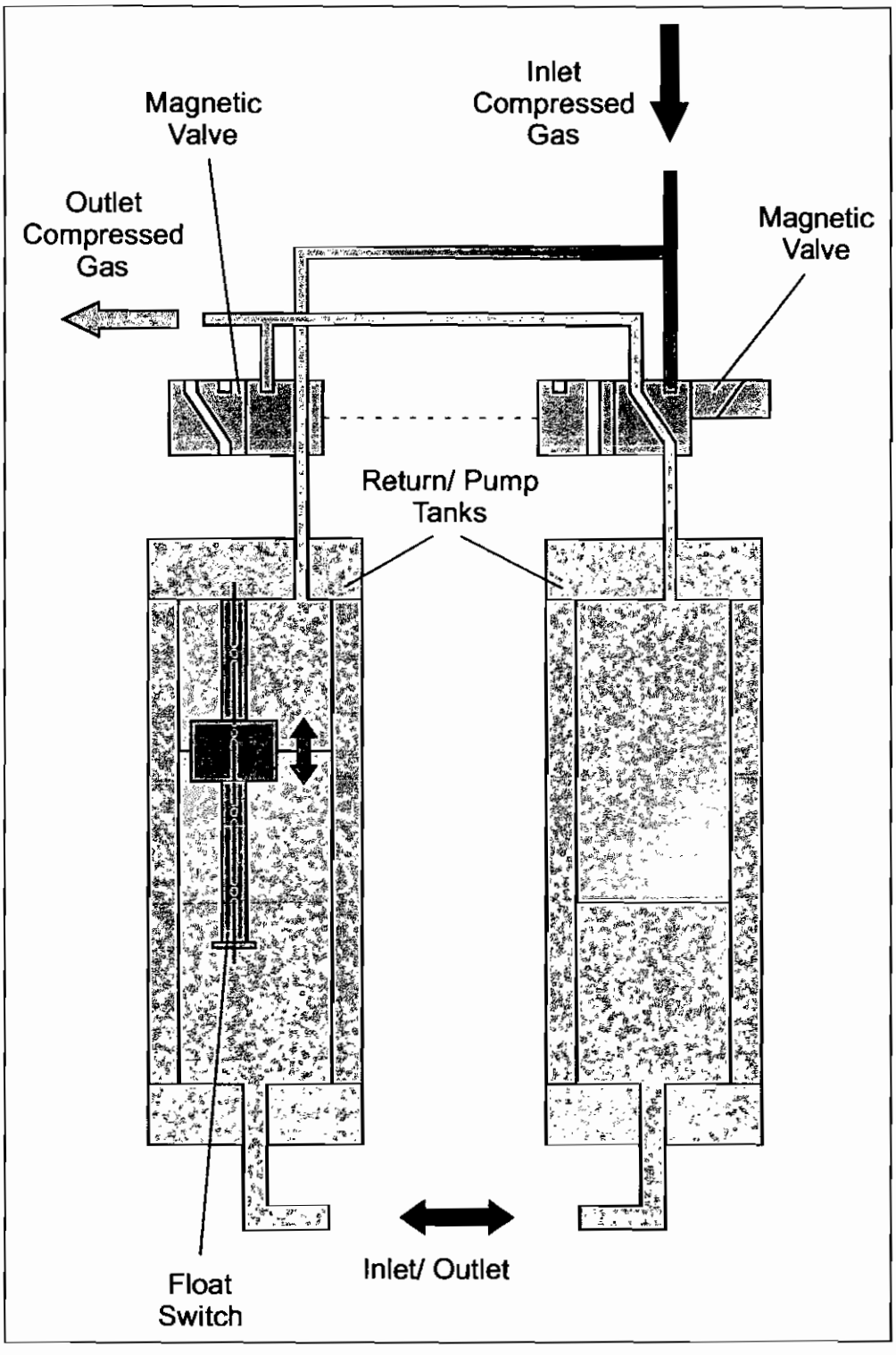

Figure 3-9: Schematic cross-section of a gas pump with two tanks

The experiment was carried out with a fuel cell. The pressures in the two tanks and the inlet pressure were recorded (in bar). The measurement values were plotted against the time (in seconds).

In Diagram 3-1, the switching points of the magnetic valve can be seen. The inlet pressure is alternately conducted to the two tanks.

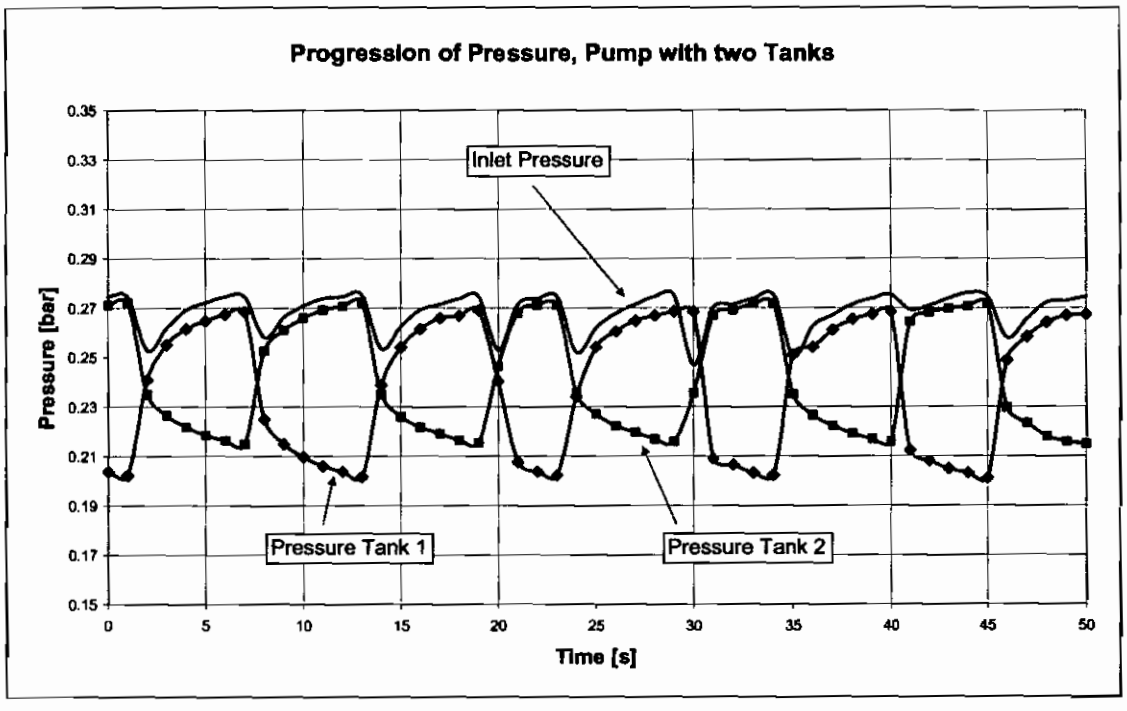

Diagram 3-1: Characteristic of the gas pump, alternating pressurisation of the tanks

3.1.3.2 System with one Pump Tank and one Storage Tank

In parallel to the development of a pump system with two tanks, another system with one pump tank and one storage tank was developed as well. Here, the purpose of the two tanks are clear. One tank always acts as a pump tank, while the other acts alternately as storage tank and return tank respectively. The hydroxide flow always takes place in one direction and there is no backwards flow through the cell.

The system operates as follows:

Initially the pump tank is filled up to the upper level with the liquid electrolyte. The level indicator is in an open state. The current-less position of the 3/2 valve allows the compressed gas to flow into the pump tank from the pressure cylinder. The compressed gas is stored in a high-pressure gas cylinder (200 bar or 300 bar). A pressure reducer lowers the pressure down to the operating pressure of the fuel cell. The pressure-reduced gas continues to flow into the pump tank via the 3/2 valve thus displacing the hydroxide contained in the tank. The check valve at the suction side prevents the fluid from flowing back into the storage tank. The check valve on the pressure side opens and the liquid electrolyte to be pumped can leave the pump tank and flow through the fuel cell. The reflow is directed into the storage tank.

With the liquid electrolyte flowing out, the fluid level in the pump tank is lowered until at a lower level the level indicator switches and supplies the 3/2 valve with current, thus interrupting the inflow of the compressed gas. Simultaneously a pressure equalisation between the pump tank and the storage tank takes place. Due to the height difference between storage tank and pump tank the check valve on the suction side opens. Liquid electrolyte flows from the storage tank into the pump tank, thus displacing the gas from the pump tank into the storage tank. The check valve at the pressure side is closed and meanwhile prevents the reflow of fluid from the fuel cell into the storage tank.

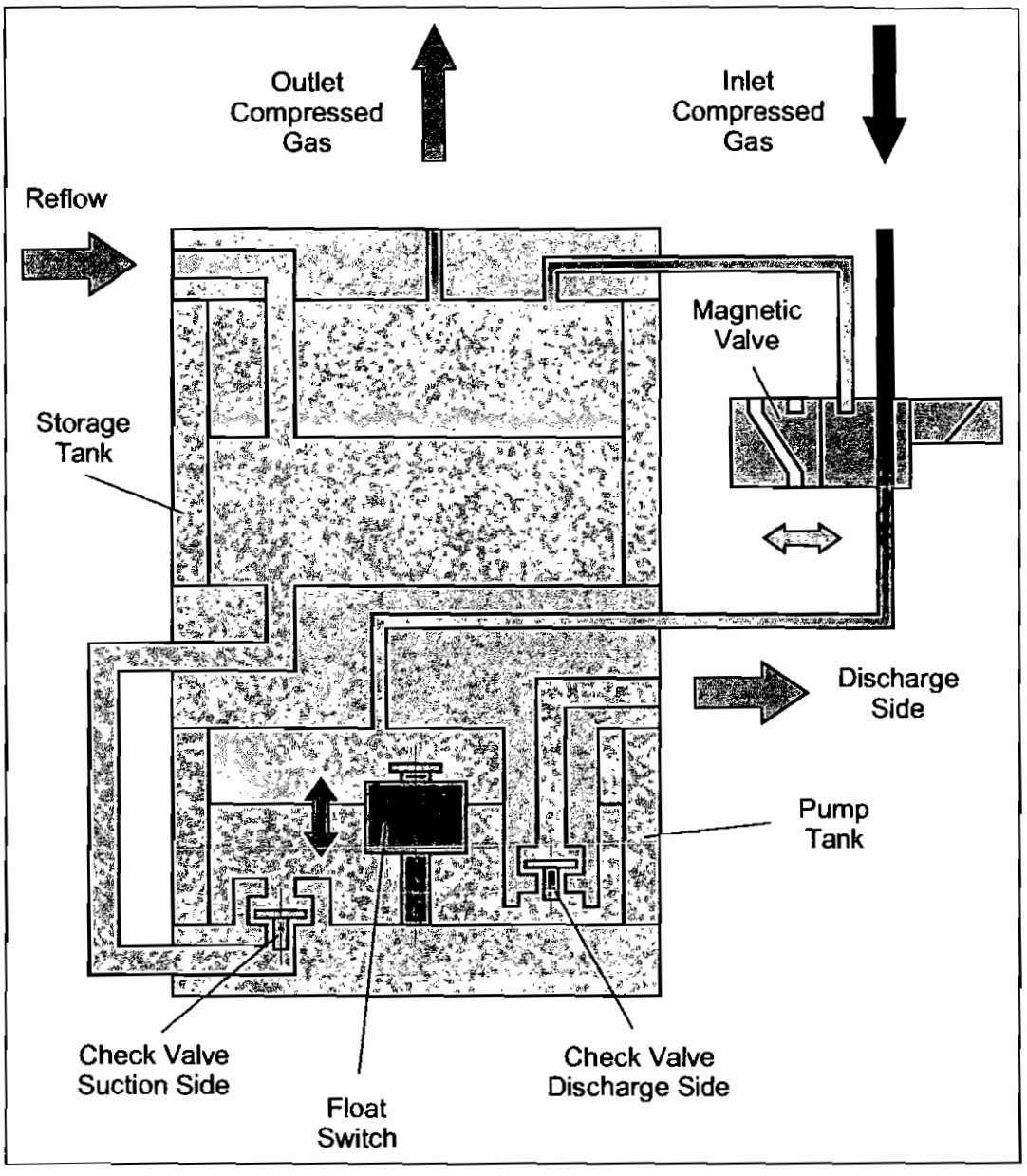

Figure 3-10: Schematic cross-section of the gas pump with separate pump and storage

The storage tank is connected to the gas inlet of the fuel cell. Hence, the gas from the pump tank can flow into the fuel cell via the storage tank. In case the cell does not consume any gas, the pumping continues until the pressure after the pressure reducer and the pressure in the storage tank are equal. In case the cell consumes gas a small difference results between the two pressures. The pressure after the pressure reducer is slightly higher than the pressure in the storage tank. This pressure difference is sufficient to pump the hydroxide solution.

When current flows through the magnetic valve, hydroxide solution flows from the storage tank into the pump tank, thus causing the fluid level to rise. In case the upper switching level is reached, the valve is toggled into the current-less state and the pump tank is again exposed to the gas pressure after the pressure reducer; the pumping cycle starts again
(see also Figure 3-10).
The specifications for the tanks are the same as for the system with two pump tanks. In addition to that, the position of the check valves is fixed. Since they have to open at low pressures they are designed in such a way that they close solely due to gravity, which means that their mounting position is determined.
The gas pump described above was tested in an electrolyser system. During electrolysis, water or water contained in the potassium hydroxide solution respectively is separated into hydrogen and oxygen. For this an electric DC current is required. The electrolysis process is the reverse process of the fuel cell process. For the function of the pump it is irrelevant whether the tests are carried out with an electrolyser or a fuel cell system.

3.1.4 System without Pump, Diffusion Processes

The gas pumps described in Section 3.1.3 work very reliably and have low energy requirements. They are, however, electromechanical systems with the possibility to fail. Even though the probability is low, the risk still exists. It was considered to find an alternative and manage completely without a pump.

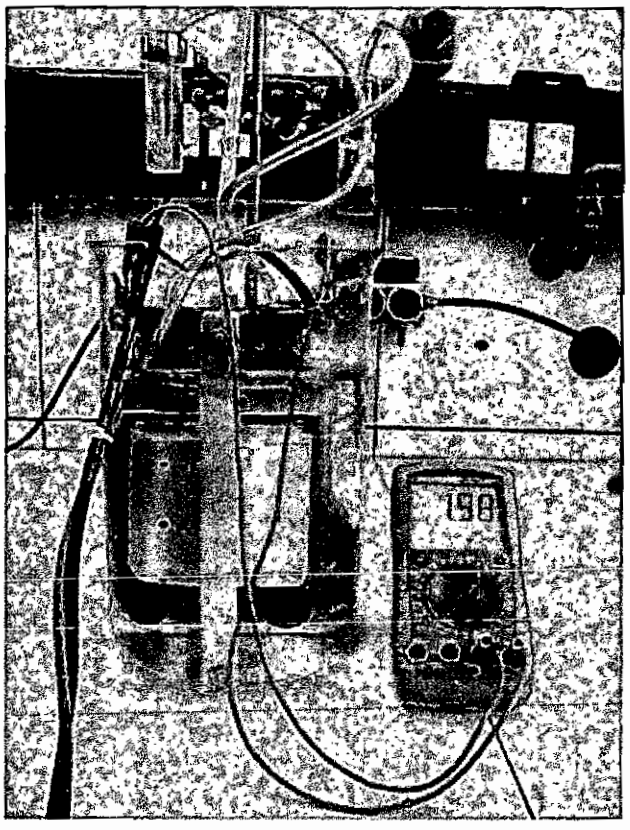

Figure 3-11: Open electrolyser

Since the mass transport in the fuel cell mainly takes place through diffusion processes it seemed reasonable to resort to diffusion processes as well for the mass transport outside the cell (see also Section 3.4).

During the operation of a fuel cell, concentration differences occur. They are found inside between the hydrogen and the oxygen electrode, but they also occur between the fuel cell and the tank.

In a system driven by diffusion the KOH circulation system would only consist of the fuel cell and the storage tank, which is connected to the fuel cell via conduits.

The distance between the fuel cell and the storage tank is to be kept as small as possible as thus promoting the mass transport. During operation, for such a system the concentration in the tank is always higher than in the fuel cell. Since the system operates completely without any electrical or mechanical components the failure probability is extremely low.

In order to further improve the mass exchange, the cell could be mounted directly inside the KOH storage tank. Openings in the fuel cell housing connecting the storage tank with the electrolyte distributor would reduce the paths to a minimum and would considerably enlarge the contact area of the hydroxide. An electrolysis system was successfully operated in that manner (see Figure 3-11).

3.2 Flow Rate and Tightness Test Stand

Before being used, each manufactured fuel cell is tested for the flow of gases and fluids as well as for its tightness. This is to ensure that from the beginning the cell will not have any supply problems with gases or potassium hydroxide, and that there are no damages at the separator and no failures in the casting. The test is carried out with compressed air and distilled water.

The test stand features a tank for the water; a pump is used to move the water. At the water side, pressure and flow rate are measured. At the air side, for the oxygen electrode and for the hydrogen electrode pressure and flow rate are measured respectively. The pressures are measured with tube spring-manometers while the water flow rate is measured by volume per time. In order to measure the flow rate of the air, a mass flow rate meter and regulator of the Manger & Wittmann company is installed in the supply conduit to the cell.

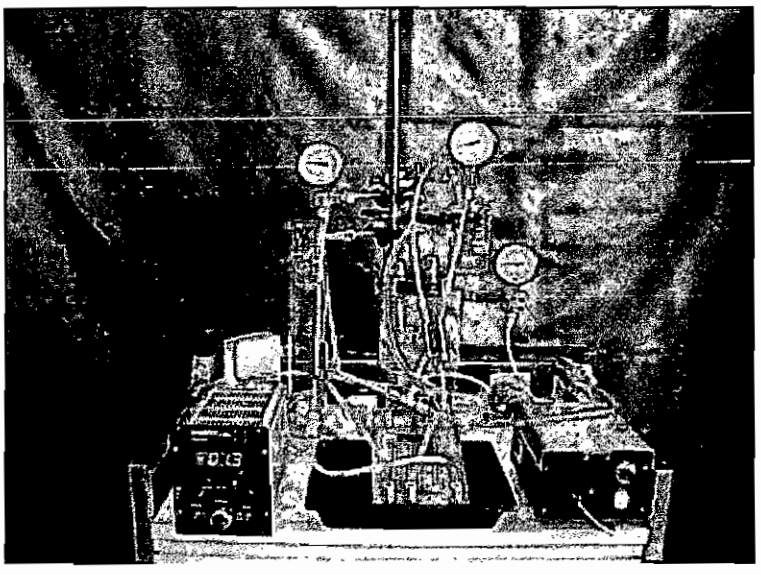

Figure 3-12: Flow rate and tightness test stand

The following values were measured:

- flow rate air in dry state
- flow rate air in wet state
- permeation (water) of the separator
- pressure loss at the electrodes
- EloFlux flow

3.3 Pressure-Dependent Flow Measurement

Mass transport processes play an important role in a fuel cell. Water and potassium hydroxide have to be transported through the electrodes and the separators. Hence, the pressure-dependent flow of water and potassium hydroxide through the electrodes and separators is a very important factor. Here, the pressure gradient is the driving force. With the use of a suitable experimental set-up the properties can be determined.

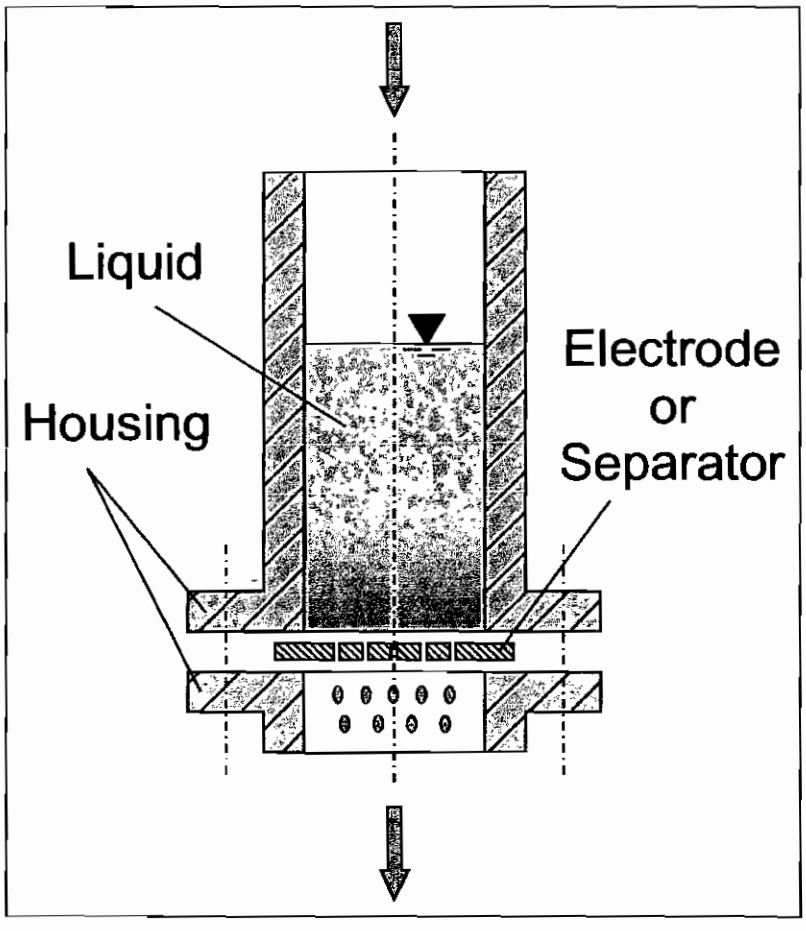

Figure 3-13: Schematic cross-section of the flow measurement device

The main part is a double-walled metal pipe (stainless steel). The space in between the two pipes can be circulated with warm water in order to heat up the test fluid. The test fluid is filled into the inner pipe. At the upper end of the pipe a connector is located for compressed air. At the lower end the probe support is located. Here, a cylinder with a diameter of 25 mm can be mounted.

The experiment starts by mounting the sample under test. Then the test fluid is filled into the inner pipe. Now the test fluid is pressurised with circa 100 mbar. The fluid flowing through the sample under test is collected in a measuring cylinder. Additionally, the time required for a certain test fluid volume to flow through the sample is measured. From this the flow rate value can be calculated; its unit is s/ml/bar/cm². The flow rate depends on the pressure, the cross-sectional area, the pore size, the number of pores and the viscosity of the test fluid. Furthermore, the wetting properties of the sample under test are important. The test fluids used were potassium hydroxide solution, water and octane.

The first measurements taken for the separators could hardly be reproduced. This had various reasons. One of them was that the seal for mounting the samples caused problems. Initially, an elastic O-ring of EPDM was inserted into the device, which was inserted between the gland nut and the sample. There was no seal used in between the sample and the thread. In this variant, the O-ring can be displaced from its position when fastening the gland nut, so it cannot seal reliably any more. The rotational movement of the gland nut caused damage to the test samples or deformed it. Furthermore, the tightness between the sample and the thread was not guaranteed. Leakages at these locations introduce errors into the measurements. Since the fluid volumes are very small even small leakages lead to significant measurement errors.

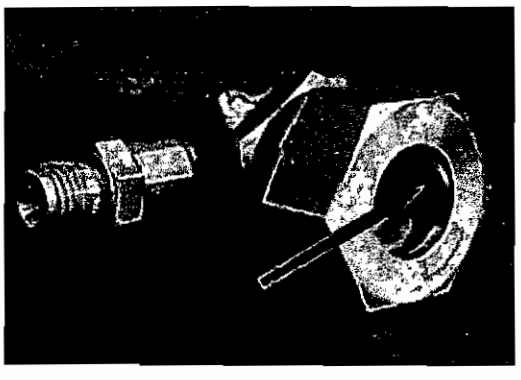

Figure 3-14: Faulty O-ring seal

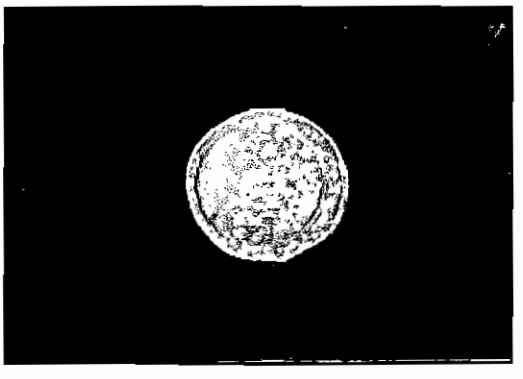

Figure 3-15: Deformations of the sample

The O-ring seal was replaced with a flat gasket made of EPDM. Thus it could be achieve that the gasket was held in its position. The deformation problem has to be

seen in the context of the turning movement, the elastic seal and the good friction properties of EPDM on metal and the sample respectively. Before the gasket is pressed sufficiently strongly against the sample the gasket is initially deformed. Here, the gland nut has to be turned further, causing deformations of the sample. The elastic EPDM seal rings were replaced with plastic seal rings. Compared to EPDM they are not elastic and exhibit a lower friction so that the above mentioned effects do not occur any more. The mounting of the sample is now done between two plastic rings. After implementing these modifications the functionality of the set-up was tested. For this, a porous plastic foil of polyethersulfone (PESU) was used as sample. The pore radius was 0.1 µm. Three times consecutively 20 ml distilled water were pressed through the probe at a detected pressure of 100 mbar. For each repetition, the flow times became longer from circa 7 min to 14 and finally to over 20 min. After the sample was taken out of the device contaminations could be seen on the sample, probably blocking the pores successively. A contamination of the water could be excluded as a cause. To investigate this, a different sample support of PESU was used. However, contaminations could not be detected. Further examinations of the storage tank showed that the stainless steel exhibited abrasion, presumably especially in the area of the welding seams.

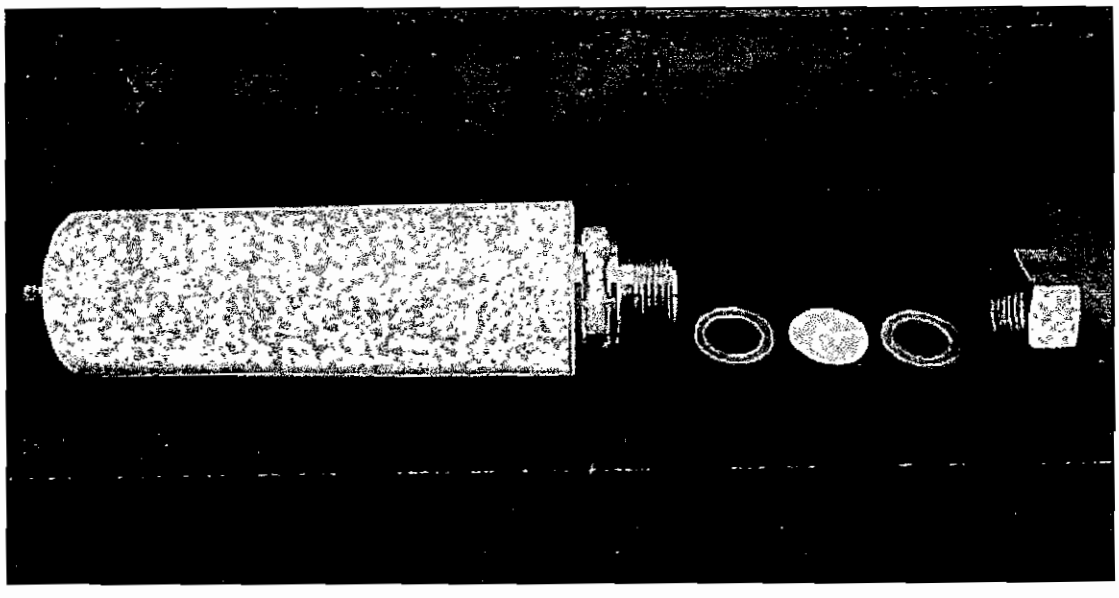

Figure 3-16: Flow rate measurement device of polypropylene for water, not heated

The device was partly used in change with water, KOH and octane, which can lead to increased abrasion. This led to the decision to manufacture such a device from polypropylene. The threaded part was still manufactured from stainless steel. This should not present a problem since no welding seam is needed and for each of the three fluids a dedicated set-up was manufactured. The initial measurements with the above described probe made from PESU produced satisfactory results. The flow times were between 6:50 and 7:08 minutes.

After the functionality of this set-up had been confirmed another set-up was made. The latter featured the possibility to heat up the fluid in order to be able to take measurements at the same temperatures as they occur inside the fuel cell.

3.4 Diffusion-Dependent Mass Transport

Next to the mass transport through a pressure-dependent flow there is also a mass transport through diffusion. Here, the concentration gradient is the driving force for the transport. Diffusion processes are temperature-dependent; with decreasing temperature the diffusion slows down.

The main part of the experimental set-up is made of three Perspex parts. It can hold cylindrical parts with a diameter of 40 mm. Both sides of the device hold a chamber that can be filled with fluids. Changes in the fluid volumes can be caught with one conduit per chamber. Electrodes as well as separators can be tested. In order to achieve a more accurate measurement of the change of volume the individual chambers were connected to measurement pipettes. This permitted to accurately read the fluid level. The temporal progression was recorded with a stopwatch. The height difference between the upper and the lower level of the pipette was limited to circa 1 cm in order to minimise the influence of gravitational pressure as much as possible. During the measurements various smaller problems of the set-up became apparent, which complicated carrying out the experiments. These problems are elaborated in the following and solutions to the problems are shown as well.

The experimental set-up is in principle well suited for the diffusion measurements. Merely the handling of the set-up and the carrying out of the experiments had potential for improvements.

Caused by the position of the fluid inlet and the outlet towards the measurement pipette air bubbles are formed in the fluid chambers when the cell is being filled. These air bubbles are very difficult to eliminate. They influence the fluid volume thus introducing errors into the analysis of the results.

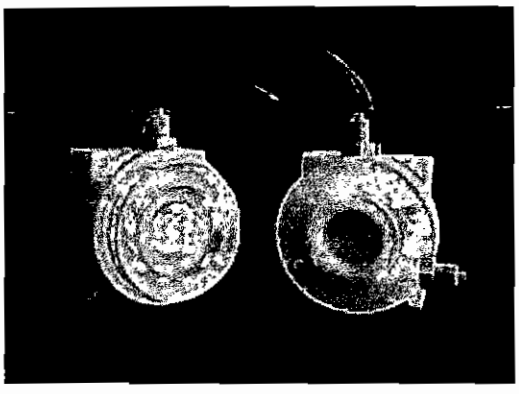

Fig. 3-17: PTFE measuring cell with heating

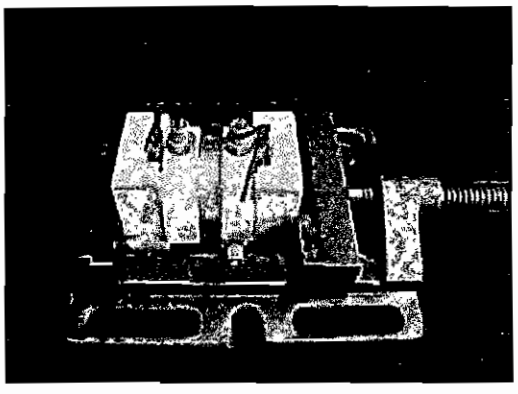

Fig. 3-18: Measuring cell in a vice

Furthermore, the two fluid compartments are different in size. This can be taken into consideration for the calculations, but it could also cause measurement errors due to mix-ups.

Another disadvantage of this set-up are the screw joints of the housing. The sample is placed between two EPDM seal rings. By means of four screws the two housing halves are pressed against each other with the samples and the seals placed in between. In order to evenly distribute the pressure across the seal face the four screws would have to be tightened with equal force. This requires some effort and thus makes the handling difficult.

Another problem is the material for the housing, i.e. Perspex. In the long run it is not persistent against potassium hydroxide, especially if hydroxide and water are filled in alternately. Furthermore, the absorption and emission of hydroxide and water could falsify the concentration measurement.

The diffusive mass transport is also temperature dependent and the fuel cell is usually operated at c. 50 to 60 °C. Since the measurements of the test cell can only be carried out at room temperature a heating should be provided.

The above mentioned disadvantages of the hitherto used measurement set-up led to the construction of a new measurement set-up.

The problem of air bubble inclusion was solved by a suitable choice of the position of the inlet and outlet borings. Potentially developing air bubbles are now flushed out through the exit during the filling process.

The fluid chambers were manufactured in such a way that they have the same dimensions. The two housing halves are now pressed together in a vice which makes the handling significantly easier. The material chosen for the housing was polytetrafluoroethylene (PTFE) which has the advantage that it does not interact with the measurement fluids. For the heating of the test cell electric heating elements (PTC elements) were used.

Concluding it can be noted, that measurement pipettes with a volume of 5 cm^3 are best suited for the presently used samples (materials). This volume is usually sufficient. For probes causing only a minor change of volume, occasionally pipettes with a volume of 1 cm^3 were also used which can be read more easily. However, this has the disadvantage that the overall volume is changed. Hence, the measurement time (standard 50 minutes) should preferably be modified. This can be taken into consideration more easily in the interpretation.

3.5 Half Cell Measurement Set-Up

Half cell measurements are to measure the characteristics of the gas diffusion electrodes. Hereby, the capacity of the electrodes can be tested individually. The probes have a diameter of 39 mm. The advantage of this set-up is that the electrochemical properties of the electrodes can be tested initially without the necessity to build a full cell, thus saving time and costs.

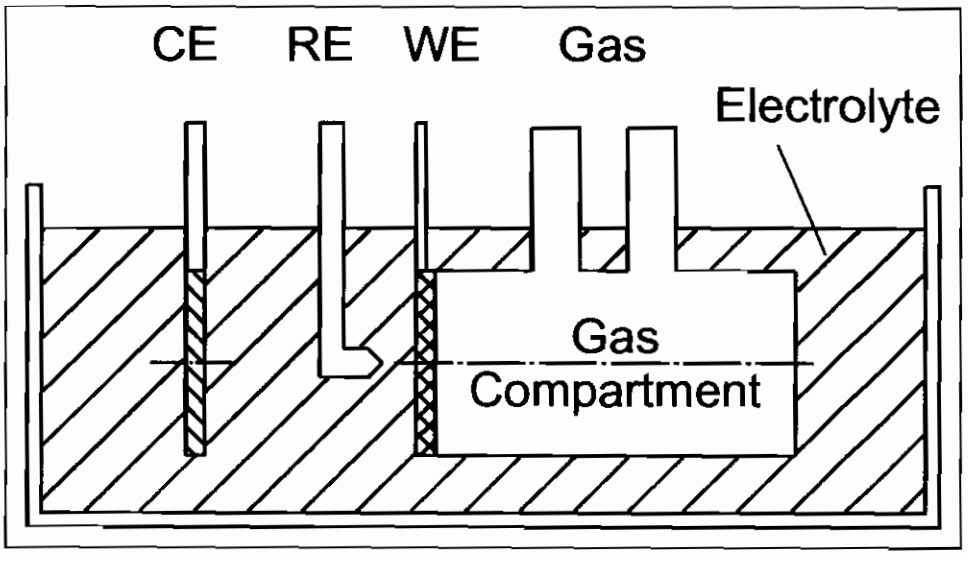

Figure 3-19: Schematic construction of a half cell

The measurement set-up is suitable for electrodes used in fuel cells, as well as for electrodes used in electrolysers. This means, that the electrodes are operated consuming gas or producing gas, provided their electrochemical properties permit this.

Figure 3-19 schematically shows the construction of a half cell. The reference electrode (RE) is placed in between the counter electrode (CE) and the working electrode (WE). Working electrode is the name for the electrode under test; it is placed next to the gas compartment.

Since only the results of the half cell measurements are relevant for this research a detailed elaboration of the tests is omitted here.

3.6 Gas Permeability (Permeation)

For the operation of a fuel cell the proper supply with the reaction gases is of great importance. For the gases to be able to react at the electrode they have to reach the triple phase boundary. The gas permeability as a quantity allows to compare different electrodes and to have an influence on this property during the manufacturing process.

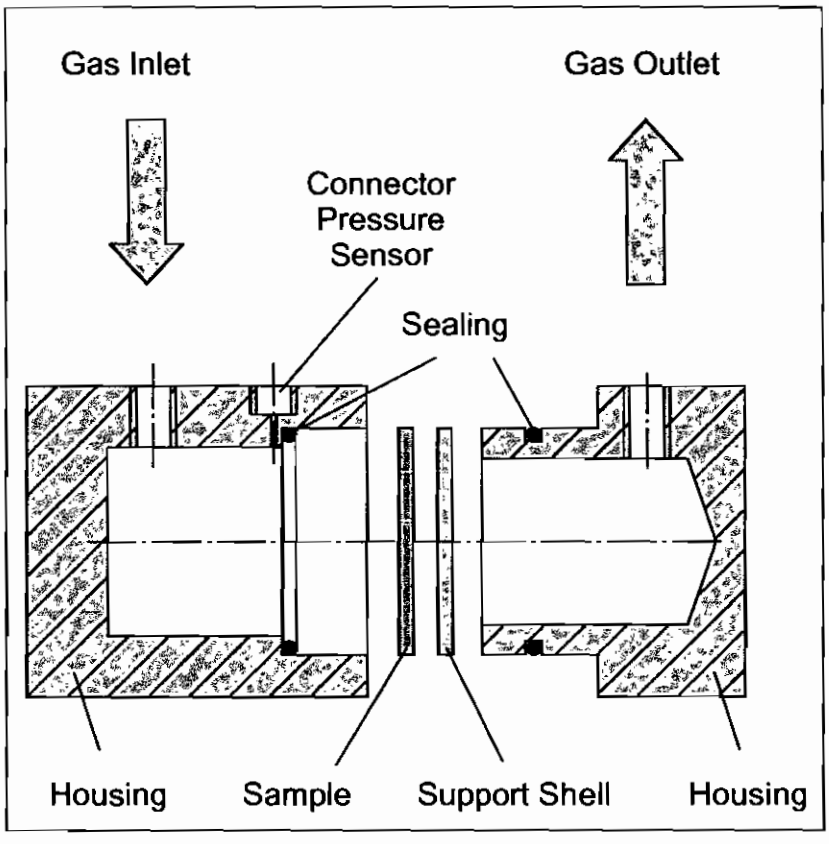

Figure 3-20: Construction for gas flow rate measurement

Figure 3-20 shows the experimental set-up for the gas permeability measurement. Samples with a diameter of circa 39 mm can be mounted into the set-up. If necessary (i.e. if the mechanical stability is too low) a support shell can be mounted additionally with the sample. The gas under test then flows from the gas inlet into the housing, permeates the sample and, if present, the support shell and then leaves the housing via the gas outlet. Before the gas inlet the gas flow rate is measured.

Immediately before the sample the gas pressure is recorded. At the gas outlet the gas is discharged against the ambient pressure. The seal rings prevent leakages and make certain that no gas can flow around the sample.

After inserting the sample and the support shell into the two housing halves the latter are mounted against each other under pressure in a vice.

The measured values for the flow rate and the pressure are recorded with a PC. The latter then calculates the characteristic gas permeation (GP) value as a function of the pressure (p), the area (A) and the gas flow ($\dot{V}$).

$$GP = \frac{\dot{V}}{p \cdot A} = \frac{l}{bar \cdot cm^2 \cdot \min} \qquad \textbf{(Eq.: 3-2)}$$

3.7 Concentration Sensor for KOH, Densoflex

For a continuous measurement of the potassium hydroxide concentration of a fuel cell in operation the concentration sensor Densoflex is used. The sensor was originally developed to measure the acid concentration in lead-acid batteries. Since the sensor does not measure the acid portion of the solution but the water portion, it can as well be used with potassium hydroxide.

The measurement probe is a plastic thread which experiences an elongation in the aqueous potassium hydrate solution. The elongation is stronger the weaker the concentration of the potassium hydrate solution. The plastic thread is fixed at the lower end of a ceramic dip pipe and is put under tension via a strain-gauge in the sensor housing. An electric displacement sensor inside the housing measures the elongation and converts it into an electric signal. Since the elongation is directly proportional to the hydroxide density the output signal corresponds to the hydroxide concentration in the electrolyte distributors of the fuel cell.

The length of the measurement probe is not only changed with the hydroxide density but also with the temperature. Therefore, a temperature sensor is included in the ceramic pipe. An electronic circuit corrects the electric output signal accordingly. Consequently, the Densoflex sensor provides the possibility to continuously determine the density of the hydroxide solution and hence the concentration of the potassium hydroxide, with a temperature compensation.

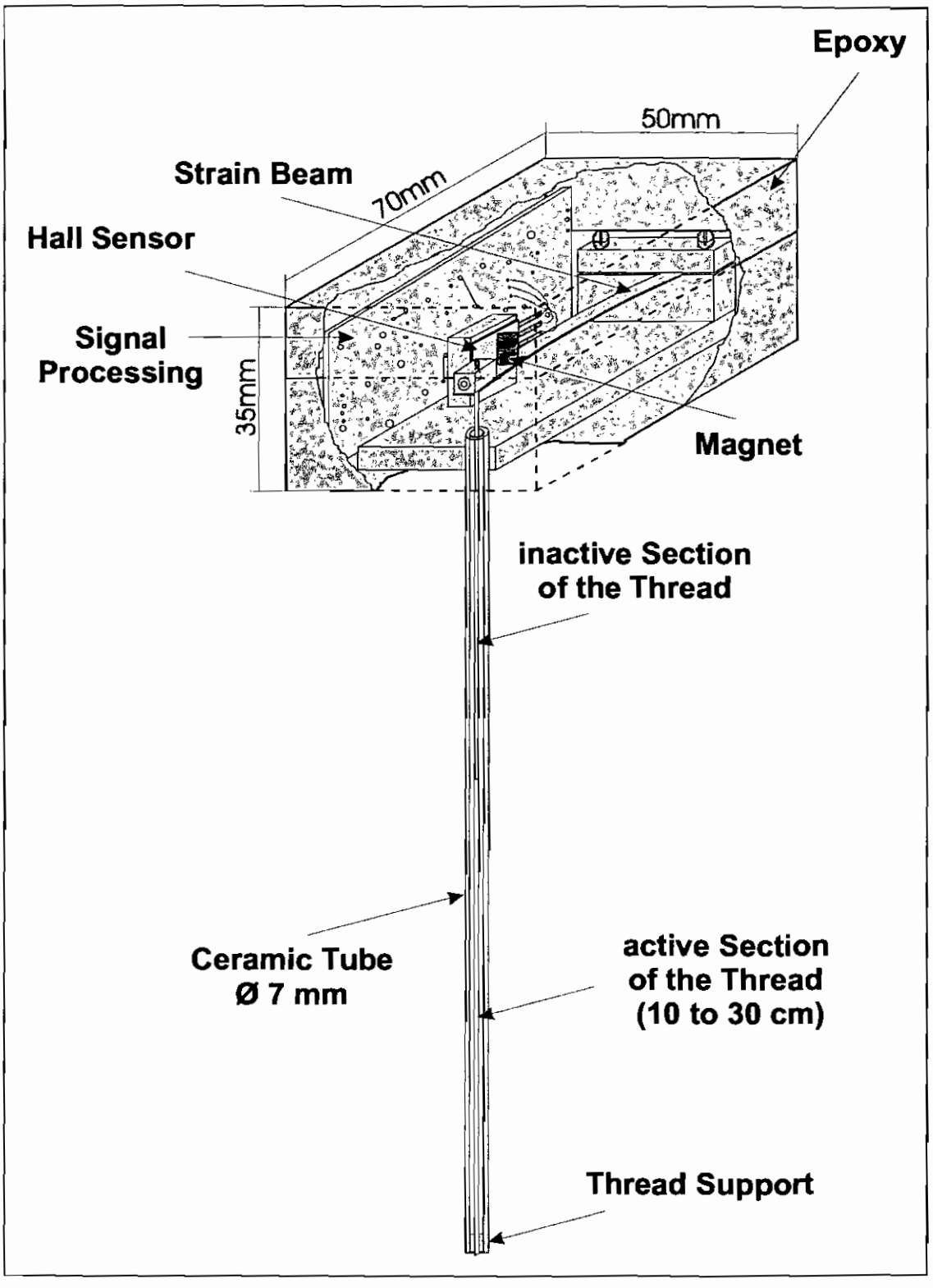

Figure 3-21: Schematic construction of a concentration sensor Densoflex

3.8 Low Temperature Tests with Diffusion

This section describes the test stand where the diffusion tests were conducted at 5 °C. Firstly, the mass flows and the utilised instruments are illustrated. Furthermore, some special parts of the test stand are described.

3.8.1 Mass Flows of the Test Stand

The test stand to carry out experiments with regards to deep sea applications is different to the standard test stand. Two tanks, two condensate traps, two needle valves, two manometers, two heat exchange plates and one fuel cell were used. In order to load the cell an electronic load is required, which converts the electric energy of the fuel cell into heat.

In order to control the cell temperature an electrically operated thermostat is used. Two heat exchange plates are mounted to the fuel cell. The heat transfer fluid of the thermostat flows through the heat exchange plates. The fluid subsequently flows back to the thermostat.

The reaction gases are supplied from gas cylinders or an electrolyser. The hydrogen gas is conducted into the fuel cell via a purification stage. In the purification stage the remaining oxygen in the hydrogen reacts with the hydrogen to form water (purification stage only for electrolytically produced hydrogen). Connected to the hydrogen outlet of the cell are a manometer as well as a condensate trap and a needle valve.

The oxygen gas is directly conducted into the cell. A manometer, a condensate trap and a needle valve are also connected to the outlet.

The KOH supply could be provided using two different methods. For the first method, only the two electrolyte compartments were filled with hydroxide solution. The hydrogen electrode as well as the oxygen electrode have their own electrolyte compartment. Two ball valves are connected to the KOH inlets of the cell (at the bottom), via which the cell can be filled. Conduits are connected to the KOH outlets (at the top) to conduct the reaction water from the respective electrode.

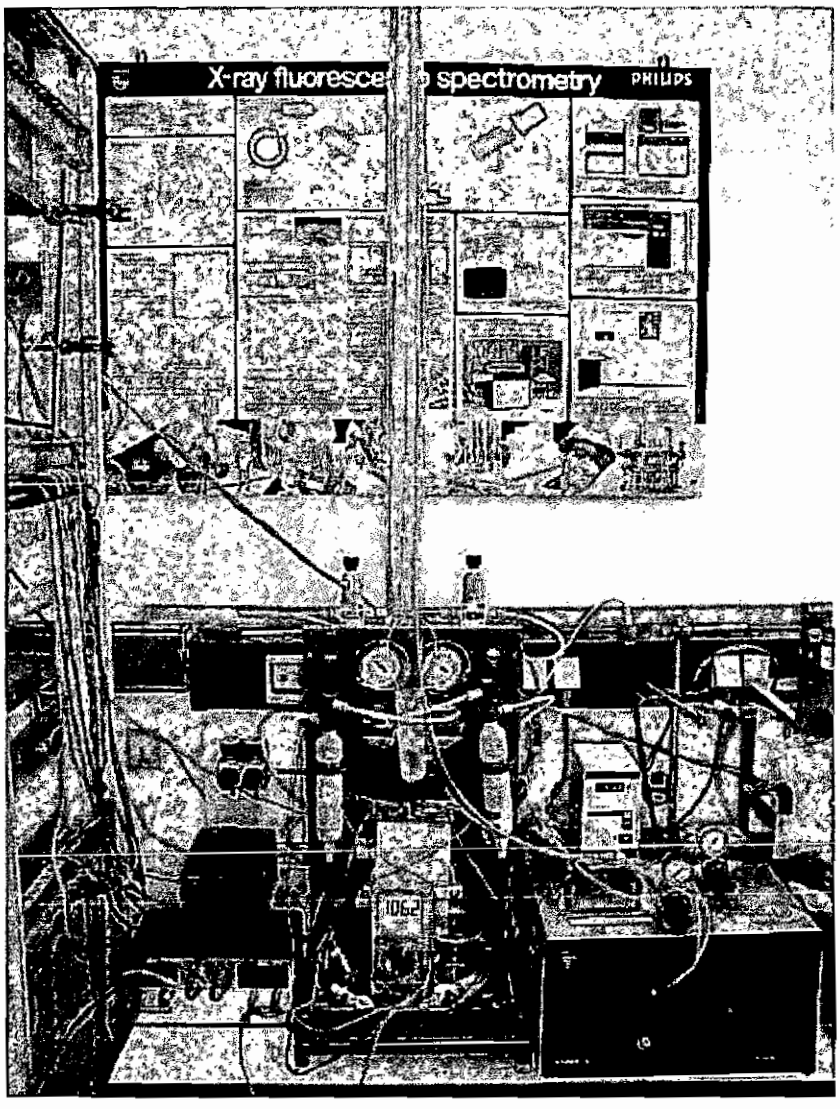

Fig. 3-22: Test stand: experiments at circa 5 °C; left: load; middle: AFC; right: thermostat

The second possibility was to connect both lower KOH sockets to a reservoir filled with KOH. The upper KOH sockets were connected to a catch tank for the reaction water.

Various parameters were recorded, which were the load current, the cell voltage, the gas pressures for hydrogen and oxygen and the cell temperature.

The acquisition of voltage, current and temperature was computer aided. A multimeter from Keithley and an electronic load from Höcherl & Hackl were connected to the computer via an IEEE-bus. The current could be adjusted by software. The measured values were represented in a table and a diagram. The pressures were displayed on tube spring-manometers.

3.8.2 Plastic Tanks

In order to operate an AFC for an extended period of time a certain supply of KOH is required, because the electrolyte is diluted by the reaction water. The size of the storage tank is determined by the operating time, the current extent, the number of cells and the acceptable hydroxide concentration.

The tank consists of a plastic pipe with seal rings, a lid and a bottom. The parts are held together by a threaded rod and two lathed parts with inside threads and integrated seals. The plastic pipe has an inner diameter of circa 80 mm and an outer diameter of 110 mm and consists of fibre-reinforced polypropylene. The two lids have a diameter of also 110 mm and a thickness of 20 mm. The lids also consist of polypropylene and they carry the conduit connection as well. Polypropylene was chosen, because it is resistant to potassium hydroxide. The threaded parts are lathed from stainless steel. They carry the seals and the threads (M6). The threaded rod is also made from stainless steel.

Additionally, condensate traps (EM-Technik company, Germany) are used before the needle valve. They protect the needle valves from fluid, which prevents a malfunctioning of the valves. The tanks consist of polypropylene and are welded. Their volume is circa 0.1 dm^3.

The tanks are to collect the condensate. The actual separator is lathed from plastic and a special feed-through enables the separation of the fluid. The fluid drops fall into the tank due to gravity.

3.8.3 Valves

For longer test durations, it is from time to time required to discharge inert gases. This is achieved with the aid of needle valves at the hydrogen and oxygen outlets of the cell.

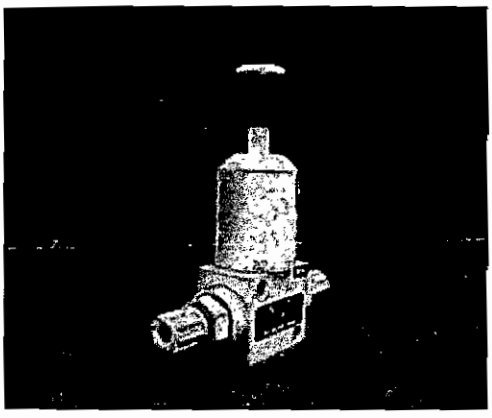

Figure 3-23: Needle valve (PP)

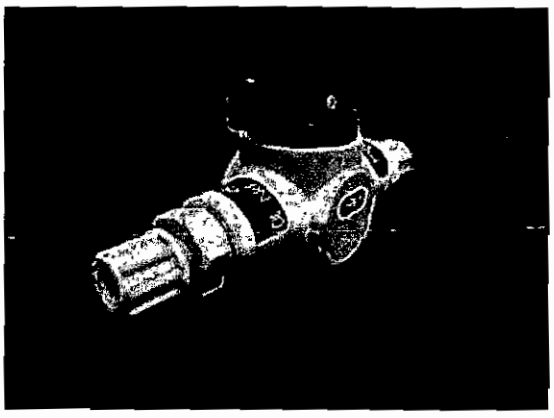

Figure 3-24: Ball valve (PP)

An even gas flow through the cell is adjusted easily. It is useful to insert a fluid separator before the valves since small fluid drops carried along in the gas flow could block the small diameters of the valve thus preventing the gas flow. The valves also consist of polypropylene.

Furthermore, ball valves made of polypropylene were used. They make it possible to quickly open and close ducts.

3.8.4 Screw Joints and Conduits

In order to conduct gases and fluids and to connect the individual parts, fittings consisting of PA and PP are used (EM-Technik). The fittings are available in many different variations. The conduits can be mounted by hand. They are inexpensive and can withstand potassium hydroxide. The PA screw joints can be used at a temperature range of –20 °C to +60 °C, while the PP screw joints can be used between +5 °C and +90 °C.

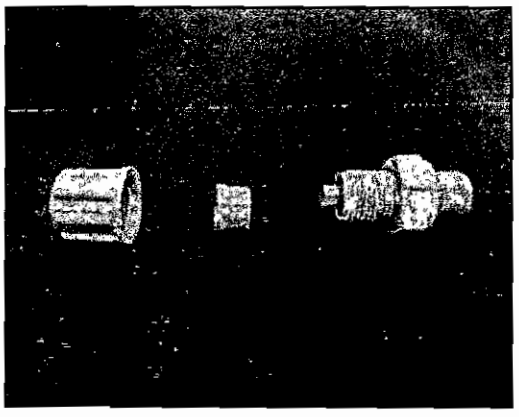

Figure 3-25: Clamping ring screw joint (PP)

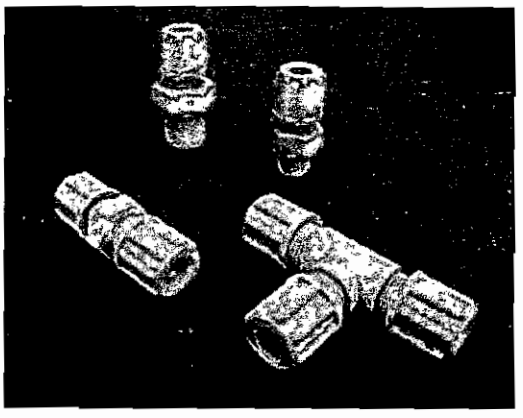

Fig. 3-26: Various fittings (PP)

The conduits consist of transparent PVC or coloured PA. Over time, PVC is not resistant to KOH; it changes its colour to brown and also hardens. The advantage of these conduits is in their high flexibility also providing for the realisation of small bending radiuses. Conduits with the dimensions 6x4 and 8x6 mm were used.

3.8.5 Framework and Cell Support

The fuel cell and the individual components were mounted to a framework of stainless steel. The framework was fitted with a PVC drip pan.

The fuel cell was mounted under pressure with two threaded bolts and two yokes. Within the pressure mounting two heat exchanger plates made of PP were integrated, which could be circulated with fluid to condition the cell temperature.

3.8.6 Electronic Load

The fuel cell can only be tested when current is draw from it, i.e. if the cell is loaded. For this two different loads were used. One of them was a type DS4806 by the company Höcherl & Hackl. A disadvantage of this load is that the current can only be adjusted in steps of 1 A. Furthermore, a minimum cell voltage of 450 mV is required under which the load does not operate.

In order to also be able to adjust the load current in steps of 0.1 A another electronic load was used which was developed and built by FH Darmstadt, Germany.

3.9 Experiments on the Mass Transport in the AFC

In order to obtain further information on the mass transport in the fuel cell the concentrations in both electrolyte distributors were measured. The set-up of the test stand was essentially identical to the set-up described in Section 3.7. Only the KOH reservoirs were removed, since the duration of the experiment was very short.

Furthermore, a modified fuel cell had to be build for this experiment. The end plates needed to be modified in order to integrate the concentration sensor. A Perspex pipe was cast into the end plate. The Perspex pipe had ten small holes through which it was connected with the electrolyte distributor. The concentration sensor could be inserted into the Perspex pipe.

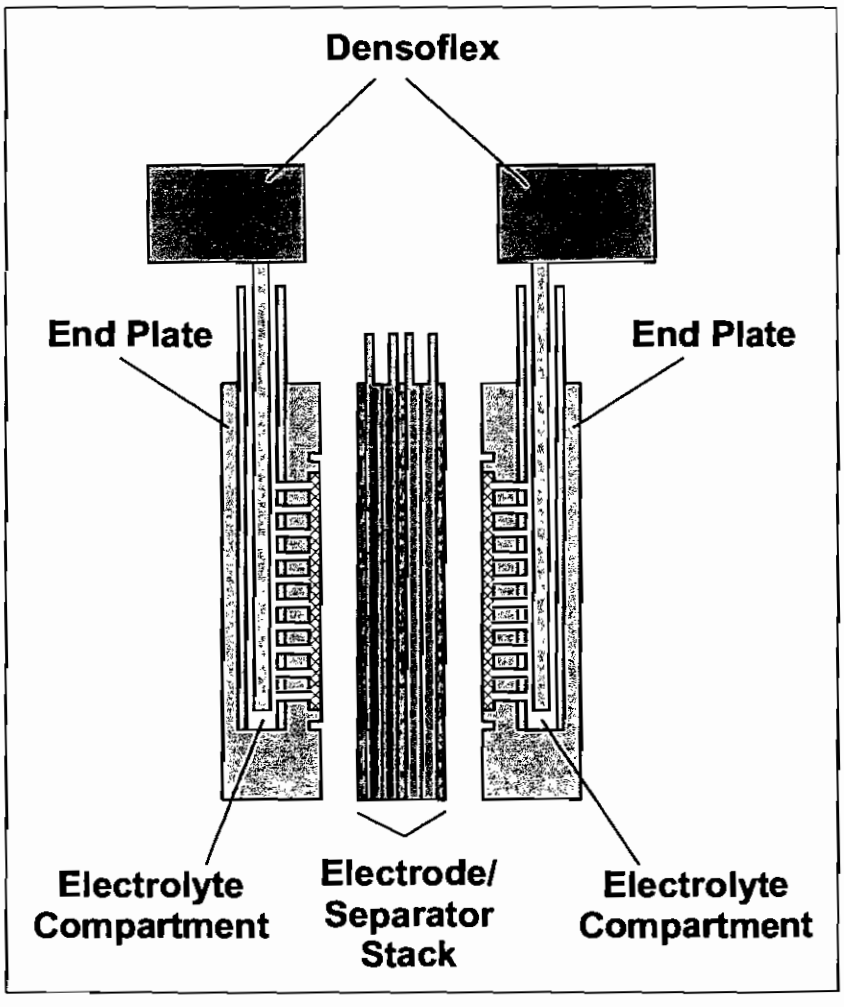

Figure 3-27: Schematic construction: fuel cell with integrated concentration sensor

4 Experiment Results

In this chapter the results of the experiments are presented. Firstly, the results of the electrode characterisation experiments are discussed.
In detail these are:

- experiments on diffusion behaviour
- determination of the density and area density
- experiments on gas permeation
- experiments on pressure-dependent flow rate measurement
- experiments on the bubble point
- absorption of liquids

Then the results of the fuel cell experiments are elaborated in detail. Here, a special focus is put on the experiments on diffusion and matter transport in the fuel cell.

4.1 Tests on Electrodes and Separators

Before electrodes and separators are used in a fuel cell they are tested and the characteristic features of the electrode and the separators respectively are measured. In the following the results of the tests are explained in more detail.

Table 4-1 below presents a list of the electrodes used in fuel cells. Electrodes #130 and #314 were used on the hydrogen side and consist of Raney nickel. Electrodes #249, #366 and Oxag were used on the oxygen side. The Oxag electrode is made from silver oxide. Before the electrode can be used in the fuel cell the silver oxide has to be reduced to silver. The material used for the other two oxygen electrodes was Silflon which consists of silver and does not need to be reduced.

Electrode	#314	#130	#366	#249	Oxag
Catalyst	90 % Nickel	90 % Nickel	85 % Silflon	100 % Silflon	90 % Ag2O
PTFE	7 %	7 %	in catalyst	in catalyst	5 %
Activated carbon	-	-	10 %	-	5 %
Graphite	3 %	3 %	5 %	-	-
Pore builder	-	-	-	80 %	-

Table 4-1: Composition of the used electrodes

The nickel catalyst used is Raney nickel. The Silflon catalyst consists of a mixture of silver and PTFE. Electrode #249 was the only one which was manufactured using a pore builder.

4.1.1 Diffusion Experiments

The charge transport inside an AFC is effected by OH^--ions. At the same time water is produced as well as consumed (see also Section 2.4.3). In order to maintain the power delivery of an AFC the internal matter transport has to be provided for. The matter circulation of OH^-, K^+ and H_2O is influenced by the components (electrodes, separators).

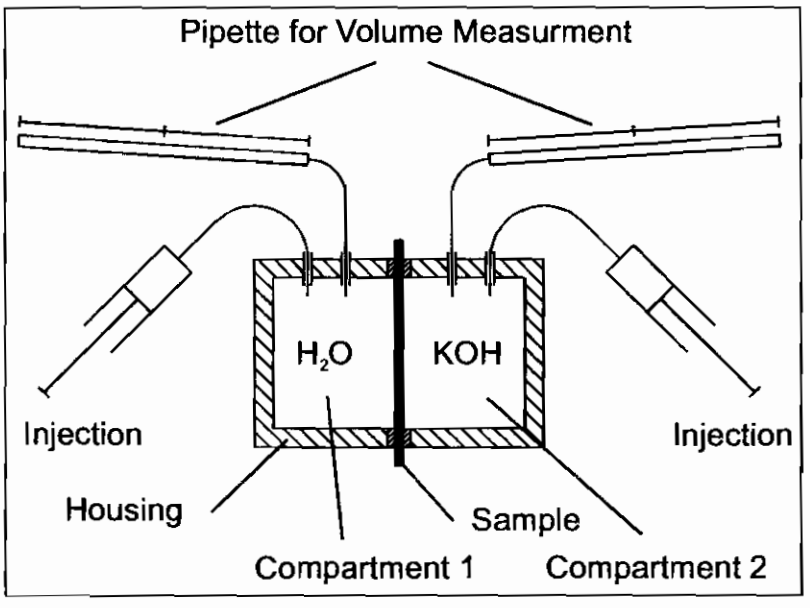

Figure 4-1: Test cell for diffusion measurement

A concentration gradient is the driving force for a matter transport by diffusion. As will be explained further down at least the water transport takes place mainly by diffusion.

The KOH transport is only partially effected by diffusion. As will become clear later in particular the transport of OH^-- and K^+-ions has to be caused by the electric field. The diffusive matter transport would not suffice to enable the high load currents. The water is in most part uneffected by the electric field. A water transport due to the electric field is not possible since a water molecule is not electrically charged. In order to investigate the water transport tests were carried out to test the diffusion behaviour of the electrodes and separators individually.

The test cell (see Figure 4-1) used for the experiments consists of two chambers separated by the component under test. At the beginning of the experiment one compartment (also called compartment 1 in the following) contains distilled water. The other chamber (also called compartment 2 in the following) contains 7.0 M KOH. The fluid levels were measured in appropriate intervals. At the end of the experiment the KOH concentrations were measured additionally.

Theoretical considerations lead to the conclusion that there are five possibilities in which the transport behaviour of a component can be explained. These possibilities are elaborated in the following.

The following figures show a schematic representation of the test cell. Compartment 2 is on the left hand side and is initially filled with 7.0 M KOH. The dashed line represents the device or sample to be tested. Compartment 1 is on the right hand side and initially contains distilled water. At the origin of the arrow the substance is denoted which is being transported in the direction of the arrow.

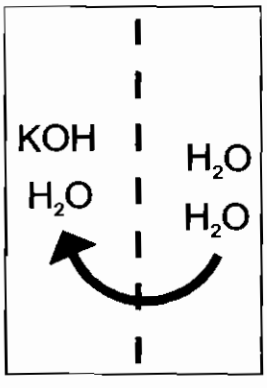

Figure 4-2: Water is transported exclusively from compartment 1 to compartment 2.

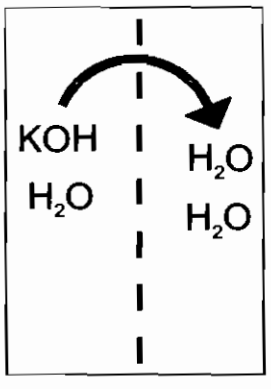

Figure 4-3: KOH moves exclusively from compartment 2 to compartment 1.

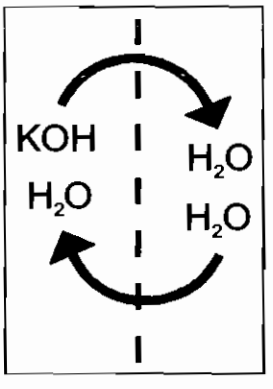

Figure 4-4: KOH from compartment 1 is moved to compartment 2 and water moves from compartment 1 to compartment 2.

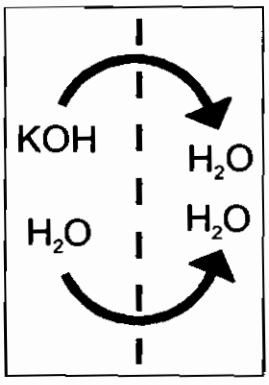

Figure 4-5: KOH and water move from compartment 2 to compartment 1.

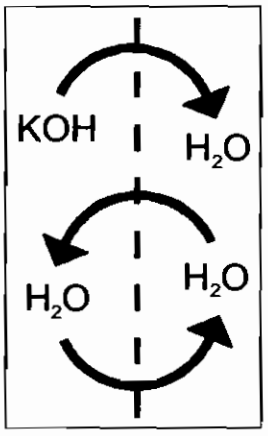

Figure 4-6: KOH and water move from compartment 2 to compartment 1. At the same time water moves from compartment 1 to compartment 2.

The potassium hydroxide solution consists of a mixture of KOH and water. The K^+-ions and the OH^--ions are enclosed in a hydrate shell.

Figure 4-2 shows the situation when only water moves from compartment 1 to compartment 2. In Figure 4-3 only the K^+- and OH^--ions would move to the other side, without their hydrate shell. In Figure 4-5 the ions would migrate with their hydrate shells. Since a hydrate shell consists of several water molecules it is possible that only a part of it is taken along while the rest remains behind.

In Figure 4-6 KOH as well as water is transported from compartment 2 to compartment 1. At the same time water is transported from compartment 1 to compartment 2. However, this cannot be illustrated with the experimental set-up as described above. Only the net amount of the transported water can be determined.

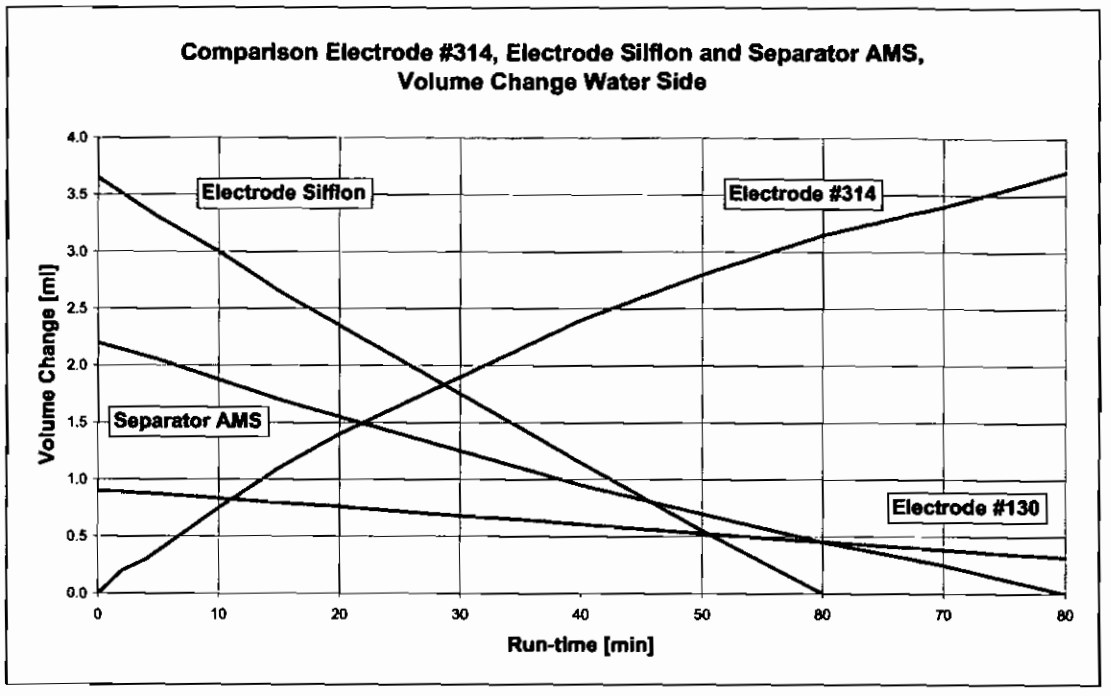

Diagram 4-1: Comparison of the volume change at the water side

Diagram 4-1 shows the temporal progression of the volume changes in ml in compartment 1 for electrode #314, electrode #130, the Silflon electrode and the separator AMS. The volume measurements alone do not allow to make detailed statements about the matter transport. This is only possible when also considering the concentration values, which is elaborated later. The volume measurements allow, however, an estimation of the tendencies.

It is noteworthy that the volume in compartment 1 increases for electrode #314. This indicates that water does not move towards the KOH, but KOH moves towards the water.

Contrary to this, the behaviour of the Silflon electrode and the separator AMS was different. Here, more or less water moved towards the KOH.

The experiments were carried out with all samples for a minimum of three times. Even though quantitative deviations of the magnitudes were detected, the basic qualitative behaviour was the same.

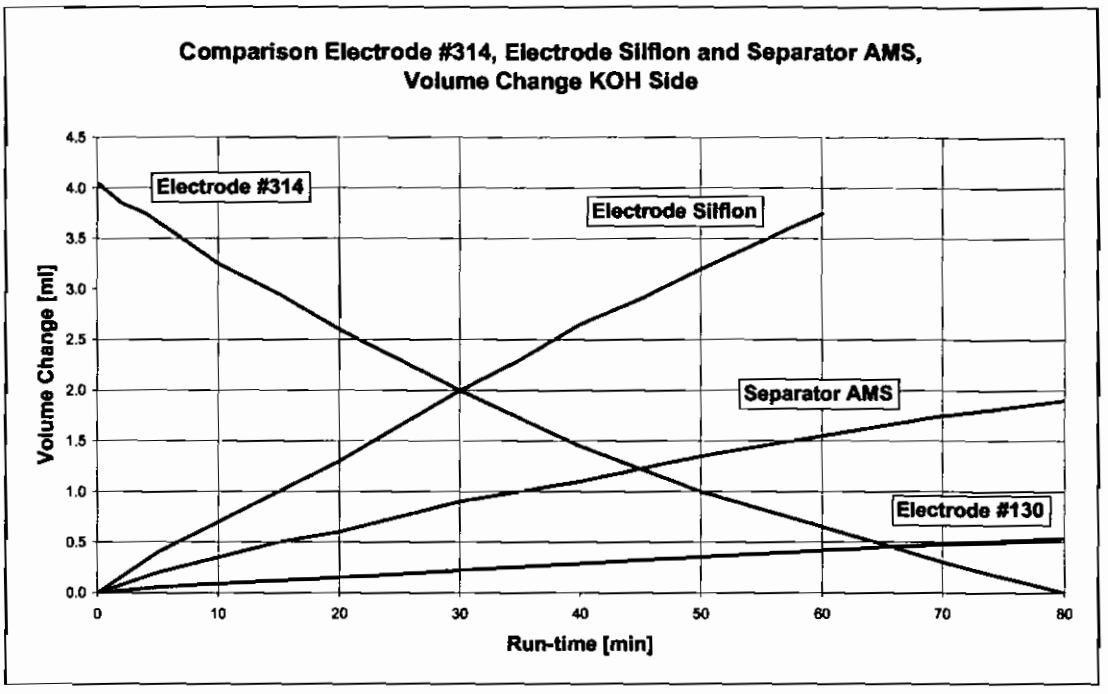

Diagram 4-2: Comparison of the volume change at the KOH side

Diagram 4-2 shows the temporal progression of the volume change in ml in compartment 2 for electrode #314, electrode #130, the Silflon electrode and the separator AMS. Here, the behaviour is similar to the one on the water side, only the other way around. While the volume increases continuously for electrode #130, the Silflon electrode and the separator AMS the volume decreases for electrode #314.

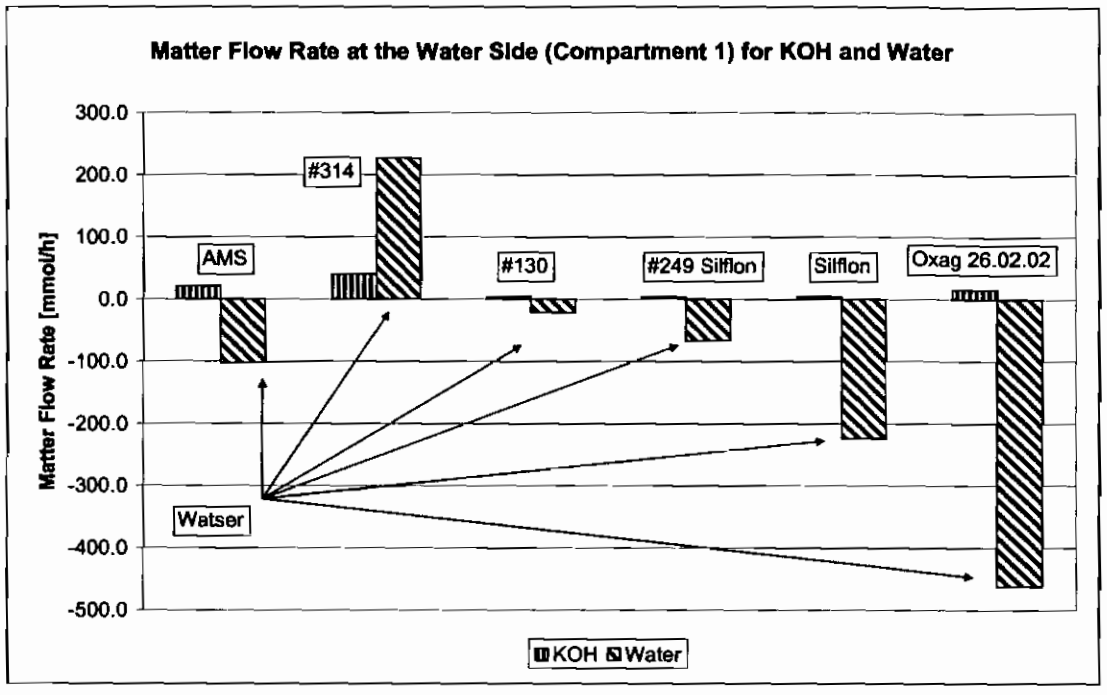

Diagram 4-3: Matter flow rate at the water side (compartment 1) for KOH and water

Diagram 4-3 shows the matter flow rate in mmol/h for KOH and water for compartment 1 for the experimental set-up. The results of the concentration measurement at the end of each experiment are included. From this the number of particles and the particle flow respectively can be calculated. A positive sign indicates matter moving into compartment 1 while a negative sign indicates matter leaving compartment 1.

Similar to the above diagrams it stands out that electrode #314 behaves differently for water transport than the other electrodes and separators. KOH and water move from compartment 1 to compartment 2. This corresponds to a matter transport behaviour as presented in Figure 4-5.

For the other electrodes KOH moves with or without water into compartment 1 and water moves from compartment 1 into compartment 2. The amount of transported water is significantly larger than the amount of KOH. This behaviour would correspond to Figure 4-4 and 4-6 respectively.

The measured values for compartment 2 can be compared to the ones from compartment 1 with inverted signs. Matter leaving compartment 1 has to arrive in compartment 2 and vice versa.

			V_S	V_E	c_S (KOH)	c_E (KOH)	Δn (KOH)	Δn (H_2O)
			[ml]	[ml]	[M]	[M]	[mmol/h]	[mmol/h]
AMS	C2	KOH	21.0	22.9	7.000	5.081	-23	104
	C1	H_2O	27.0	24.8	0.000	1.148	21	-102
#314	C2	KOH	22.0	18.0	6.907	6.704	-38	-238
	C1	H_2O	25.0	28.7	0.000	1.161	40	227
#130	C2	KOH	20.0	20.8	7.180	6.126	-6	29
	C1	H_2O	23.9	23.0	0.000	0.447	4	-21
#249 Silflon	C2	KOH	23.0	24.6	7.180	6.355	-6	77
	C1	H_2O	28.0	26.3	0.000	0.195	3	-67
#366 Silflon	C2	KOH	23.0	26.7	7.180	5.369	-22	246
	C1	H_2O	28.0	24.0	0.000	0.168	4	-224
Oxag	C2	KOH	22.0	26.0	7.793	6.550	-2	464
	C1	H_2O	25.0	20.9	0.000	0.375	16	-462

Table 4-2: Overview of the most important diffusion values

Table 4-2 shows the measured values of the diffusion measurement and the calculated values for the amount of particles. The measured values are the starting volume V_S, the final volume V_E, the starting concentration c_S and the final concentration c_E. The change of the number of particles Δn for KOH and for water are calculated values. Compartment 1 is denoted by C1 and contains distilled water at the beginning of the experiment. Compartment 2 is denoted by C2 and contains c. 7 M KOH at the beginning of the experiment. A negative sign indicates that matter moves out of the compartment while a positive sign indicates that matter moves into the respective compartment.

4.1.2 Further characteristic Electrode Parameters

In order to obtain further insights about the properties of the electrodes other values are measured apart from the diffusion properties. Using these measured values electrodes of different or identical consistencies can be compared with each other.

4.1.2.1 Density and Area Density

Initially the weight and the thickness of a circular piece of electrode with a diameter of 3.9 cm (corresponding to an area of circa 12 cm^2) are determined. From this the density and the density per area (also called area density) can be calculated.
The density of the electrode is a measure for its porosity, i.e. how much hollow space (pores) the electrode contains. It is not possible to make a statement about the number of pores or the pore size.

Parameters	**Medium**	**O_2-Electrodes**			**H_2-Electrodes**	
		#366	#249	Oxag	#314	#130
Electrode thickness [µm]	dry	430	310	380	270	465
Weight [mg]	dry	1759	1001	1670	1220	1659
Electrode density [g/cm^3]	dry	3.426	1.949	3.25	2.376	3.23
Area density [g/cm^2]	dry	0.147	0.084	0.140	0.102	0.139
Electrode volume [cm^3]	dry	0.516	0.372	0.456	0.324	0.558

Table 4-3: Electrode thickness, weight, density, area density and volume

The results are presented in Table 4-3. Even though electrodes #314 and #130 have the same consistency their thickness and density are quite different. This shows that the mixing and rolling processes have a great influence on these properties. Since

both electrodes are Raney nickel electrodes the passivating process prior to the mixing process also has a great influence on the resulting electrode.
Both silver electrodes, #366 and Oxag, are quire similar. Their difference to #249 can only be explained with the fact that this electrode was manufactured using a pore builder.

4.1.2.2 Permeability and Bubble point

For the permeability measurement of a sample the flow rate dependent pressure loss at a gas flow rate of 100 ml/min through the sample is measured.
In order for the AFC to have an optimal power delivery it has to be supplied optimally with the different reaction substances. Furthermore, it is essential that the reaction products can be removed efficiently. These conditions pose certain constraints for the electrodes.
For the reactions to be able to take place optimally and numerously a sufficient number of triple phase boundaries have to exist. The triple phase boundary denotes the boundary formed by the reaction gas, the electrolyte and the catalyst. If one component is not available the reaction cannot take place.
The electrode must not be wetted to the extent that all pores are filled with the electrolyte. On the other hand it must not be wetted so sparsely that all pores are filled with gas. In order to obtain further insights about the pore structure further values are determined.
The permeability measurement allows to make statements about how well gases can penetrate the electrode. Again, air flows through a circular sample with a diameter of 3.9 cm. Initially, the experiment is carried out with a dry electrode and then with electrodes wetted with octane, water and KOH. In an AFC the electrode also has to distribute the reaction gas over the entire electrode area. In order to fulfil this task the electrode has to feature pores for the gas transport. This experiment allows to measure the change of gas permeability when the electrode is partially filled with fluid, as is the case in an AFC.

Parameter	Medium	O_2-Electrodes			H_2-Electrodes	
		#366	#249	Oxag	#314	#130
Permeability [ml/bar/cm²/min]	dry	32	3780	154.5	205.9	127.5
	Octane	21	2191	167.9	231.8	-
	Water	27.9	2750	21.7	72.6	24.5
	7 M KOH	11.4	1396	13.3	15.6	15.86

Table 4-4: Permeability for gases

Table 4-4 shows the results of the permeability measurement which partly show some quite large differences. Electrode #249 exhibits the highest flow rate values. This is because this electrode was manufactured using pore builder which makes the electrode very porous.

The permeability is a measure of how well fluids can permeate the electrode. The flow rate is measured at a pressure difference of 100 mbar. This value is important for the electrolyte transport in the cell, in particular for removing the reaction water from the cell. The reaction water has to pass at least two electrodes and one separator before it reaches the electrolyte compartment.

Parameter	Medium	O_2-Electrodes			H_2-Electrodes	
		#366	#249	Oxag	#314	#130
Permeability [ml/min]	Octane	0.6	5	0.2	2.4	0
	Water	0	0	0.8	2.0	0.1
	7 M KOH	0.06	5.3	0.7	1.7	0.3

Table 4-5: Permeability for liquids

Table 4-5 shows the measured values of the permeability measurement. Electrode #249 delivers the best results which is due to its large porosity (it was manufactured with a pore builder). Of the electrodes manufactured without a pore builder electrode #314 had the best permeability values.

The bubble point indicates the pressure necessary to force a gas bubble through the largest pore of a porous material wetted with a fluid. This allows to assess the suitability of an electrode for use in a fuel cell.

If an electrode has a high bubble point it is difficult or even impossible to clear the pores of the electrolyte once the electrodes is wetted with it. The required pressure difference is difficult to achieve. If the bubble point is low the electrolyte is easily displaced from the pores by the gas.

Parameter	Medium	O_2-Elektrodes			H_2-Elektrodes	
		#366	#249	Oxag	#314	#130
Bubble point [mbar]	Octane	214	1	550	232	200
	Water	20	10	250	87	210
	7 M KOH	415	20	600	130	770

Table 4-6: Bubble point measurement

Table 4-6 shows the results of the bubble point measurement. Electrode #249 has the lowest bubble point. This leads to the conclusion that the pores are relatively large. According to the different surface tensions of the measurement fluids the bubble point has to be smallest for octane, medium for water and highest for KOH.

The deviations could be related to the different wetting properties of the measurement fluids. Octane has the best wetting properties of the three measurement fluids. As a consequence, also smaller pores can be filled which in return require a higher pressure to be cleared resulting in a higher bubble point.

4.1.2.3 Fluid Absorption

The fluid absorption allows to draw conclusions about the wetting properties. For this the electrode is first weighed in a dry state. Then the sample is placed in the according test fluid for a certain time. The electrode is then removed from the fluid, slightly dried and reweighed.

Due to the different densities of the used test fluids the absorbed amount of fluid in grams is not very meaningful. The conversion into the absorbed fluid volume allows to better compare the results. The three test fluids have different wetting properties, octane wets very well while KOH has the worst wetting properties.

Parameters	Medium	O_2-Electrodes			H_2-Electrodes	
		#366	#249	Oxag	#314	#130
Net weight [mg]	Octane	128	147	116	47	25
	Water	83	13	156	59	46
	7 M KOH	203	82	279	80	105
Volume [µl]	Octane	182	210	165	67	35
	Water	83	13	156	59	46
	7 M KOH	156	63	214	61	80

Table 4-7: Net weight and recorded volume

Table 4-7 shows the results of the wetting measurement. The results are very inconsistent. None of the electrodes behaves in a way that could be expected. Electrode #314 absorbs all three measurement fluids to the same extent. Electrode #130 behaves contrary as expected as KOH wets it best and octane least.

4.1.3 Characteristic Measurement Values Separator

The separator consists of a porous plastic film and in a fuel cell one of its functions is to keep the two reaction gases separate. In order to achieve this the pores have to be filled with liquid KOH. The bubble point should be as high as possible. At Gaskatel pressure differences larger than 1 bar were rated suitable. The separator materials listed below all have a bubble point larger than 1 bar.

The separator should furthermore electrically isolate (for electron flow) the two electrodes from each other. On the one hand this is achieved by the separator which acts as a spacer preventing the electrodes from getting in touch with each other. On the other hand the separator material has to consist of an electrically isolating material, such as plastic.

Some separator materials contain fillers. Here care has to be taken that the fillers are not electrically conducting and remain that way when used in a fuel cell.

The third important criterion is that the separator inhibits the charge transport through the electrolyte, which is effected by OH^--ions, as little as possible. This

property is also called diaphragm resistance. The pressure-dependent hydroxide flow rate through the separator is a first orientation point. If the flow rate is high the charge transport via the electrolyte is good as well. Filled separators are an exception here as the flow rate is usually very low due to the absence of actual pores. However, the filler enhances the ion transport which takes place through diffusion. In order to produce the cross flow EloFlux electrodes as well as separators require a very good permeability while the pressure loss needs to be as low as possible.

In order to determine the flow rate values circular samples (diameter 3.9 cm) are first soaked in the fluid to be measured to completely wet them. Then they are mounted into the appropriate sample mount. Finally, the respective measurement fluid is pressed through the sample with a pressure difference of 0.1 bar. The time required for 20 ml measurement fluid to pass the sample is measured and used to calculate the flow rate.

Separator		**AMS Fas 1000**	**Zirfon**	**Supor 45**	**Supor 80**
Weight cylinder (dry) ∅ = 39.5 mm	[mg]	489	604	83	93
Thickness	[µm]	200	212	234	230
Flow rate H_2O 0.1 bar, 20 °C	[ml/min]	0.03	5.5	20	60
Flow rate 7 M KOH 0.1bar, 70 °C	[ml/min]	0.3	4	20	43
Flow rate 7 M KOH 0.1 bar, 70 °C over night	[ml/min]	0.2	4	20	26

Table 4-8: Characteristic measurement values for different separators

Table 4-8 shows the measurement results of selected separators. The separators AMS and Zirfon are separators with fillers. Accordingly, they exhibit the worst flow rates. The separator AMS was used in the fuel cells where it became apparent that the good diffusion properties are sufficient to ensure the charge transport. The separators

Supor 45 (pore size 0.45 µm) and Supor 80 (pore size 0.80 µm) are porous plastic films and hence they exhibit comparatively good flow rates.

4.2 Experiments with Alkaline Fuel Cells

In the following the results of the experiments are presented which are in a direct connection to the deep see project. The experimental conditions were comparable to the conditions in the deep sea. The obtained measurement data provide insights into the application under optimal conditions.

The following experiments showed that the increase in volume due to the reaction water almost exclusively occurred at the oxygen side. The reaction equations for the AFC lead to the expectation that this would happen at the hydrogen side. This behaviour is examined in greater detail in Section 4.3.

4.2.1 Experiments at Room Temperature

The objective of this experiment was to show if it is possible to operate an AFC without a stimulated electrolyte circulation at a lower temperature of c. 25 °C. This was the first time that an AFC was operated under such conditions at the Gaskatel company and it hence was the first experience of that kind.

Decreasing the operating temperature from c. 50–60 °C to c. 25 °C yielded the advantage that no cooling device was required. Apart from the temperature the operating parameters are quite close to the conditions in the deep sea probe.

The experiment was carried out using the test stand as described in Section 3.2. A KOH tank was not connected during the experiment. The KOH supply available was only the volume in the electrolyte distributors and the conduits. The potassium hydroxide solution was not pumped and not pressurized. The gas pressure for hydrogen and oxygen were c. 0.6 bar. At the beginning of the experiment the concentration of the potassium hydroxide solution was 7.0 M. At the end of the experiment the concentration had fallen to 3.5 M which was due to the reaction water.

The temperature of the fuel cell was between 24.0 °C and 25.5 °C during the experiment. The load current was adjusted to 2.1 A. The thermostat was not used. The experiment duration was c. 44 hours. After this time the supply of KOH had decreased in concentration from 7.0 M to 3.5 M.

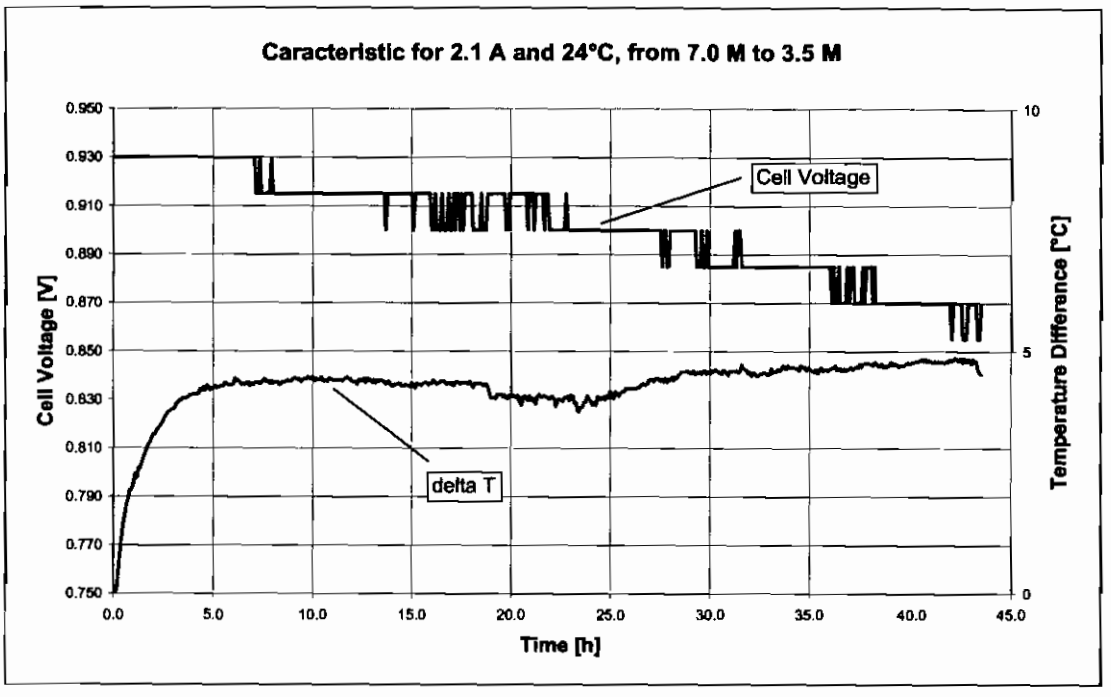

Diagram 4-4: Characteristic curve at 2.1 A and 24 °C, from 7.0 M to 3.5 M

Diagram 4-4 shows the cell voltage in volts and the temperature difference between the room temperature and the fuel cell temperature in °C. The values are plotted against the time in hours.

The cell voltage drops from circa 930 mV to 875 mV. This behaviour was unexpected and several causes for it are conceivable. Due to the decrease of the KOH concentration the conductivity of the hydroxide solution is also reduced. This decline of conductivity leads to an increase of the voltage drop across the electrolyte. As will be shown later the concentration can decrease down to 0.01 M before a voltage drop can be measured at a current of 1 A. It could be measured that the electrolyte concentration decreased to only 3.5 M. However, it cannot be completely excluded that the local concentration in the electrode was significantly lower.

This behaviour shows that the set current was too high under these conditions which means, that the supply of the electrodes with electrolyte or reaction gases was inhibited. Since the electrodes have a certain storage capacity the phenomenon did not immediately become apparent. A more detailed discussion of the causes of the voltage drop is presented in Section 5.2.3.1.

The cell temperature was c. 5 °C above the room temperature. This indicates that to a certain extent the cell is able to heat itself up. By applying suitable measures for a thermal insulation the operating temperature of the fuel cell could be increased further. The cell efficiency increases with a higher temperature.

During the experiment an unexpected behaviour became apparent with regards to the produced reaction water volume. The outlets of the two separated electrolyte compartments were each connected to a plastic tube. The plastic tubes hold the produced reaction water. The fluid level increased almost exclusively at the oxygen side.

According to the chemical reactions it was expected that the volume would occur at the hydrogen side. This behaviour is examined in greater detail in Section 4.3.

4.2.2 Experiment at 5 °C

After the above experiment had shown that it is possible to operate an AFC at room temperature without electrolyte circulation a further experiment investigating this was carried out.

A current of 2 A resulted in a relatively high cell voltage drop so that the current was lowered to 1 A. It was intended to counteract the transport problem with this and lessen or stop the cell voltage drop. Furthermore, the operating temperature was now lowered to the specified value of 5 °C.

The experimental set-up was identical to the set-up described in Section 4.2.1. In addition the cell temperature was lowered to 5 °C using a thermostat. The gas pressures for hydrogen and oxygen were circa 0.6 bar. The load current was adjusted to 1.1 A. At the beginning of the experiment the concentration of the potassium

hydroxide solution was 4.2 M. The cell was operated until the concentration had decreased to 3.5 M. The experiment duration was 20 h.

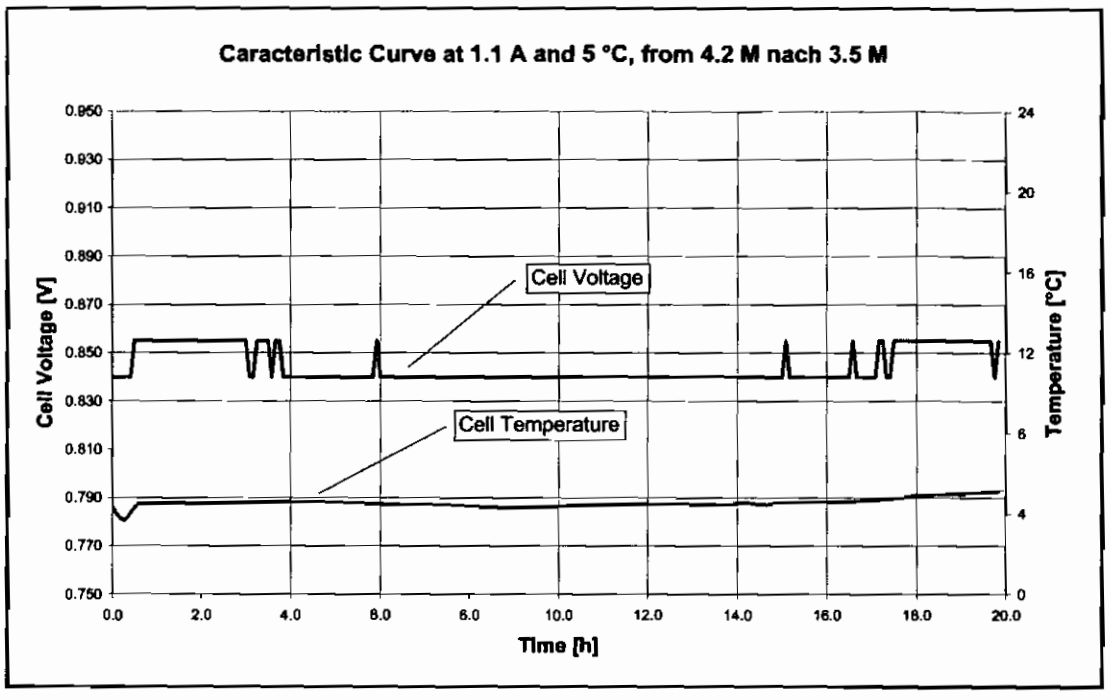

Diagram 4-5: Characteristic curve at 1.1 A and 5 °C, from 4.2 M to 3.5 M

Diagram 4-5 shows the cell voltage in volts and the cell temperature in °C plotted against the time in hours. The cell voltage did not change over the time. This shows that the current at which the matter transport is just about sufficient to maintain the cell voltage lies between 1.1 A and 2.1 A. A further lowering of the temperature did not result in further disadvantages.

As observed in Section 4.2.1 almost the entire volume was produced at the oxygen side. This behaviour is examined in more detail in Section 4.3.

4.2.3 Experiment at 5 °C with a KOH Tank

The experiment described in Section 4.2.2 was carried out without a KOH storage tank. The only KOH supply was in the electrolyte distributors of the AFC. Because of the long operating time of the measurement probe it is essential to have a

sufficient supply of KOH. The supply volume would absorb the reaction water without diluting the hydroxide solution too much. The following experiment was aimed at proving that the exchange of potassium hydroxide solution does not only work inside the fuel cell but also between the fuel cell and the storage tank. Due to the large amount of KOH in the storage tank observing the natural concentration decline would be very time consuming. Therefore the 7.0 M KOH was exchanged with 3.5 M after c. 43. h.

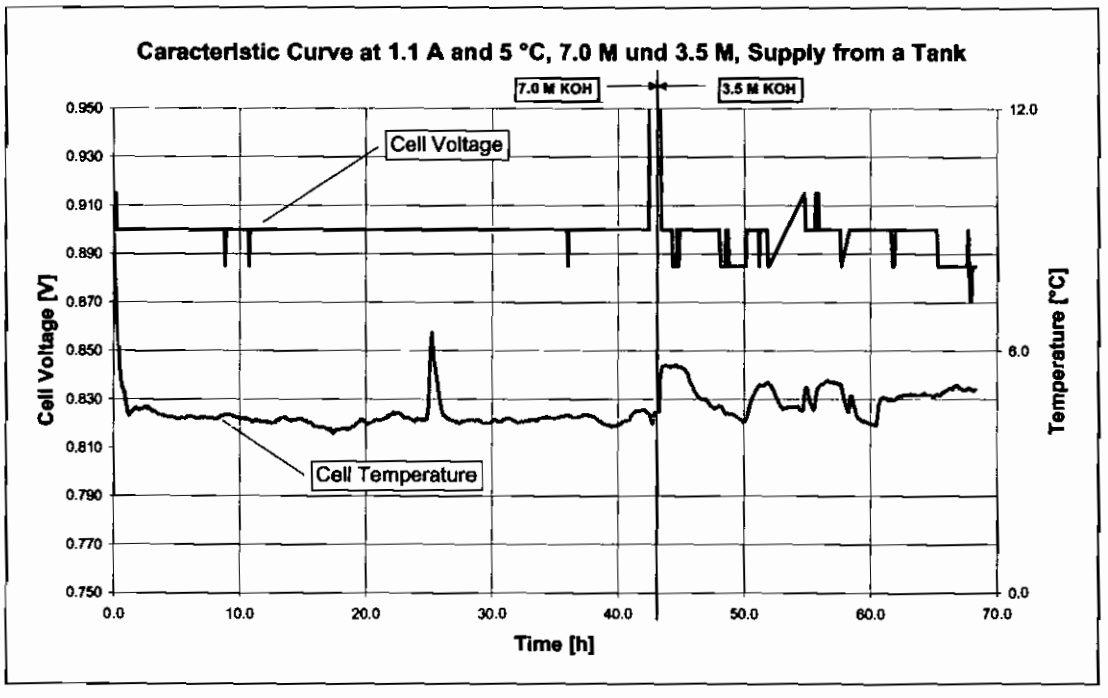

Diagram 4-6: Characteristic curve at 1.1 A and 5 °C, supply from a tank

The experimental set-up is identical with the one described in Section 4.1. In addition the cell temperature was lowered to 5 °C using a thermostat. The main difference was the additionally connected KOH tank. The gas pressures for hydrogen and oxygen were circa 0.6 bar and the load current was adjusted to 1.1 A. The concentration was 7.0 M at the beginning of the experiment. The 7.0 M KOH was exchanged with 3.5 M KOH after c. 43 h and the cell was loaded with 1.1A for another c. 25 h.

Diagram 4-6 shows the cell voltage in volts and the temperature of the fuel cell in °C plotted against the time. The progression of the cell voltage remains nearly constant. The supply of the cell with KOH from a tank and the extraction of the reaction water into a tank worked well and the use of a pump is not required as the matter transport caused by diffusion was sufficient. The cell temperature remained largely constant at 5 °C, so the cell also met this specification.

4.3 Experiments on Water Extraction

For the deep sea application a fuel cell system without a pump is used which means that the matter transport cannot take place by stimulated convection. As will be explained later the matter transport takes place through diffusion processes and/or the electric field inside the AFC.

The experiments described in Sections 4.2.1 and 4.2.2 already yielded that the volume increase almost exclusively takes place at the oxygen side. This behaviour is now investigated in greater detail. The increase of volume was not expected to that extent and the results of the corresponding experiments are presented in the following.

4.3.1 Volume Measurement and Reaction Water Extraction

The objective of the experiment was to gain an understanding of the water extraction from the cell. Furthermore, the experiment was aimed at showing how the water extraction changes dependent on the current. Three experiments were carried out for this with 2.1 A, 5 A and 10 A. The experiment duration became shorter each time, from 28 h to 9 h to finally 5 h.

The test stand used for the experiments was the same as described in Section 3.2. A KOH tank was not connected in the experiment. The KOH supply comprised only of the volume in the electrolyte distributors and the conduits. The potassium hydroxide solution was not pumped or pressurised. The gas pressures of hydrogen and oxygen were c. 0.6 bar. The initial concentration of the potassium hydroxide solution was

7.0 M. The temperature of the fuel cell was adjusted with a thermostat at c. 40 °C. This was necessary as the experiments were carried out with different currents. Caused by the higher heat dissipation at higher currents the cell would heat up to different extents. A comparison for different temperatures would be difficult. The use of the thermostat allowed to maintain the operating temperature even for different load currents.

The increasing volume caused by the reaction water was initially metered via the level in the vertically mounted conduits and then converted into volume.

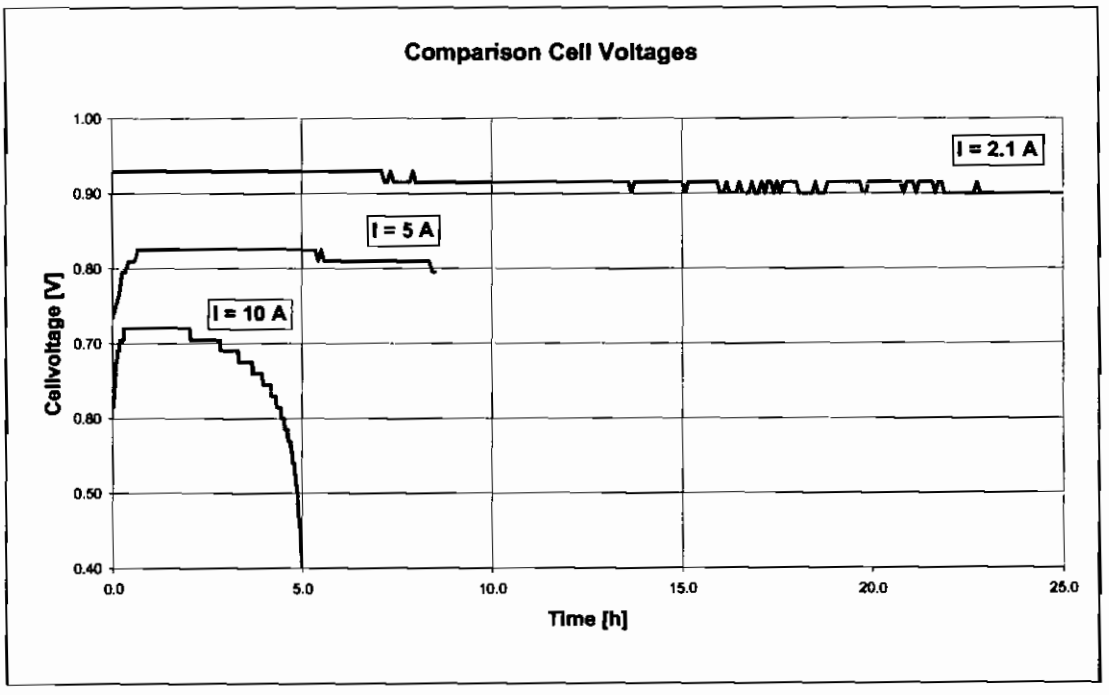

Diagram 4-7: Comparison cell voltage at I = 10 A, I = 5 A and I = 2.1 A, at 40 °C

Diagram 4-7 shows the cell voltage in volts for different currents plotted against the time in h. The higher the current the faster decreases the cell voltage. The voltage decline is non-linear over time. This shows clearest for the measured curve with I = 10 A. As already seen in Section 4.2.1 the current limit of this cell was between 1.1 and 2.1 A. The supply problem becomes stronger with increasing current.

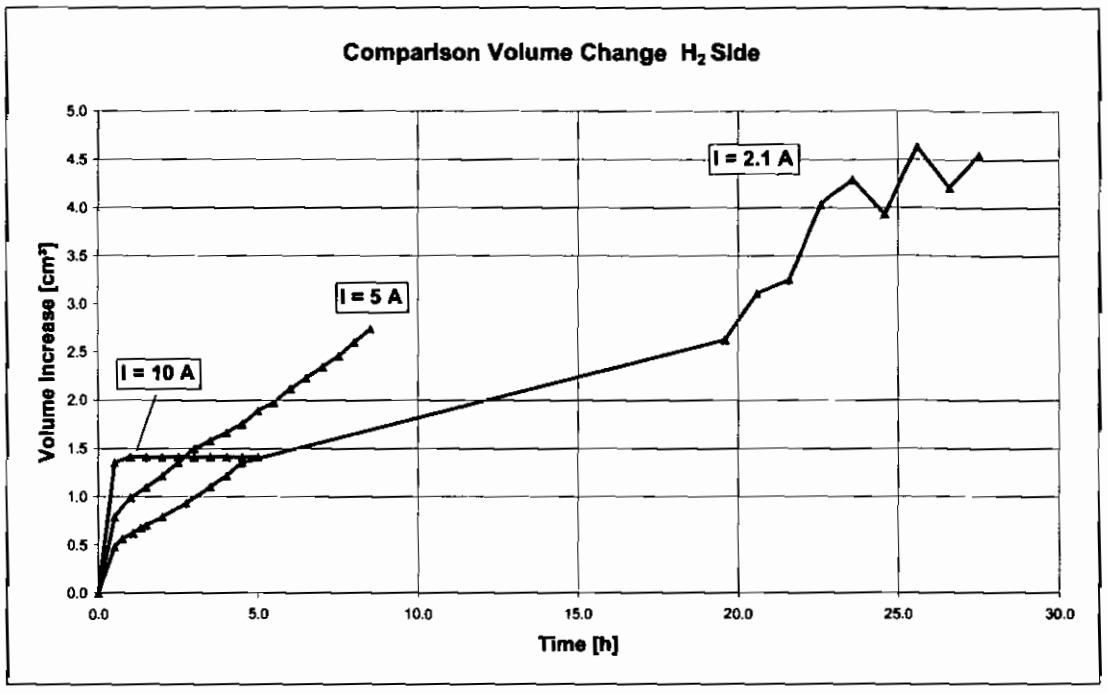

Diagram 4-8: Comparison volume change, H_2 side, at T = 40 °C

Diagram 4-8 shows the volume increase at the hydrogen side in cm^3 for different currents over the time in h. The measured curve for I = 10 A increases to a certain value shortly after the current was switched on and remains stable after that.

For I = 5 A also a quick increase is seen at the beginning which is not as high as for I = 10 A. From then on the volume increases with a constant rate. For I = 2.1 A also a quick increase occurs shortly after switching on, which is again lower than for I = 5 A. From then on also a linear increase can be observed with a lower slope than for I = 5 A.

The quick volume increase during the first 30 min is elaborated later. The volume increase at the hydrogen side is influenced by the current. A clear relationship is not apparent here. Only when plotting the volume over the charge in Ah the relationship shows (see Diagram 4-9)

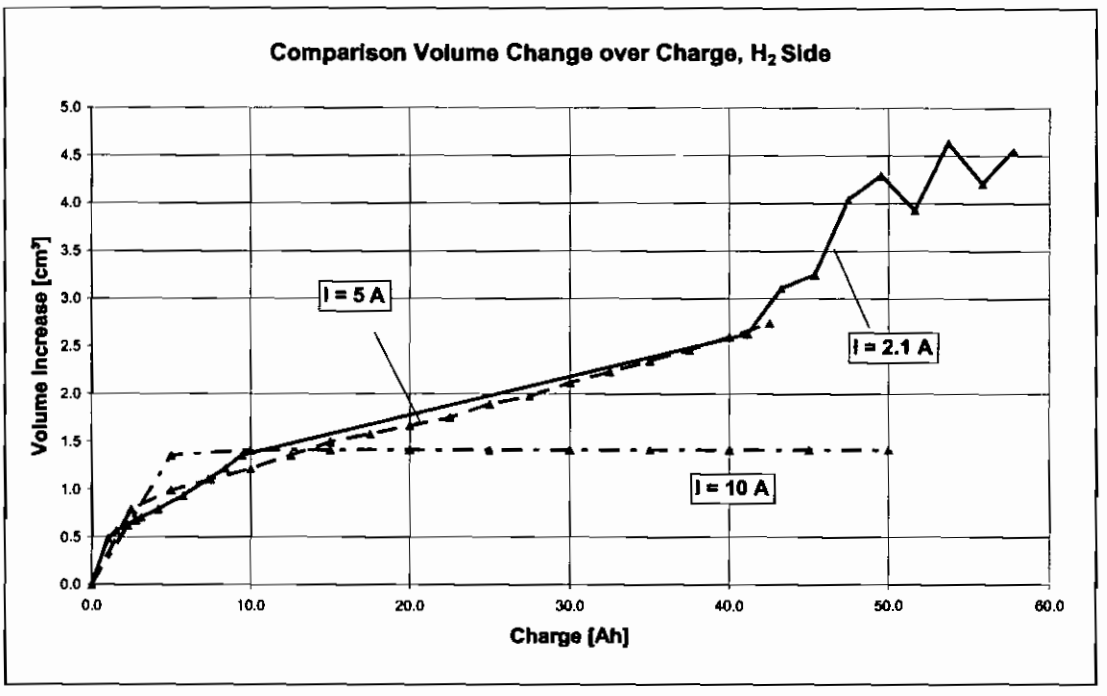

Diagram 4-9: Volume change as a function of the charge in Ah, H_2 side, at T = 40 °C

In order to simplify the comparison of the measured values the volume increase at the hydrogen side was plotted against the charge in Ah in Diagram 4-9. The volume increase is given in cm^3.

The measured curve for I = 10 A increases shortly after switching on the current to a certain value and remains stable afterwards. For I = 5 A a fast increase at the beginning can be seen which is not as high as for I = 10 A. From then onwards the volume increases with a constant rate.

For I = 2.1 A also an increase shortly after switching on can be observed which is again lower than for I = 5 A. From this value on also a constant increase occurs. The slope is slightly steeper than for I = 5 A.

Now a clear relationship shows between current and volume increase. The higher the current the lower is the volume increase at the hydrogen side. Apart for an increase shortly after switching on the current no further increase could be measured for a current of 10 A. It cannot be stated whether the volume would even decrease when increasing the load current, but this is possible.

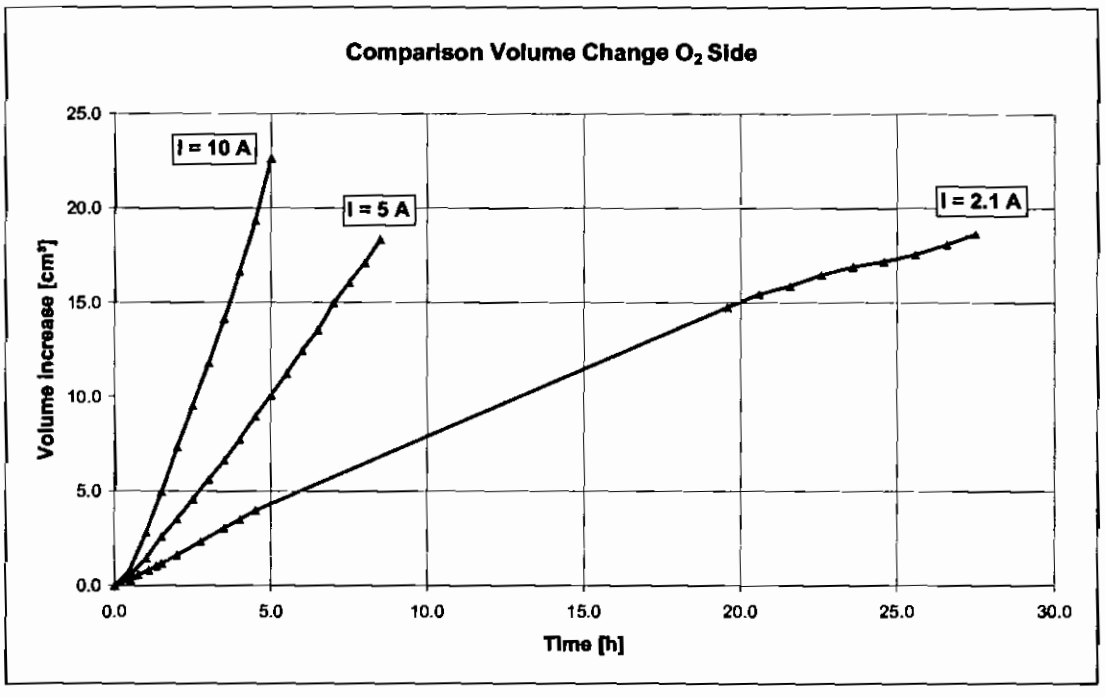

Diagram 4-10: Comparison volume change, O_2 side, at T = 40 °C

Diagram 4-10 shows the volume increase in cm^3 at the oxygen side for different currents plotted against the time in h. The larger the current the higher is the volume increase, which is linear. Here, also shortly after switching on a change of the slope of the volume change curve can be seen. Initially, the increase for the first 30 min is low. Then the increase is significantly higher (detailed representation in Diagram 4-13). The relationship between current and produced reaction water is described by Faraday's law of electrolysis which states that the amount of reaction water is proportional to the current. Here, almost the entire reaction water is removed. The hydrogen side additionally influences the volume extraction at the oxygen side.

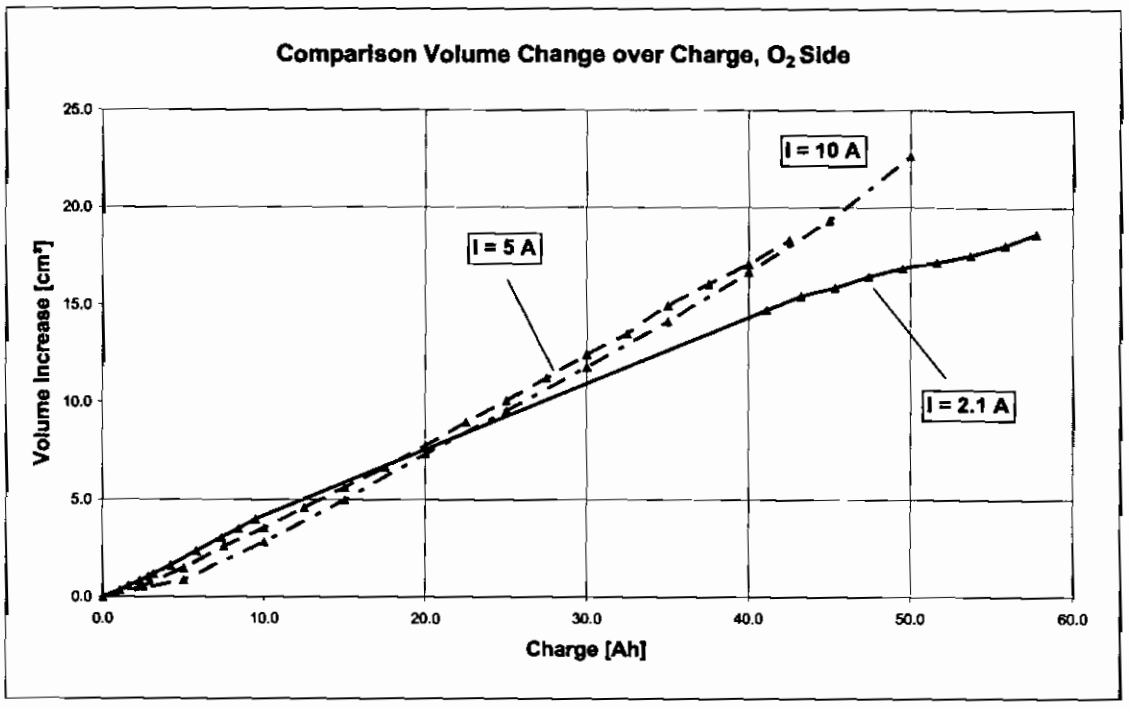

Diagram 4-11: Volume change as a function of charge in Ah, O_2 side, at T = 40 °C

Diagram 4-11 shows the volume increase in cm^3 at the oxygen side for different currents against the charge in Ah. The slope of the measured curves for 5 A and 10 A is nearly identical. For 2.1 A the slope declines slightly after a load of 10 Ah.

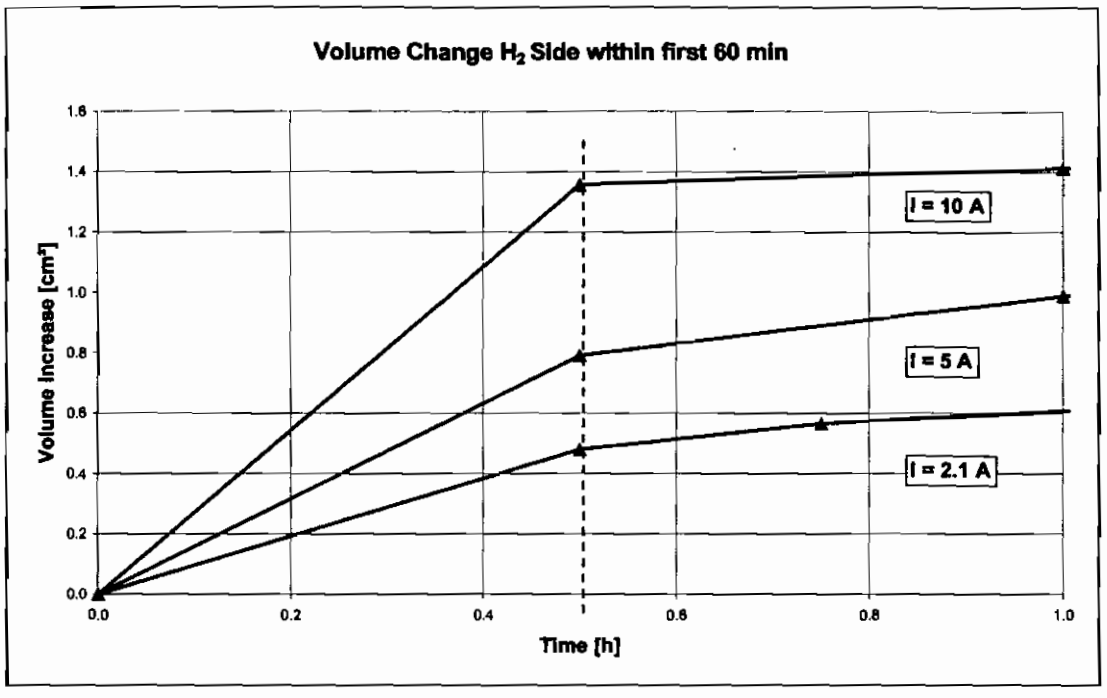

Diagram 4-12: Volume change H_2 side within the first 60 min, at T = 40 °C

Diagram 4-12 shows the first 60 min of the curve seen in Diagram 4-9 in greater detail. Up to a run-time of up to c. 30 min the volume increases strongly, then the curve continues clearly flatter. Since the first measurement was only taken 0.5 h after the start it cannot be stated whether the increase occurred earlier.

The extent of the increase correlates with the current. The higher the current the higher the volume increases. This behaviour indicates that the electrodes reach some sort of equilibrium which obviously has a relationship to the current.

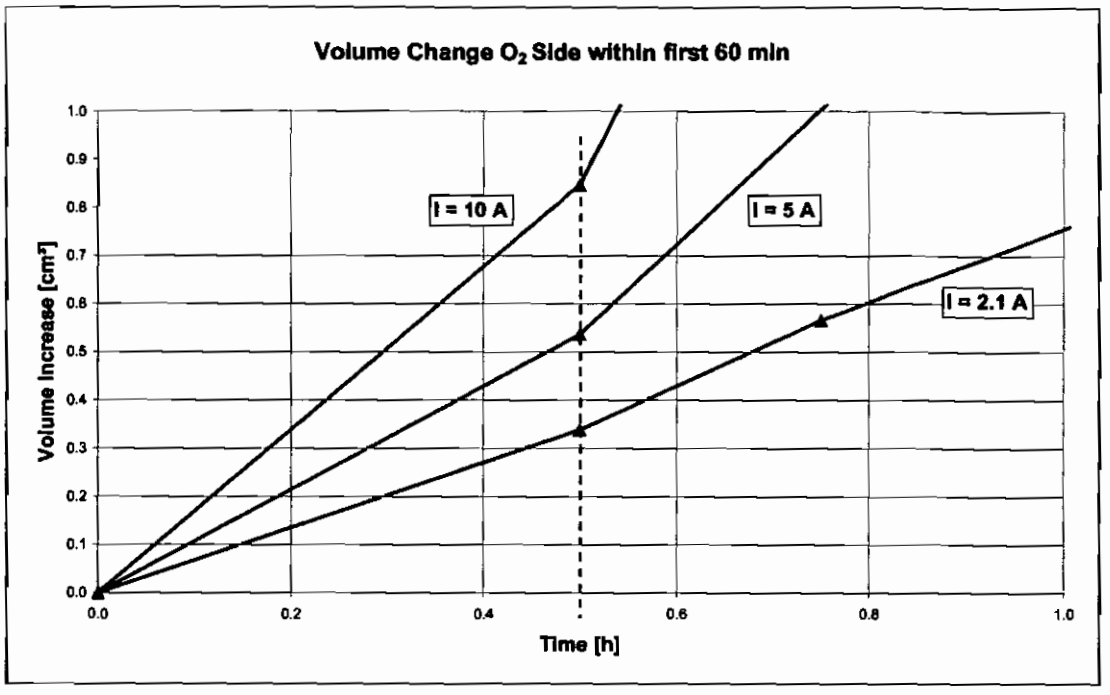

Diagram 4-13: Volume change O_2 side with the first 60 min, at T = 40 °C

Diagram 4-13 shows the first 60 min of the curve seen in Diagram 4-9 in greater detail. Up to a run-time of circa 30 min the volume increases steadily. After this the volume increase is significantly higher. It should be noted that the first reading after the start of the experiment was taken at 30 min. It is therefore not possible to identify whether the increase had not occurred earlier.

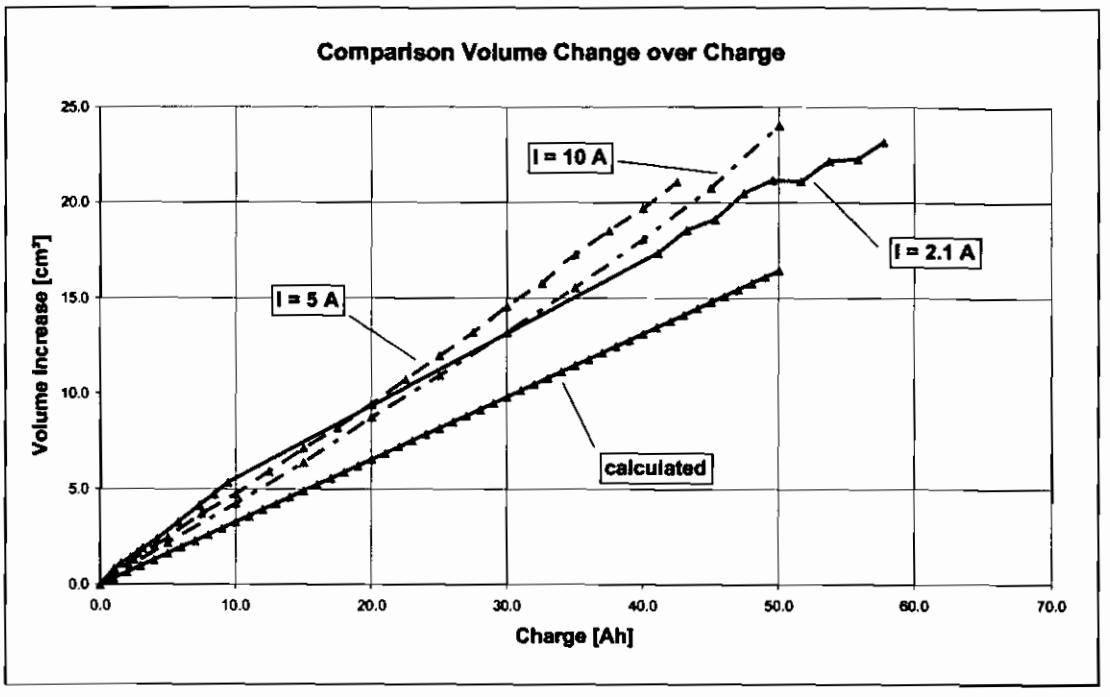

Diagram 4-14: Total volume change at I = I0 A, I = 5 A, I = 2.1 A and calculated, at T = 40 °C

Diagram 4-14 shows the total volume changes against the charge. The volumes at the hydrogen side were added to the volumes at the oxygen side. For the same charge the same amount of reaction water should be produced which should make the comparison of the measured value easier. The theoretical progression was plotted additionally. Here, a significant deviation to the calculated values can be seen. The reasons for this are discussed in Section 5.3

At the end of the experiments the hydroxide solution in the electrolyte compartment was exchanged with fresh solution. The concentration of the used (i.e. diluted) hydroxide solution was measured separately for both electrolyte compartments. This was done to find out whether different concentrations occur at the hydrogen side and the oxygen side. According to the reaction equation it was to be expected that the concentration at the oxygen side would be higher than at the hydrogen side.

	10 A	5 A	2.1 A
Start concentration	7.0 M	7.0 M	7.0 M
H_2 side, experiment	5.148 M	4.918 M	4.852 M
O_2 side, experiment	5.074 M	5.411 M	5.040 M
Δ c O_2 side H_2 side	-0.074 M	0.493 M	0.188 M
Start concentration	7.0 M	7.0 M	7.0 M
H_2 side, calculated	3.590 M	3.838 M	3.590 M
O_2 side, calculated	4.186 M	4.802 M	4.235 M
Δ c H_2	1.558 M	1.080 M	1.262 M
Δ c O_2	0.888 M	0.609 M	0.805 M

Table 4-9: Concentration Comparison: Measured values and calculated values

Table 4-9 shows the concentrations in M at the end of the experiments. For comparison, the calculated values are given as well. The calculation takes into consideration the size of the electrolyte compartments and the theoretically produced amount of reaction water. Furthermore, the different volumes at the hydrogen and oxygen side are taken into consideration in the calculation as well (see Appendix).

The concentration differences between hydrogen and oxygen side are not very large. As illustrated in Section 5.4 the water removal functions well, otherwise larger concentration differences would occur.

The calculated values are always below the ones measured in the experiment. This indicates that concentrations in the electrodes are assumingly smaller than in the electrolyte compartments. The two bottom lines show the difference between the calculated and measured values.

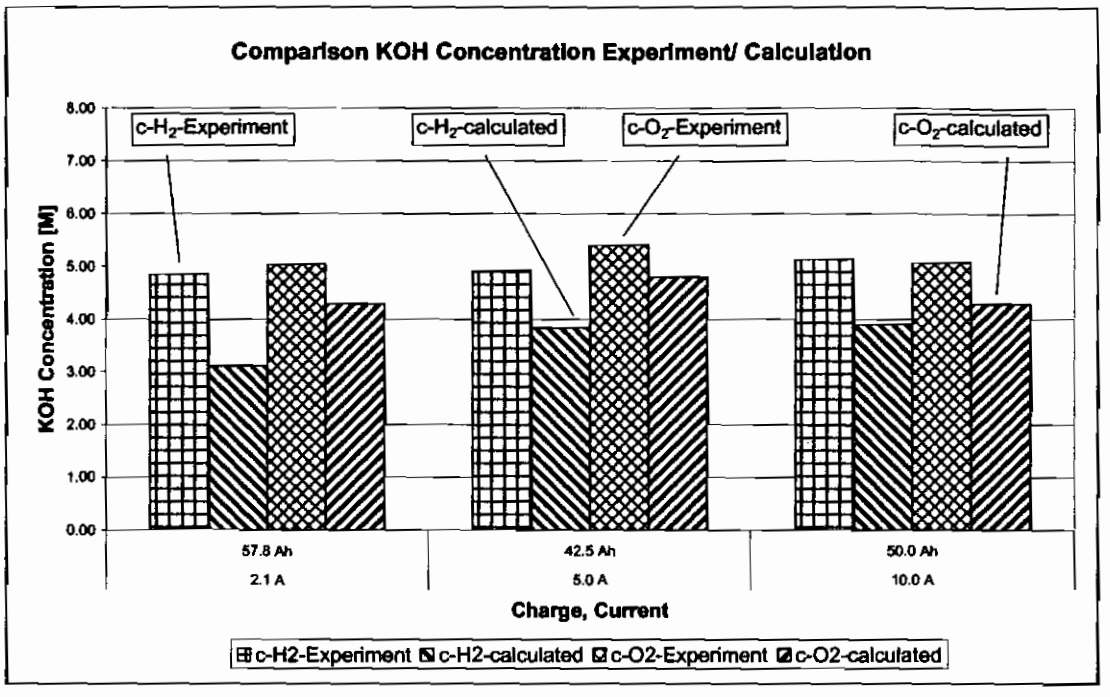

Diagram 4-15: Concentration comparison measured values and calculated values

In Diagram 4-15 the values of Table 4-9 are represented graphically. In addition the load currents and the ampere hours are given.

4.3.2 Concentration Measurement in the Fuel Cell

The above experiments with regards to the reaction water extraction did not yet deliver any indications about the concentrations in the electrolyte distributors. So far, only the volumes could be determined. As the concentrations were always measured at the end of the experiments the progression of the concentration change could not be represented. The following experiment was aimed at a continuous concentration measurement in both electrolyte distributors while the fuel cell was in operation.
For these measurements the fuel cell described in Section 3.9 was used. This cell was prepared to take the concentration sensors. The voltage signal of the concentration sensor was converted into the hydroxide concentration in M.

4.3.2.1 Total Overview

Diagram 4-14 shows the progression of the concentration of the hydroxide solution in M at the hydrogen side and the oxygen side as well as the cell voltage over the time in h. The experiment duration was circa 90 h. The initial concentration in both electrolyte distributors was 7.0 M. The load current was set to 1.1 A for the entire experiment. The cell temperature was controlled using a thermostat and was kept almost constant at 30 °C.

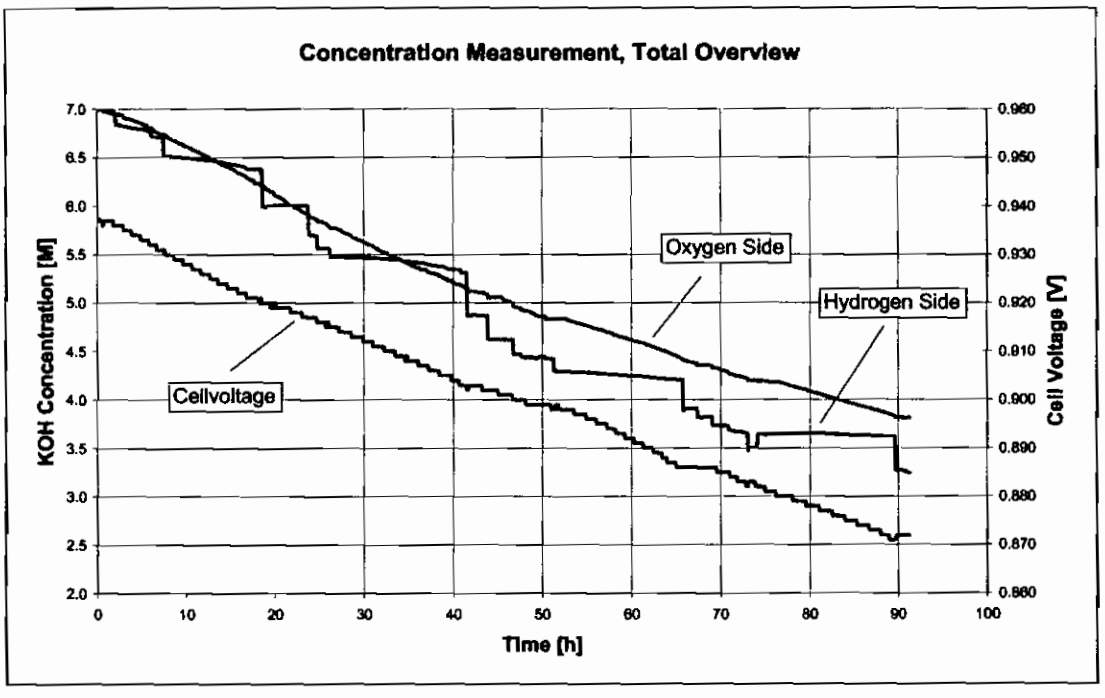

Diagram 4-16: Concentration measurement, total overview

Up to c. 25 h after the start the concentration decreased evenly at both sides. After that the concentration at the hydrogen side decreased significantly faster than on the oxygen side, or the concentration at the oxygen side decreased more slowly respectively. After circa 20 h the cell voltage decreased slower than before.

The step-wise concentration decline at the hydrogen side is prominent. The measurement indicates that the water is not removed continuously but in steps.

4.3.2.2 Detailed Representation between 20 h and 80 h

In order to more precisely evaluate the measured curves it is necessary to represent certain ranges in greater detail. The range between 20 and 80 h is investigated more closely. In this area the step-like concentration decline occurred at the hydrogen side.

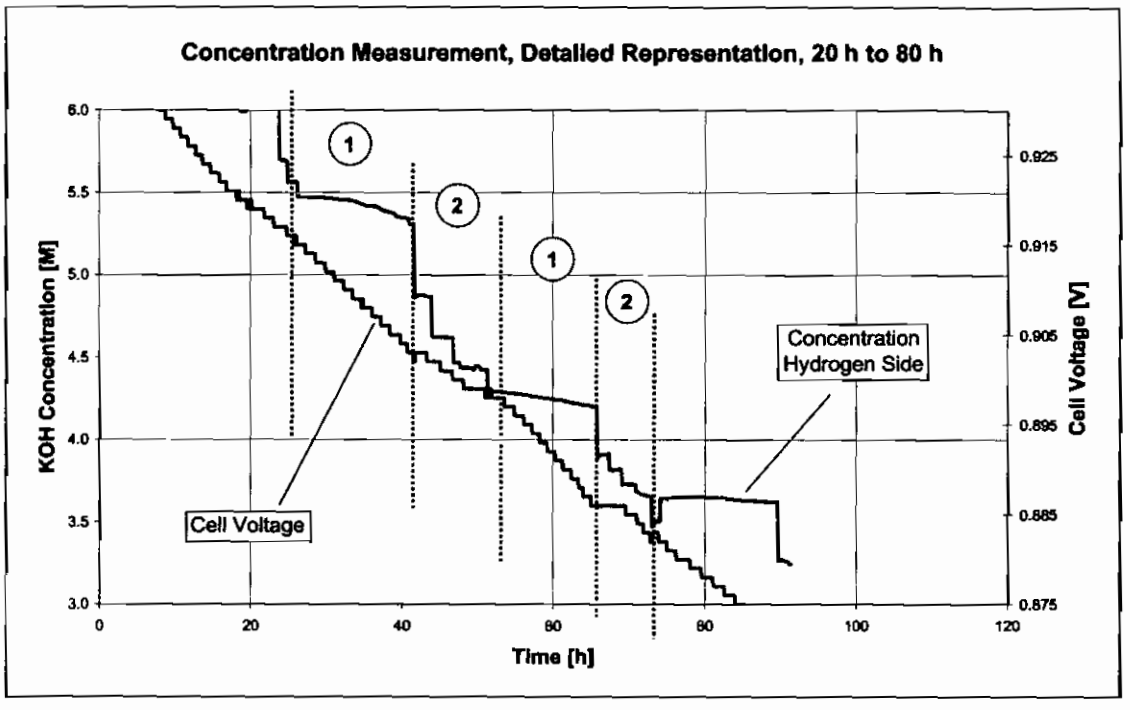

Diagram 4-17: Concentration measurement, detailed representation, H_2 side

Diagram 4-17 shows the range between 20 h and 80 h. The progression of the concentration at the oxygen side and the cell voltage are plotted against the time. A relationship between the decline of the concentration and the decline of the cell voltage becomes apparent.

The measured curve can be divided into two ranges:

1 The concentration hardly changes while the cell voltage continuously declines.
2 The concentration drops suddenly while the cell voltage recovers slightly.

The recovery of the cell voltage becomes more prominent with increasing run-time. This behaviour could be caused by two effects. On the one hand the cell voltage improves if the reaction water is removed and fresh hydroxide solution can flow into the electrode. On the other hand it is possible that the gas pores fill more and more with fluid if the water cannot be removed. This would cause less and less gas to be in the pores. If the water is now removed then fresh reaction gas can again flow into the pores.

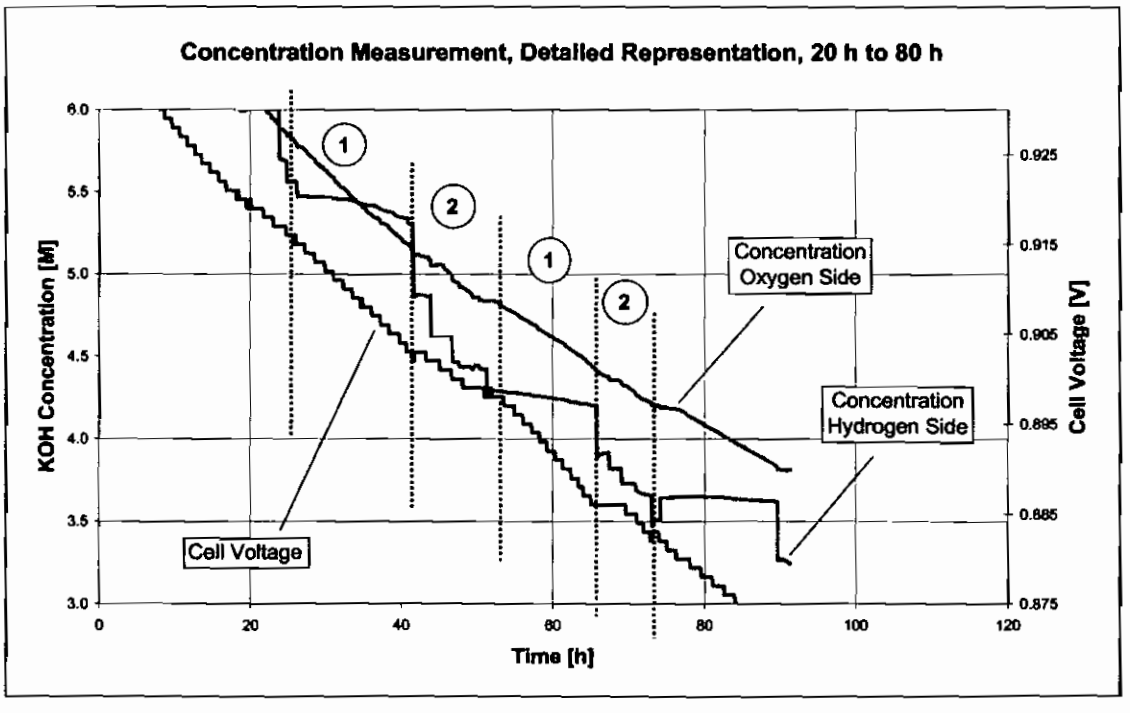

Diagram 4-18: Concentration measurement, detailed representation, O_2 side

Diagram 4-18 is the same as Diagram 4-17, with the difference that the progression of the concentration at the oxygen side is also shown. The progression of the

concentration basically declines steadily. However, the sudden concentration drop at the hydrogen side has not only an influence on the cell voltage but also on the progression of the concentration at the oxygen side.

4.3.2.3 Electrode Potential

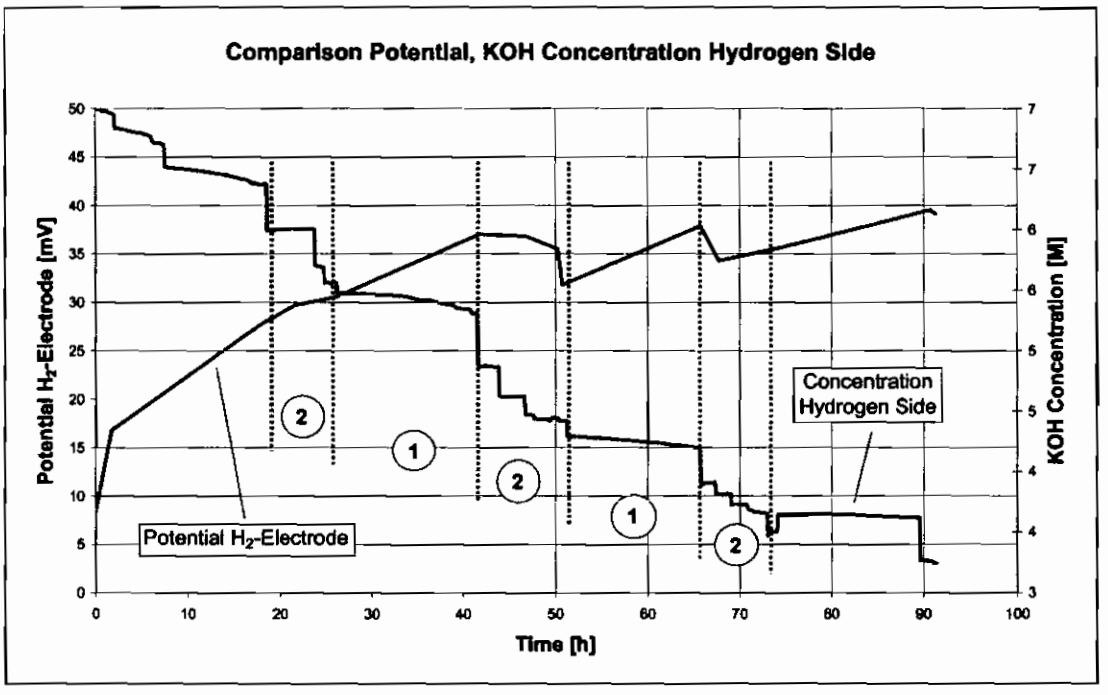

Diagram 4-19: Potential and concentration at the hydrogen side

Diagram 4-19 shows the progression of the electric potential at the hydrogen electrode in comparison with the concentration change at the hydrogen side. The measured values are plotted against the time in h. In the ranges marked with (2) the potential does not increase further or even drops again respectively. In comparison with the hydrogen reference electrode the electrode potential without a load is 0 V (i.e. both electrodes have hydrogen potential). Increasing the load current causes an increase of the electrode potential, it becomes more positive than the H_2 reference electrode. This means that the cell voltage decreases. In case the electrode potential

at the hydrogen electrode increases this means that the latter deteriorates. Removing the water has a positive effect on the electrode and the potential stabilises again.

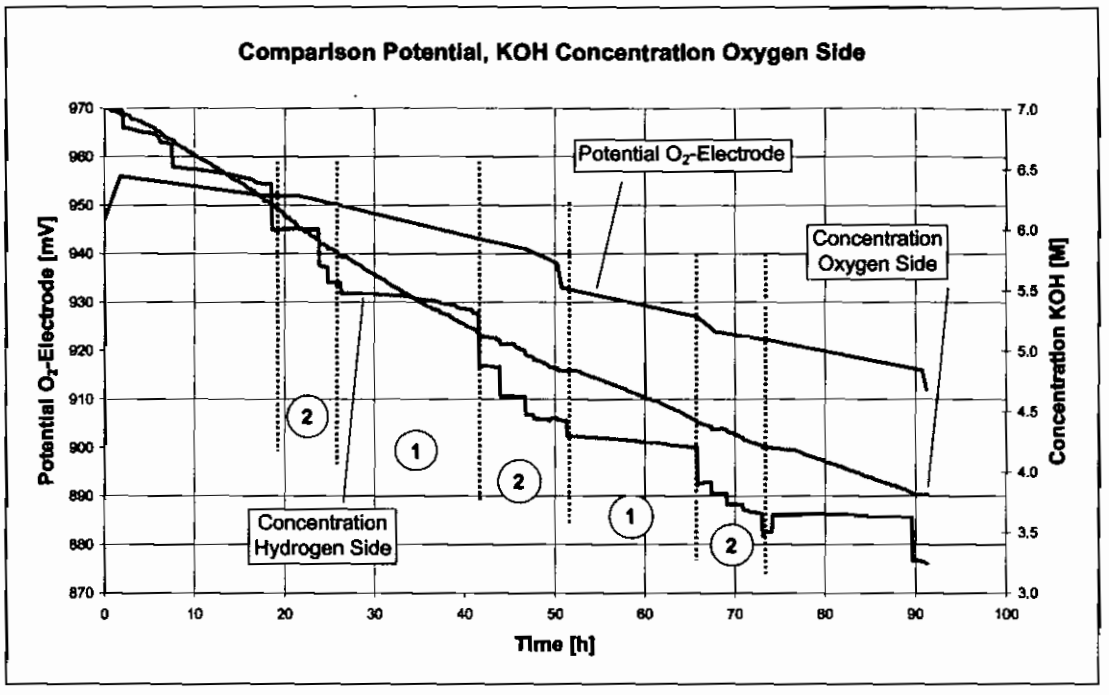

Diagram 4-20: Potential and concentration at the oxygen side

Diagram 4-20 shows the progression of the potential of the oxygen electrode compared to the concentration change at the oxygen and hydrogen side. The measured values are represented over the time in h. In the areas marked by (2) the potential decreases stronger than in the areas marked with (1).

In order to obtain an additional comparison the concentration progression at the hydrogen side was recorded as well. Compared to the hydrogen reference electrode the electrode potential of the oxygen electrode is theoretically 1.23 V (without a load current). Practically voltages of c. 1.1 V (without a load current) are achieved. If the load current is increased the potential of the oxygen electrode decreases.

Here, it also shows that the sudden water extraction at the hydrogen side has an influence on the potential of the oxygen electrode. At the hydrogen side the water extraction has a positive influence on the potential of the hydrogen electrode. However, the potential of the oxygen electrode decreases and thus deteriorates.

5 Discussion of the Results

In this chapter the measurement results which were presented in Chapter 4 are discussed. Initially, the preliminary experiments on electrodes and separators are elaborated, which are in detail:

- measurements on diffusion behaviour
- determination of the density and area density
- measurements on gas permeation
- measurements on fluid permeability
- bubble point measurement
- fluid absorption

This is followed by a discussion of the results obtained from the fuel cells.

5.1 Electrode and Separator Examinations

To remind the reader: prior to their use in an AFC electrodes and separators are examined in preliminary tests. This allows to make first statements about their suitability for the application in an AFC. Furthermore, some electrode properties can be specifically influenced during the manufacturing process. The preliminary tests also allow to compare different electrodes with each other. The measurement methods are shortly recalled in the following and some fundamental insights are illustrated.

5.1.1 Diffusion Measurement

The diffusion properties of the electrodes and separators were determined using the experimental set-up shown in Figure 5-1. Two compartments are separated by the sample under test. At the beginning of the experiment, compartment 1 contains distilled water while compartment 2 contains 7.0 M KOH.

The exchange of the fluids can in principle take place in both directions. Therefore, after the measurement time the change of volume as well as the change of concentration on both sides were measured in order to determine the matter transport.

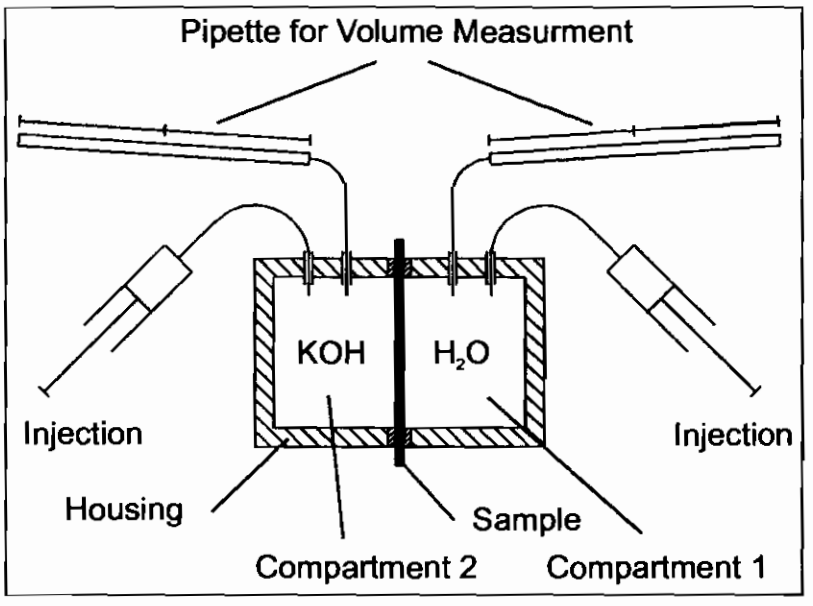

Figure 5-1: Test cell for diffusion measurement

The balancing of the concentrations is effected by the Brownian molecular movements, which are temperature-dependent, chaotic random movements of the molecules. The friction of and collisions with other particles counteract these movements. From a macroscopic viewpoint the concentration gradient is the driving force for a matter transport.

Potassium hydroxide solution is a mixture of K^+-ions, OH^--ions and water. The (charged) ions are surrounded by water molecules (hydrate shell) to shield their charge. This is due to the dipole properties of water. Because of the size differences between ions with a hydrate shell and water molecules it can be assumed that the smaller water molecules can move faster than the large ions with their hydrate shell. The ion mobility could easily be determined using the diffusion coefficient which after all describes the mobility of particles. This value is available for KOH in water; however, for water in KOH no values could be found.

While usually water moves towards KOH, K^+-ions and OH^--ions move towards the water. The electrodes and separators provide resistance against the molecular movement. The influence of the sample on the matter transport depends on the extent of the interaction between the fluid molecules and the sample molecules.

The K^+-ions and OH^--ions as well as the water exhibit quite different properties. K^+-ions have a positive charge while OH^--ions have a negative charge. Water has dipole properties.

The arrangement of the atoms in a water molecule cause an accumulation of positive charges in the region of the hydrogen atoms while negative charge carriers accumulate in the region of the oxygen atom (see Figure 5-2). This constellation leads to the mentioned dipole properties. As a consequence, the water molecules around a K^+-ion arrange themselves with the oxygen atom towards the K^+-ion. For an OH^--ion, the water molecules are positioned around the ion with the hydrogen atoms towards the OH^--ion. The principle holds that like charges repel each other while unlike charges attract each other.

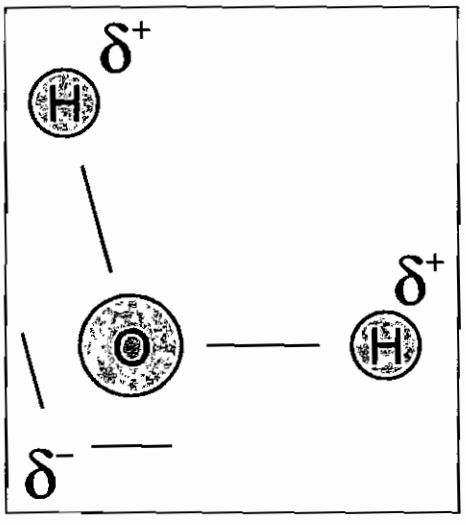

Figure 5-2: Water molecule; the negative charge carriers concentrate in the region of the oxygen atom (O), while the positive charge carriers concentrate in the region of the hydrogen atoms

Since the different samples also have very different properties due to the different materials and pore structures the matter transport is not expected to be uniform. The volume measurements already indicated that the samples are very different with regards to their diffusive transport behaviour.

The results of the diffusion measurement allow to also approximately calculate the diffusion coefficients of the various parts. For this, Fick's first law was used [5-1]:

$$J = -D \cdot \frac{dc}{dx} \rightarrow D = -J \cdot \frac{dx}{dc} \qquad \text{(Eq. 5-1)}$$

where J is the particle flow, D the diffusion coefficient, dx the thickness of the electrode/ the separator and dc denotes the concentration difference.

This calculation, however, exhibits errors. The concentrations at the beginning and at the end of the experiment were known, but the concentrations did not remain constant. This means, that the concentration gradient changed during the progression of the experiment. In the equation an average concentration gradient was used.

The diffusion coefficients calculated here allow to calculate the required concentration gradients in an AFC that have to adjust if a certain amount of particles is to be transported. The results are presented in Table 5-1. The particle flow for a current of I = 1 A was calculated to be c. 37 mmol/h. The cell area was 100 cm².

	Diffusion coefficient KOH in water 10^{-5} [cm²/s]	Diffusion coefficient water in KOH 10^{-5} [cm²/s]	Δc cell for KOH [M]	Δc cell for H_2O [M]
Reference table	2.855	-	0.108	-
AMS	0.532	4.758	0.580	0.065
#314	0.894	7.090	0.345	0.043
#130	0.126	0.918	2.453	0.336
#249 Silflon	0.114	2.249	2.709	0.137
#366 Silflon	0.426	8.982	0.724	0.034
Oxag	0.042	13.152	7.369	0.023

Table 5-1: Diffusion coefficients and required Δc for I = 1 A

The diffusion coefficient D_{salt} for KOH in water is calculated as:

$$D_{salt} = \frac{(z_+ + |z_-|) \cdot D_+ \cdot D_-}{z_+ \cdot D_+ + |z_-| \cdot D_-} \qquad \text{(Eq. 5-2)}$$

where z is the ion charge, D_+ is the diffusion coefficient of the positively charged ions and D_- denotes the diffusion coefficient of the negatively charged ions. KOH consists of K^+ ($D = 1.957 \cdot 10^{-5} cm^2 \cdot s^{-1}$) and OH^- ($D = 5.273 \cdot 10^{-5} cm^2 \cdot s^{-1}$). For the diffusion coefficient this yields $D_{salt} = 2.855 \cdot 10^{-5} cm^2 \cdot s^{-1}$. These values are valid for solutions with a low concentration. For high concentrations no values could be found [5-2].

Apart from electrode #314 no statement can be made for the other electrodes and separators respectively if and how much water is transported by the potassium hydroxide solution towards the water side. The experiment and the calculations can only determine the net amount of the transported water. It is, however, likely that the KOH transports more or less water.

The size of the hydrate shell of the ions depends on the concentration. Whether an ion releases parts of or its entire hydrate shell depends on whether the energetic state of the ion improves or at least does not get worse. If an ion has to partly or entirely leave its hydrate shell behind the hydrate shell has to be replaced by other particles for the transition through the electrode or the separator. In biology science, such a mechanism was verified for the migration of potassium ions through a cell membrane [5-3]. In this context the term potassium channels is used. These passages through the membrane have a diameter just about the diameter of the potassium ion. The wall of the channel is covered with oxygen molecules which replace the water molecules of the hydrate shell for the migration of the ion through the channel. At the other end of the channel the hydrate shell reforms around the ion. The electrode material could exhibit properties similar to the oxygen molecules of the ion channel. If this actually takes place inside the electrodes cannot be stated here, but it was pointed out that it is possible.

5.1.2 Area and Area Density

A circular probe with a diameter of c. 3.9 cm is punched out of an electrode piece, corresponding to an area of circa 12 cm^2. From these values the area and the area density can be calculated.

The density of the electrode allows to determine how porous the latter is, i.e. what portion of hollow space (pores) the electrode contains. The number of pores and the pore size cannot be determined from this.

5.1.3 Gas Permeation

For the permeability the gas permeation of the sample is measured. For this the flow-dependent pressure loss at a gas flow rate of 100 ml/min through the sample is determined.

5.1.4 Fluid Permeability

Here, the permeability for fluids is measured. The time is measured that 10 ml of a measurement fluid require to flow through the sample at a pressure difference of 100 mbar. Table 5-2 shows the physical properties of the used test fluids.

	Density	Dynamic Viscosity	Surface tension
	g/cm^3	mPas	mN/m
Octane	0.703	0.508	22
Water	1.000	1.004	74
7 M KOH	1.295	2.357	93

Table 5-2: Physical properties of the test fluids octane, water and 7 M KOH [5-4]

5.1.5 Bubble point

The bubble point states the pressure required to press the first gas bubbles through a porous material which is completely soaked with a fluid. This test allows to determine the size of the largest pore. The surface tension of the test fluid and the wetting angle between test fluid and the tested material (solid state surface) are used for the calculation [5-5].

$$d_x = \frac{4 \cdot \sigma \cdot \cos \alpha}{\Delta p} \qquad \text{(Eq. 5-3)}$$

where d_x denotes the pore diameter in metres, σ is the surface tension in N/m, α is the wetting angle between the fluid and the solid state surface and Δp denotes the pressure difference in Pa across the sample (electrode or separator).

5.1.6 The Electrodes at the Hydrogen Side

At the hydrogen side Raney nickel is used as catalyst. Electrodes #314 and #130 mainly consist of this material. At the hydrogen electrode the hydrogen is consumed while reacting with the OH^--ions thus forming the reaction water. The electrode should be able to release the water well and absorb OH^--ions in return.

5.1.6.1 Electrode #314

Electrode #314 behaves different than the other electrodes in the diffusion measurement in so far that KOH as well as water migrate from compartment 2 to compartment 1, while circa six times more water than KOH is transported. Despite the fact that this electrode was manufactured without a pore builder it is however relatively porous, which is also confirmed by the permeation and flow rate measurements. Compared to other electrodes its bubble point is rather low. An explanation for the results would be that the KOH keeps the largest part of its hydrate shells and takes it to the water side. This behaviour contradicts the above explained different mobilities of the particles. Water is expected to migrate much better towards the KOH than vice versa. The question remains why the water from the other side is not able to flow to the KOH side. It is possible that the ions can pass the

sample with their hydrate shells under the influence of the pore size and the material properties. For the water molecules these interactions could be so disadvantageous that they cannot pass the pores.

The electrode has a relatively low density and thickness, which leads to the conclusion that it is quite porous. This is confirmed by the results of the gas permeation measurement, as this electrode had the best results of all tested electrodes; the only exception is electrode #249 which was manufactured using a pore builder and hence should not be used for comparison.

The fluid permeability is also very high with the best results for octane and the poorest results for KOH, with water being in between the two. Due to the different viscosities of the fluids this behaviour was to be expected.

A concrete statement with regards to the bubble point measurement cannot be made. Since the wetting angle is not known, Equation 5-2 can only be used in a limited way to make statements.

The surface tension is lowest for octane and highest for KOH. Therefore, the bubble point of octane should be lower than for KOH or water. However, the wetting angles are very different for octane, water and KOH. The wetting angle of octane should be clearly lower than for KOH or water; at least this was shown using some simple experiments. For octane, the wetting angle probably converges towards zero. This means, that the cosine of the angle converges towards one, so both properties have opposing effects. It can furthermore not be completely excluded that the samples were not entirely wetted which would introduce errors into the bubble point measurement.

The results of the fluid volume absorbed by the electrode were unexpected. Due to the different wetting properties of the test fluids, the volume absorption of octane should be clearly higher than for KOH or water. Electrode #314 was used for the fuel cells manufactured for this research.

5.1.6.2 Electrode #130

Even though the consistency of this electrode is identical to electrode #314, the obtained measurement results are completely different. For the diffusion measurement the water moves towards the KOH and the KOH moves towards the water, but circa five times more water moves towards the KOH than vice versa. However, the overall transported amount of water is only 10 % of the value of electrode #314.

The electrode has the largest thickness of all tested electrodes thus resulting in a high density and area density, which results in a poor gas permeability. The porosity of electrode #130 is clearly smaller than of #314, which is also reflected in the fluid permeability.

For the bubble point measurement the same holds as for electrode #314. It is surprising that the bubble point for KOH is significantly higher than for octane and water. The absorbed fluid volume is in the same range as for electrode #314. #130 absorbs more KOH than #314. The comparison of these two electrodes shows that the manufacturing process has a strong influence on the electrode properties.

5.1.7 The Electrodes at the Oxygen Side

At the oxygen side silver is used as catalyst. Electrodes #249 and #366 were manufactured from a pre-mixed silver-PTFE mixture. For #249 a pore builder was additionally used. For #366 activated carbon and graphite were added to the mixture. The Oxag electrode is made of silver oxide. Prior to its usage for oxygen consumption it has to be reduced to pure silver.

At the oxygen electrode the oxygen is consumed. It reacts with water molecules and forms new OH^--ions. The electrode should be able to absorb the water well and release OH^--ions in return. A good release of OH^--ions is very important since the silver could corrode due to the concentration increase.

5.1.7.1 The Oxag Electrode

The Oxag electrode exhibits a diffusion behaviour as expected. The water moves towards the KOH and the KOH moves towards the water. Of all tested electrodes it

transports the largest amount of water. The KOH transport is very low. Furthermore, deviations occur for the KOH measurement values. There are considerable differences between the released and the absorbed amounts of particles; less KOH is released than arrives at the other side. A probable cause for this is the pre-treatment of the samples with potassium hydroxide solution. The samples were previously soaked in 7 M KOH for at least one hour. This was done to ensure that the pores of the samples were completely filled. Whether this succeeded is questionable. The pore system of the samples was presumably only partly filled with hydroxide solution. In case during the experiment the sample gets in touch with water on one side and with KOH on the other side, the KOH concentration of the sample changes. This causes the sample to either release further KOH or absorb more fluid. In the substance amount balance this appears as excess or loss.

The thickness and density of the electrode do not exhibit any unusual values. The gas permeation is similar to #314. The fluid permeability is quite poor. If seen in the context with the high bubble point, this could mean that the pores have relatively small diameters. The gas permeation can still be ensured, but for the fluid permeability the viscosity difference between gas and fluid is very important. The flow resistance is much higher for the fluid in small pores.

The high bubble point poses a serious problem for the operation. Once the pores are filled with fluid they can only be cleared again with a large effort or not at all. The supply with reaction gas is inhibited and the power delivery of the cell collapses. Compared to the other electrode this electrode absorbs the largest fluid volume.

5.1.7.2 Electrode #366

This electrode also behaves as expected with regards to the diffusion behaviour, which is similar to the Oxag electrode. The transported amount of water is c. 50 % lower than for the Oxag electrode. Here also considerable differences occur for the transported amount of KOH. The electrode was also previously soaked in 7.0 M KOH. At the KOH side more particles disappear than arrive at the water side, which means that the electrode absorbs KOH. This behaviour is contrary to the Oxag electrode, which released KOH.

At the water side also deviations occurred, which were in the range of c. 10 %. The electrode still absorbs water. This could mean, that the soaking in KOH was not sufficient to fill the pores. During the experiment further pores were filled with fluid. The electrode thickness and density were within a normal range. The measurement results are similar to the Oxag electrode; the gas permeation was the poorest in the comparison. The fluid permeability was also very poor. This leads to the conclusion that the electrode is not very porous.

The results of the bubble point measurement are similar to the Oxag electrode. However, the bubble point in water is considerably lower and is only circa 5 % of the value measured for KOH. Therefore, this value has to be considered critically. It is possible that the electrode was not entirely wetted and hence a too low value was measured.

The absorbed fluid volume also indicates that a considerably lower amount of water was absorbed. This would explain why the fluid permeability and the bubble point for water were so poor. The electrode is water repelling.

5.1.7.3 Electrode #249

For this electrode the KOH also moves towards the water and the water moves towards the KOH. The amount of transported water again declines and is only circa 30 % of the value of #366. The KOH transport is very poor and comparable to #130. Here, also deviations for the matter transport occur. More KOH is released than arrives at the water side. Furthermore, less water is released than arrives at the KOH side. The cause for this is probably also the electrode absorbing and releasing particles respectively.

Due to the high porosity and the relatively large pore diameter (which is explained below) this electrode shows that a porous electrode exhibiting a good fluid permeability can have a very poor diffusion behaviour. The electrode density is very low and the electrode is very porous which is caused by the addition of pore builder. Pore builders are solid state substances added as a powder to the electrode powder. After the rolling process the electrode is heated up and the pore builder evaporates thus leaving pores were the grains were previously. The process can be compared to

the addition of baking powder when baking. The large porosity is confirmed by the gas permeation measurement; the values are circa 20 times higher than for the other electrodes. With the exception of water the fluid permeability is also very high. It was unexpected that the electrode does not let water pass. The measurement value is questionable. However, during the volume absorption measurement, the electrode absorbed very little water. The low bubble point admittedly shows that the pores have to be relatively large. It is hence remarkable that the electrode hardly absorbs any water or lets it pass. The large pore diameter should only marginally influence the fluid absorption.

5.2 Experiments with the Fuel Cells

The optimal operating temperature for AFCs is between 40 °C and 80 °C. For the deep sea application two parameters important for AFCs had to be changed: on the one hand the operating temperature had to be lowered; on the other hand the potassium hydroxide solution is neither circulated nor is the reaction water extracted, thus leading to a decline of the KOH concentration.

5.2.1 Test at Room Temperature

The first experiment was carried out at c. 30 °C. The advantage of this was that the operating temperature was considerably lower than in a typical application of an AFC without the need to use a cooling device. With 2 A and 20 mA/cm² respectively the load current was low. This was the first experiment of the kind ever to be undertaken in the Gaskatel company and hence this experiment was important to obtain first insights.

The cell voltage declined increasingly with increasing operating time. From the start to the end of the experiment a voltage decline of c. 55 mV was observed (see Diagram 4-4). The extent of the voltage decline of circa 6 % of the starting value within 45 h was not expected. This is probably caused by a supply problem with the electrolyte or the reaction gases. Since this behaviour occurred at all experiments with the AFC this is elaborated in a separate section (see Sections 5.2.3.1 to 5.2.3.4).

Furthermore, the tubes connected to the cell for absorbing the reaction water showed that the volume increase mainly occurred at the oxygen side. This behaviour was also unexpected as the electrode reaction equations had led to the expectation that the volume increase would occur at the hydrogen side. At the end of the experiment, the KOH concentrations at the hydrogen side as well as at the oxygen side could be determined. The values were almost identical. This leads to the conclusion that at least in the outwards direction towards the electrolyte distributor a sound matter exchange took place.

Concluding the temperature progression in Diagram 4-4 is elaborated. As already mentioned above a fuel cell can heat itself up under certain conditions. Under the operating parameters adjusted here the fuel cell produces a heat dissipation power of c. 0.8 W. This is sufficient to increase the cell temperature by c. 5 °C as compared to the room temperature. For the deep sea application it follows that the cell is in fact able to heat itself up. By using a sound thermal insulation this effect can be enhanced, but not to the extent that the cell could reach its optimal operating temperature.

5.2.2 Test at 5 °C

In Section 5.2.1 the power loss of the fuel cell due to the decrease of the operating temperature to room temperature was already apparent. Since the specified temperature for the deep sea probe is only 5 °C the cell was additionally cooled down.

The experiment described in Section 5.2.1 had shown, that a load current of 2 A led to a voltage drop. This is presumably caused by a supply problem; the cell is not sufficiently supplied with the reaction gases or the electrolyte. This problem is later elaborated in detail. In order to reduce or even completely eliminate the voltage decline, the load current was reduced to half of its original value, i.e. 1 A. The hydroxide concentration was reduced to 4.2 M. After a 20 h experiment duration the hydroxide concentration had declined to 3.5 M. A critical-current behaviour like above did not occur any more. The matter transport of electrolyte and gases was sufficient to sustain a current of 1 A.

This experiment shows that it is possible to operate an AFC at a temperature of 5 °C and a current density of 10 mA/cm². However, this is already at the limit of what is possible. It was further shown that a hydroxide concentration of 3.5 M is sufficient. It now remains to clarify, whether not only the matter transport within the cell works but also between the cell and the storage tank.

5.2.3 Test at 5 °C, Supply from a Tank

In order to test whether the supply from a tank also works a further experiment was initiated, in which a fuel cell was supplied with hydroxide from a storage tank. The path the particles require to travel to achieve a concentration balance is hence significantly longer. Furthermore, the diameter the particles need to cross is considerably lower. Diagram 4-5 clearly shows that the supply of the cell from a tank with potassium hydroxide solution works fine and no voltage drop was recorded. This holds for concentration of 7.0 M as well as for a concentration of 3.5 M.
The experiments show that it is possible to operate an AFC under the specified conditions. However, the problems with respect to the matter transport become apparent with increasing current densities.

5.2.3.1 Voltage Drop

In the experiments discussed in Sections 5.2.1 to 5.2.3, but also in the experiments on the water extraction and on the concentration measurement, a voltage drop during the operating time was recurring. The causes for this are the same in all experiments and hence they are elaborated in particular in this section.
A voltage drop in a cell under load can have various reasons. Initially, a distinction has to be made between a voltage decline due to an increase of the load current and a voltage decline which occurs over the operating time.
Increasing the load current causes the cell voltage to decrease. This is caused by overvoltages at the electrodes, which are the transit overvoltage, the diffusion overvoltage and the reaction overvoltage [5-6]. These overvoltages cause a deterioration of the cell voltage. They have in common that they increase with increasing load current. In addition to this, the ohmic resistance causes a linear

voltage drop dependent on the load current. In case the load current remains constant the overvoltages have to assume a constant value. A change of the voltage drop over time has to be caused by an effect that also changes over time.

Caused by the dilution of the potassium hydroxide solution due to the reaction water the conductivity of the hydroxide solution decreases over time. This leads to an increased voltage drop across the electrolyte at a constant load current. This effect is elaborated in more detail in the section about conductivity (Section 5.2.3.2).

Another cause of the voltage drop could be a supply problem with electrolyte or the reaction gases. If one of the reaction partners (reaction gases or electrolyte) is only limitedly available, the cell reacts with a drop of the cell voltage. The cell voltage is composed of the two electrode potentials. By measuring the electrode parameters it can be found out which electrode is affected by a supply problem. A further cause could be a concentration difference in the electrolyte which also leads to a change of the electrode potentials. In the following, these three causes are discussed in more detail.

5.2.3.2 Conductivity

The conductivity of the potassium hydroxide solution depends on the temperature and the concentration. Diagram 5-2 shows these relationships [5-7]. At a temperature of 50 °C to 60 °C the conductivity reaches its maximum value for a concentration of 7.0 M. A concentration decrease causes the conductivity to decline. This effect results in a voltage drop across the electrolyte which causes a reduction of the cell voltage.

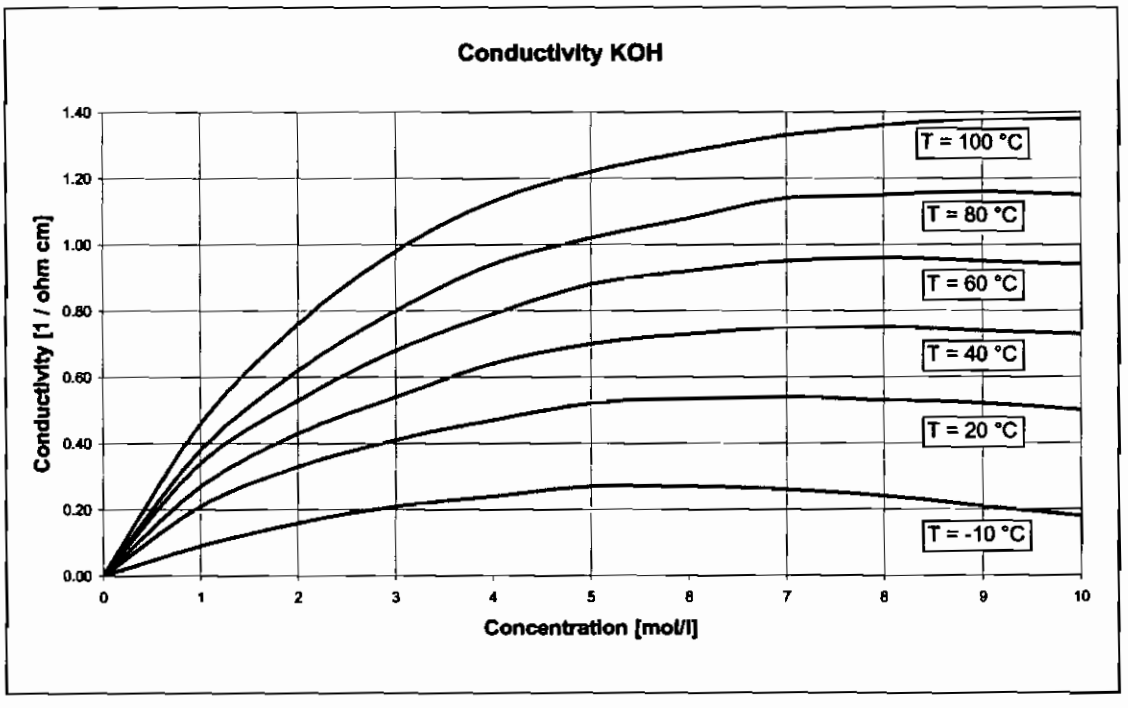

Diagram 5-1: Conductivity of potassium hydroxide solution as a function of the concentration and the temperature

During the experiment the electrolyte was diluted by the reaction water. The initial concentration of 7.0 M was reduced to 3.5 M. This resulted in a decline of the conductivity. The voltage drop across the electrolyte at such small current densities as in this case is however extremely small. The electric current (electron flow) flowing through the external circuit is effected inside the cell by an OH^--ion flow (ionic conduction) between the cathode and anode. The same laws hold for ionic flow as for electron flow. Considering the electrolyte-soaked separator as an electric

conductor with a cross-sectional area of 100 cm² and a length of 0.2 mm yields a voltage drop of only several mV.

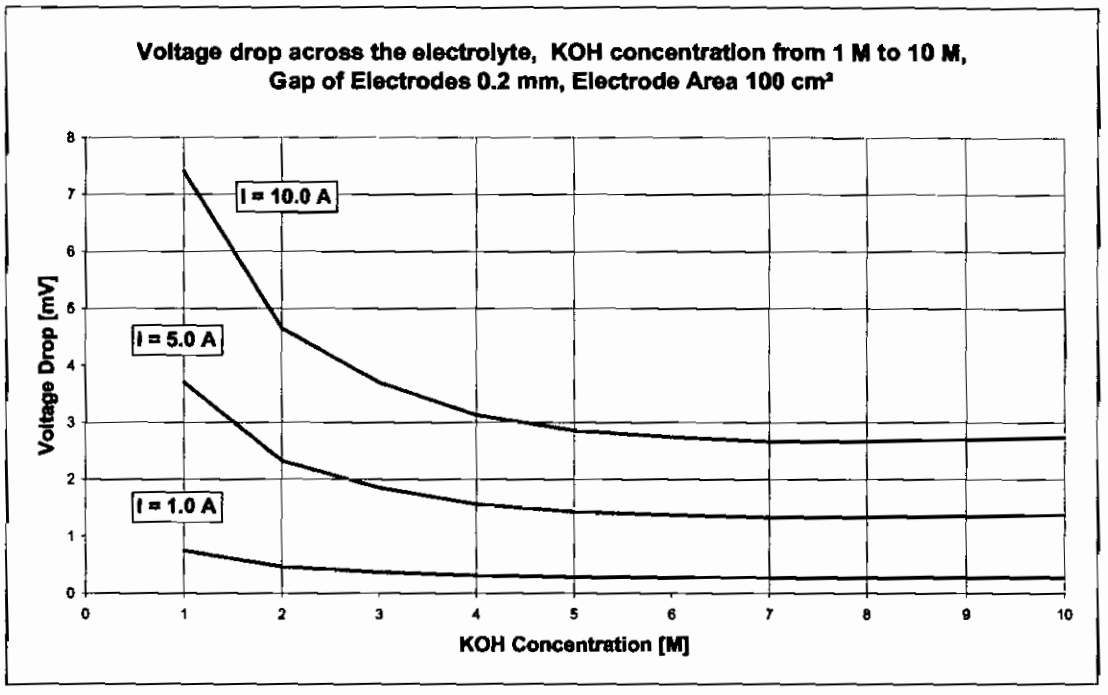

Diagram 5-2: Voltage drop across the electrolyte at various load currents depending on the KOH concentration; KOH concentration in a range of 1 M to 10 M

Diagram 5-2 shows the voltage drop across the electrolyte depending on the concentration of the latter. The currents and current densities were 1 A, 5 A and 10 A or 10 mA/cm², 50 mA/cm² and 100 mA/cm² respectively. For a decrease of the concentration from 7.0 M to 3.5 M the voltage drop across the electrolyte is only c. 3 mV, even for a current of 10 A. At a voltage of 1 A—as specified for the deep sea application—the voltage drop is below 1 mV, even for a concentration of merely 1 M.

In case the concentration falls below 1 M the voltage drop increases rapidly. This problem will play a role further down and is hence explained again in Diagram 5-3. Down to a concentration of 0.1 M, the voltage drop increases to 100 mV at 10 A. At a cell voltage of 700 to 1000 mV this is a severe loss. Below a concentration of 0.1 M another strong increase of the voltage drop occurs. It is also visible that the

voltage drop is rather low for currents below 1 A and 10 mA/cm² respectively, even for a concentration of 0.1 M.

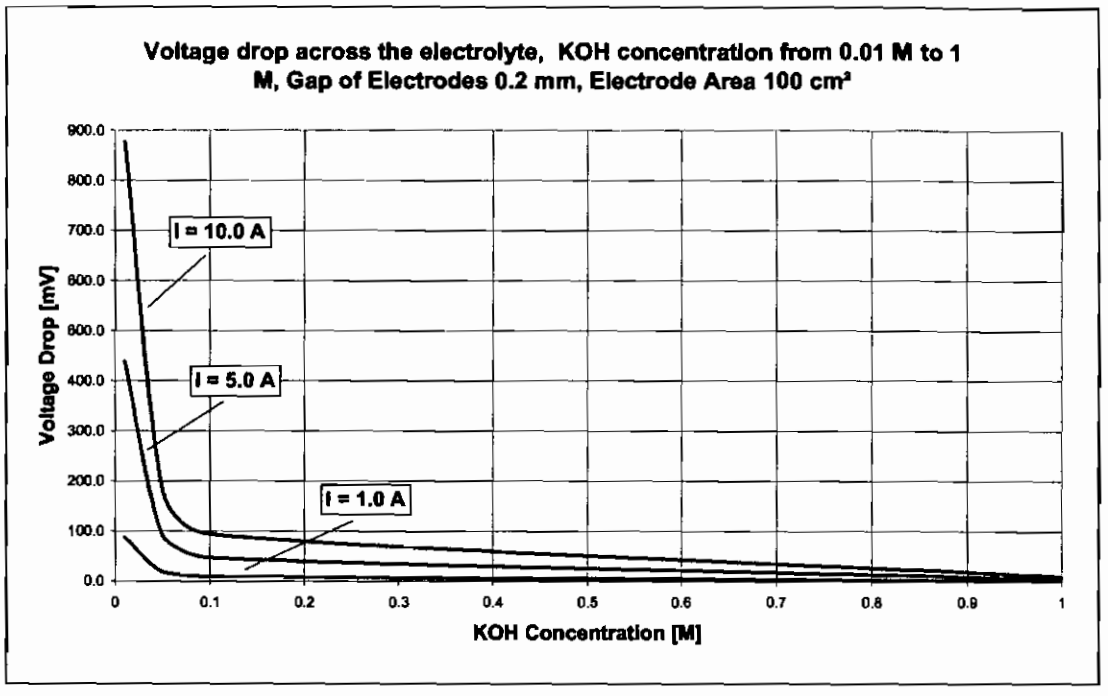

Diagram 5-3: Voltage drop across the electrolyte at various load currents depending on the KOH concentration; KOH concentration in a range of 0.01 M to 1 M

For small load currents, a voltage drop in the measured range could only be caused by a severe decrease of the KOH concentration in the electrodes. According to the concentrations measured in the electrolyte distributors, the measured voltage drop cannot be explained by the deterioration of the conductivity. It is, however, not possible to state whether the concentrations in the electrolyte distributors and in the electrodes are identical. So far there is no possibility to directly measure the KOH concentration in the electrodes. The possibility can thus not be completely excluded, that the electrolyte concentration in the electrodes differs from the concentration in the electrolyte distributors, which would enhance the voltage drop.

5.2.3.3 Critical-Current Behaviour

The term critical-current behaviour is used to describe a voltage drop caused by a supply problem. If a cell were operated with a constant voltage then with a certain current the critical current would be reached, at which the matter transport is just about sufficient for the cell. A constant voltage operation yields the advantage that the cell always delivers the highest possible current. In case the matter transport deteriorates the cell reacts with a decreased current. For constant current operation the cell responds to a deteriorated matter transport with a cell voltage drop.

To a small extent the electrodes can store (buffer) gases as well as electrolyte. If a load current is adjusted that is above the possible matter transport, the stored volume will be used. Depending on the extent of the shortfall of the matter transport a time constant attunes after which the buffer is completely exhausted.

This problem could on the one hand be linked to an inadequate supply of the electrodes with reaction gas. On the other hand, a limited supply with KOH or disposal of reaction water could be the cause. It is not yet possible here to state, whether the problem is linked with the electrolyte supply or due to reaction water disposal. Further down, considerations on that regard are presented. Since no individual electrode potentials were measured it is not clear which electrode suffered a disadvantage.

5.2.3.4 Concentration Differences

The electrode reactions cause water to be formed at the hydrogen side while OH^--ions are formed at the oxygen side. A constricted concentration balancing could lead to considerable concentration differences which would also cause a voltage drop.

In order to better estimate the situation of the concentration balancing it is shown here, how the concentration in the electrodes would change if no balancing took place between the two electrodes and between the electrode and the electrolyte distributor respectively. To facilitate a charge balancing, the transport of K^+-ions has to be enabled.

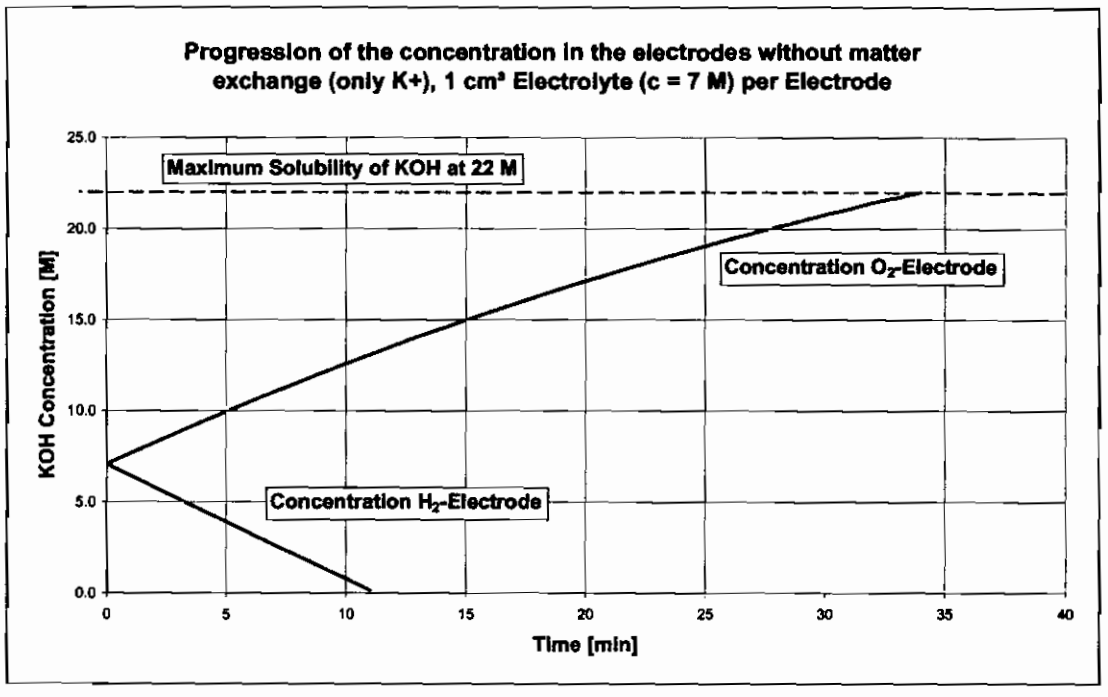

Diagram 5-4: Progression of the concentration in the electrodes without matter exchange (only K^+)

The availability of OH^--ions is important for the reaction at the hydrogen side. For the oxygen side the presence of water is necessary to sustain the reaction. Here, the process is determined by the maximum solubility of KOH, which is circa 22 M [5-4]. This consideration is very useful. It shows how fast the cell would reach concentration ranges where the performance would be strongly reduced or the reaction would stop completely respectively.

For a single cell this means, that an electrode with an active area of c. 100 cm^2 absorbs c. 1 cm^3 hydroxide solution (initial concentration 7 M). At a current of 1 A (10 mA/cm^2) the supply of OH^--ions at the hydrogen side would be exhausted after c. 11 min, at which point all OH^--ions would have been converted into water by consuming hydrogen.

At the oxygen side the situation is far less critical. The solubility limit of the potassium hydroxide solution would only be reached under comparable conditions after 34 minutes, so a factor of approximately three lies between the available times. These considerations clearly show that the hydrogen electrode is much more affected by an inhibited matter transport than the oxygen electrode. On the other hand the corrosiveness of the hydroxide increases with increasing KOH concentration, which can lead to an oxidisation of the silver. The corrosiveness is reflected in the activity coefficient of the hydroxide solution. Diagram 5-5 shows the activity coefficient over the KOH concentration. Above a concentration of c. 3 M the increase starts. At a concentration of 10 M, the activity coefficient is already five times as large.

The oxygen electrode is hence exposed to the risk of a higher corrosion. An oxidisation of the oxygen electrode could also lead to a drop of the cell voltage over the operating time. Contrary to the supply problems, this voltage drop would not be reversible.

The times until the reaction stops are reduced accordingly at higher currents. A free matter transport in the cell is therefore of utmost importance. It is the aim to maintain the hydroxide concentrations in the electrodes approximately constant. In case of the TIGER project (deep sea probe project), the electrolyte will not be regenerated and the decline of the concentration is consciously taken into consideration. However, the matter transport has to be sufficient to keep the concentration difference between hydrogen and oxygen electrode as low as possible. This can only be achieved if the electrodes and separators exhibit only low resistances against the matter exchange.

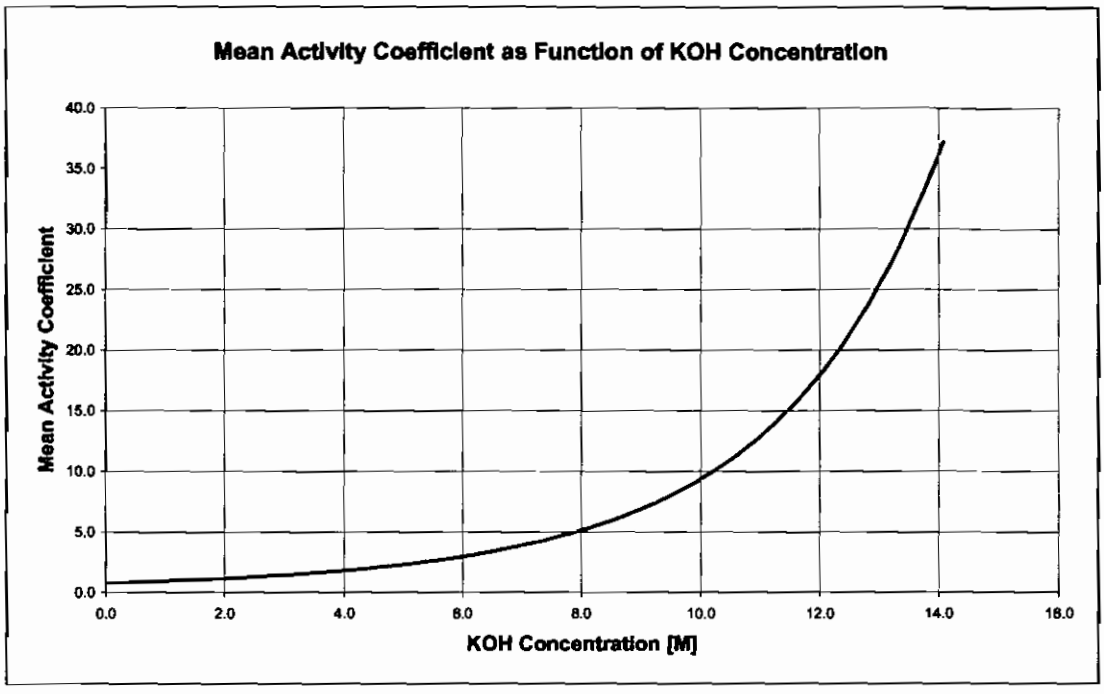

Diagram 5-5: Activity coefficient over the KOH concentration

In case concentration differences should occur due to a poor matter exchange the electrode potential is actually influenced. Using the Nernst equation the deviation from the standard electrode potential at different concentrations can be calculated. In case both electrodes have the same electrolyte concentration the deviation disappears and the overall cell voltage is unaffected. However, if a concentration difference occurs the cell voltage is changed. In the Nernst equation, the quotient of the two concentrations appears as the argument of the 10-base logarithm (see Equation 5-4). As a consequence, the cell voltage changes by only c. 59 mV, i.e. when the ratio of the two concentrations is 10. This means, that if one electrode operates with a concentration of c. 7 M, the concentration in the other electrode has to fall below 1 M to result in a clearly measurable cell voltage drop.

$$E = E_0 - \frac{R \cdot T}{n \cdot F} \cdot \ln \frac{[B]^b}{[A]^a} \qquad \text{(Eq. 5-4)}$$

where E_0 denotes the standard electrode potential, R is the universal gas constant, T is the temperature in K, n is the number of electrons involved in the reaction, F is the Faraday constant, c_0 is the standard concentration and c is the concentration of the electrolyte in the electrode.

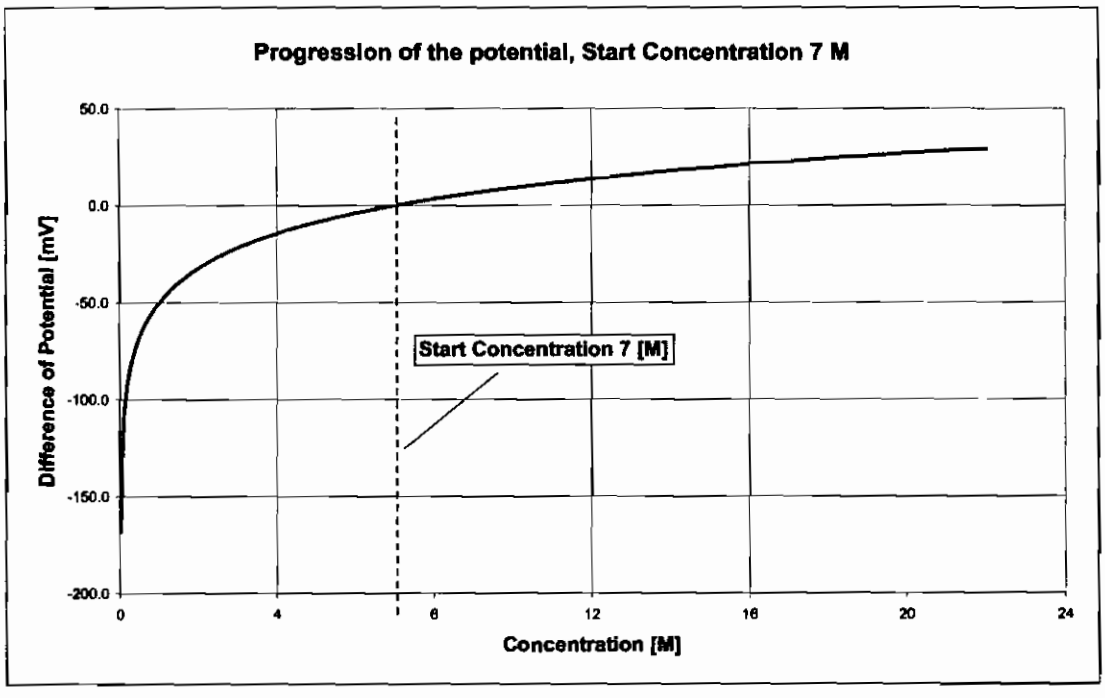

Diagram 5-6: Progression of the potential difference for different concentrations

Diagram 5-6 shows the calculated values, based on a hydroxide concentration of 7 M. It can be clearly seen that for an increase of the concentration up to the solubility limit of KOH the cell voltage would increase by only circa 30 mV. For a decline in concentration a much larger potential difference occurs, which is due to the stronger influence of the logarithm.

5.3 Experiments on Water Extraction and Matter Transport

The experiment described in Section 4-3 showed a volume increase almost exclusively at the electrolyte distributor facing the oxygen side. Furthermore, the concentrations in both electrolyte distributors were nearly identical.

5.3.1 Volume Increase

As a short reminder: according to the reaction equations the reaction water is produced at the hydrogen side, so a volume increase is expected to occur at this side. Contrary to this expectation the volume increase occurred at the oxygen side.

The appearance of the volume in an AFC is due to two reasons: one is caused by the individual reactions in the electrodes and the other is caused by the reaction water. The volume increase due to the electrode reactions takes place at the oxygen electrode and can be explained by the volumes of the participating reaction partners [5-8].

The volumes of an OH^--ion and a water molecule differ only marginally. Investigating the reaction at the hydrogen side shows that two OH^--ions form two water molecules. The volume change is not noteworthy. However, at the oxygen side one water molecule and half an oxygen molecule form two OH^--ions. The gaseous oxygen is transferred into the liquid electrolyte, thus doubling the fluid volume. This shows that a certain volume increase has nothing to do with the formation of reaction water as the latter is produced at the hydrogen side according to the reaction equations. Furthermore, it has to be considered, that the OH^--ions are surrounded by a hydrate shell which would enhance the volume increase. This behaviour can only be effected by a volume displacement. The total number of OH^--ions in a certain volume of KOH in an AFC cannot be changed. Exactly as many OH^--ions are formed at the oxygen electrode as are consumed at the hydrogen side. A volume change can only occur if the concentrations change. If the OH^- concentration increases at the oxygen electrode the concentration must decrease at the hydrogen electrode.

The volume changes measured in the experiment were caused by the reaction water. The amount of reaction water is proportional to the load current and the run-time (see Appendix). This relationship is expressed by Faraday's equation.

At the end of the experiments the KOH concentrations in the two electrolyte compartments were determined additionally. It was found that the values at both sides were approximately the same. This means that largely a concentration balancing takes place. Since the volume at the hydrogen side does only change little or not at all, the amount of reaction water absorbed at the hydrogen side is small.

In case the concentration should be lowered while the volume is kept constant this can only be achieved if water molecules join and at the same time K^+- and OH^--ions are released (or consumed). When looking at the oxygen side based on the same considerations this means that the volume can only increase if the reaction water is transported there.

5.3.1.1 Volume Measurement

The individual experimental results are elaborated in the following. When comparing the volume changes at the hydrogen side at different load currents the representation of the volume over the operating time does not yield a uniform picture (see Diagram 4-8). Even though there is an influence of the load current on the volume increase it does not correlate with the extent of the current. The strongest increase occurs at $I = 5$ A, and it is slightly lower at $I = 2.1$ A. Apart from the increase immediately after switching on the current (which is elaborated later), at $I = 10$ A no increase over time can be measured.

The step-like increases at $I = 2.1$ A could be due to measurement errors. The cause for this is probably the unnoticed accumulation of gas bubbles in the electrolyte distributor at the hydrogen side, which could have been introduced through leakages.

A logical relationship between the current and the volume increase only becomes apparent when representing the volume over the charge in Ah (see Diagram 4-9). The representation over the charge has the advantage that for the same charge the same amount of reaction water is produced. Now the dependency of volume increase and current can be seen. The lower the load current the higher is the volume increase

at the hydrogen side. At 10 A a volume increase cannot be detected any more. It is conceivable that the volume could decrease if the current were further increased.

The volume progressions at the oxygen side (Diagrams 4-10 and 4-11) are not very meaningful as they are influenced by the volume removal at the hydrogen side. Furthermore, almost the entire volume is removed, small differences do not stand out so clearly as on the hydrogen side.

To make further statements about to what extent KOH and water respectively are transported a substance amount balance was created (see Appendix). It was set up in such a way that the calculated values with regards to volume extraction and concentration can be compared to the measured values. The balancing yielded that with increasing load current more and more reaction water must be transported to the oxygen electrode. At 2 A c. 85 % of the reaction water produced at the hydrogen electrode is transported to the oxygen electrode. At 5 A the portion increases to c. 90 % and at 10 A to nearly 100 %. For the transport of OH^--ions it follows that c. 99 % to 100 % of the produced OH^--ions have to be transported to the hydrogen electrode.

It is noted here, that according to the reaction equations at the electrodes a water transport of 50 % would be sufficient. This would mean, that just about as much water would be transported to the oxygen electrode as is consumed. The remaining 50 % would be dissipated into the electrolyte.

This ideal case would however result in the KOH concentration at the oxygen side to remain constant while at the hydrogen electrode it would more and more decrease. The thus created concentration gradient leads in return to a matter transport caused by diffusion. The higher the current the higher the concentration gradient. Due to the increasing concentration gradient the water transport towards the oxygen electrode would increase.

Diagram 4-10 shows the volume change at the oxygen side. The volume increase is caused by the reaction water. It depends on the load current and the operating time. This behaviour was expected. It is, however, surprising that the volume increase occurred at the oxygen side.

Diagram 4-14 shows the total volume increase over the charge in Ah. In addition, the calculated progression was included. It was expected that all lines progress identically, since the amount of produced water is proportional to the charge. This is approximately true taking the measurement errors into account. However, it is unexpected that the calculated progression is clearly below the measured progression.

The water production of the fuel cell depends directly on the transferred charge. If, for instance, the current measurement were erroneous then more or less water could be produced than would be calculated from the measured current. For the presented measurement this can be excluded since the deviation is far too large for an erroneous current measurement to be responsible for this.

A different cause could be a gas leakage within the fuel cell. When hydrogen and oxygen mix they could be recombined to water in the presence of suitable catalysts without contributing to the current flow. However, the catalysts used in this AFC are not capable of effecting this.

An internal electric short circuit could also effect an additional water production, but this would decrease the no-load voltage of the cell. This could also not be observed.

Concluding, one reason remains that could explain the measured values. At the beginning of the experiment the fuel cell is filled with liquid KOH, including the pores of the electrodes. The characterising data show, that for instance electrode #366 absorbs more KOH than water. In case the hydroxide concentration inside the pores declines during operation the pores in the electrode could be emptied successively and be filled with oxygen gas thus releasing an additional volume.

5.3.1.2 Volume Increase shortly after switching on the Current

A further distinctive feature of the volume measurement was the step-like increase of the volume at the hydrogen side (see Diagram 4-12). At the oxygen side, however, no volume decrease could be measured (see Diagram 4-13). The increase was considerably lower compared to the value that adjusted later during operation. This takes place during the first 30 min.

The relationship between load current and volume is proportional. Whether the increase also correlates with the converted amount of substance cannot be stated here, since the first measurement values were recorded only after 30 min. In order to identify a relationship with the charge it would be necessary to know the time at which the volume increase took place. The latter could have occurred unnoticed 30 min earlier. The times should approximately double from 2 A to 5 A and finally to 10 A.

At the current state of knowledge several explanations are possible. It is conceivable that here the transport balance adjusts according to the particular load current. This would lead to a displacement of the volume until a new balance is established. Furthermore, the establishing of a balance with regards to the K^+- and OH^--ions in the electrode could play a role.

A different cause could be that due to the changed potentials the wetting properties of the electrodes could change. This results in an electrode absorbing or releasing electrolyte. Here, also a balance would be established. The individual points are discussed in the following.

5.3.1.3 Establishing of Transport Balance

For this, the substance balance can be used once more. As there is initially no concentration gradient between oxygen and hydrogen electrode the matter transport could take place in an almost ideal fashion. This means, that the reaction water leaves the cell at the hydrogen side. After a concentration gradient has gradually build up the situation changes and the water is transported towards the oxygen electrode. The balance would be reached if a stable concentration gradient had been established. As the transport properties of the AMS separator are quite good with respect to water, only a small concentration gradient is required, which will be established after a short time. The time is shorter the higher the load current.

To estimate the effects this has on the volume change, the consideration in Section 5.2.3.4 and Diagram 5-4 is used. Here, theoretically a matter transport of OH^--ions and water was prevented. Only a transport of K^+-ions due to the charge balancing could take place. This consideration would be the worst case that could occur with

regards to the concentration differences. The result is the largest possible volume change with respect to the highest and the lowest KOH concentration respectively. Diagram 5-7 shows how a KOH volume of 1 cm^3 with a concentration of 7 M changes if it is exposed to a current of 1 A in the electrodes. It can be seen clearly that the volume changes are very small.

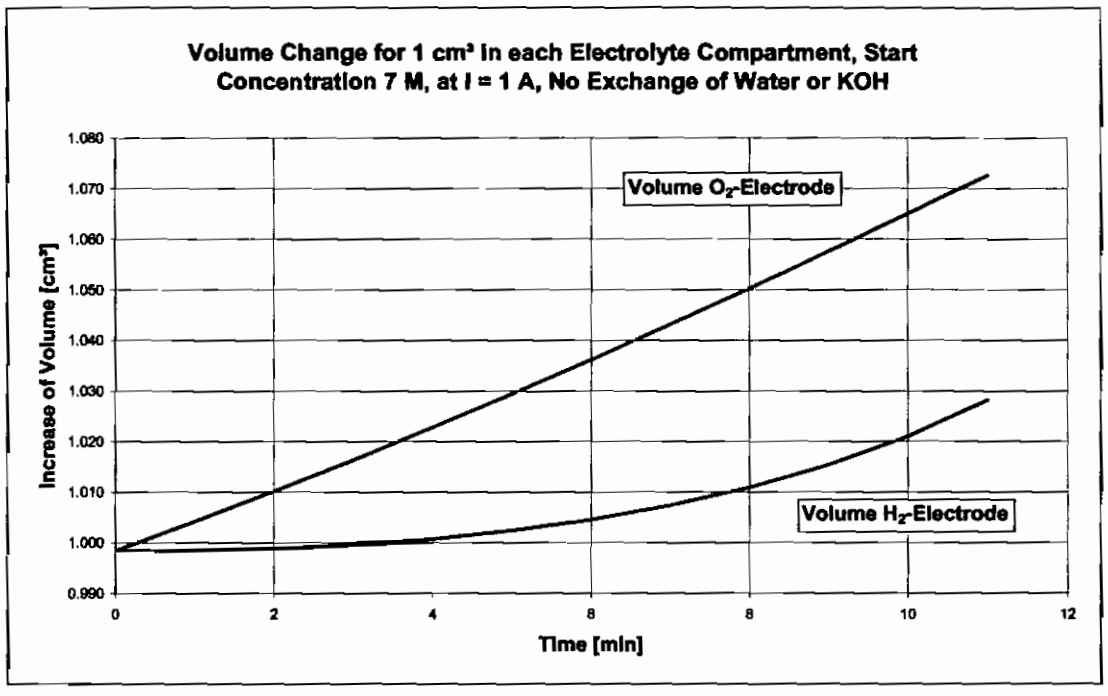

Diagram 5-7: Volume change of 1 cm^3 7 M KOH each, at a load current of I = 1 A

5.3.1.4 Ion Balance

A possible cause for the step-like volume increase could be related to the release of K^+-ions from the hydrogen electrode. When the current is switched on, suddenly a certain amount of OH^--ions are consumed. Since the latter are not available any more for the load balancing of the K^+-ions, it is possible that the K^+-ions leave the electrode in order to balance their charge with other OH^--ions. Contrary to this the OH^--ions generated at the oxygen electrode should effect a volume decrease. Since here the OH^--ions are produced which need K^+-ions for a charge balancing this could cause the K^+-ions to move into the electrode. This effect would last until the matter transport balance corresponding to certain current is established.

5.3.1.5 Changes of the Wetting Properties (Concentration-dependent)

A further explanation is that the electrodes absorb more or less electrolyte depending on the concentration. Comparing with Table 4-8 for this yields that all of the measured electrodes absorb a larger volume of KOH than of water. This is caused by a change of the wetting properties. Since the reaction water is formed at the hydrogen side, the KOH concentration will decrease there. As a consequence volume is released from the electrode.

For electrode #314, which is used at the hydrogen side, the difference between absorbed KOH and absorbed water is very small. Extrapolated to the fuel cell, the difference would only be 0.0167 cm^3 per electrode. This is not sufficient to explain the volume increase at the hydrogen side.

For the oxygen electrode (#249) the situation is somewhat different. It can absorb 0.608 cm^3 more KOH than water per electrode, so the electrode could absorb a part of the produced KOH solution. The volume could be stored for a certain time until a new balance has been established (see Section 5.2.3.4).

5.3.1.6 Changes of the Wetting Properties (Potential-dependent)

A further possibility to explain this measurement could be that the wetting angle or the wetting properties of the electrolyte respectively change depending on the electrode potential. This principle is also used to pump liquid electrolytes.

The electrodes respond to the switching on of the load current with a potential change. This would cause the electrode to absorb or release electrolyte due to the changed wetting properties.

5.3.1.7 Voltage Drop

When comparing the cell voltages of the three test series a critical-current behaviour stands out (see Diagram 4-7). As already described above this is linked to a problem with the matter transport in the electrolyte (see Sections 5.2.3.1 to 5.2.3.4). The cell voltage drop does not have a direct relationship to the transferred amount of substance. A certain matter transport takes place. For lower currents this is just sufficient. When increasing the current, an initially low substance transport

deficiency does not have a large effect. At a considerably higher current the still occurring matter transport is so low that the cell rapidly runs into a supply problem.
A first indication to a matter transport problem of the AFC is also given by the measured values in Diagram 4-13. At the end of each experiment the concentrations of the potassium hydroxide solution in the electrolyte distributors were measured. Here it showed, that the measured concentrations were always higher than the calculated ones. This leads to the conclusion that the reaction water cannot entirely leave the electrodes. The highest concentrations were reached in the measurement series with a current of 5 A. This is because here the lowest matter transfer occurred during the run-time (42.5 Ah) thus producing the lowest amount of reaction water.

5.4 Concentration Measurement in the Fuel Cell

To obtain further information about the matter transport and the water extraction a further measurement series was started, where the concentration in the two electrolyte distributors could be measured continuously. The results are presented in Diagram 4-14, which provides an overview over the entire experiment duration. The cell voltage declines continuously during the experiment, but regions with higher and lower voltage drops can be seen. In total, the cell voltage declines by c. 66 mV. When observing the curves in detail (see Diagrams 4-15 and 4-16) it can be seen that the progression of the voltage has a relationship with the concentration progressions. The concentrations at the hydrogen side progresses step-like. In the regions marked with 1 in the diagram the concentration changes only marginally. This leads to the conclusion that during this time the electrode hardly releases any reaction water. This, in return, causes a decline of the concentration of the potassium hydroxide solution which is accompanied by an increase of the potential at the hydrogen electrode (see Diagram 4-17). In the ranges marked with 2, the concentration changes within a short time. This means that reaction water is released into the electrolyte distributor and fresh KOH can be supplied to the electrode. The potential reacts positively to this and does not increase for a short time. With increasing run-time this behaviour becomes more distinctive.

The oxygen electrode reacts with a slight time delay to the pulsating water extraction. Contrary to the hydrogen electrode it reacts with a deterioration of the potential. To explain this behaviour is very difficult since various causes could interact with each other. One possibility could be that the change of the bubble point and the wettability respectively cause pores to be more or less filled with gas. According to this it takes a higher or lower effort to clear the pores.

It is also possible, that a volume increase in the fuel cell causes a pressure increase and hence the electrodes are lifted more or less off the separator. Due to the resulting poor contact the potentials also deteriorate.

Furthermore, this behaviour could also show, that the water released via the hydrogen electrode is not available to the oxygen electrode for the production of OH^--ions. As a consequence, the KOH concentration would additionally increase.

It is another question in this context which role the diffusion properties of the components play. To apply these insights to the matter transport in the cell, it makes sense to consider the cell in three sections, which are:

- internal matter transport between the hydrogen and oxygen electrodes via the active separator,
- external matter transport via the hydrogen electrode and the passive separator towards the electrolyte distributor at the hydrogen side,
- external matter transport via the oxygen electrodes and the passive separator towards the electrolyte distributor at the oxygen side.

Assuming that the reactions at the boundary between the electrode and the active separator implies that the inner matter transport is only influenced by the diffusion properties of the separator [5-9]. If a matter transport takes places through diffusion the concentration gradient corresponding to a certain current can be calculated (see Table 5-1) using the measurement values in Table 4-3.

The influence of the components on the external matter transport is more difficult to describe, since two or three components respectively interact. A possible progression could look like in Figure 5-3. Starting from the electrolyte distributor (EL) of the hydrogen electrode the concentration falls continuously to the reaction layer between the H_2-elektrode and the active separator. This is caused by a consumption of OH^--

ions and the formation of water. Across the active separator the concentration increases again. At the reaction layer between the O_2-electrode and the active separator the concentration reaches its maximum before a continuous decline up to the electrolyte distributor (EL) at the oxygen electrode occurs. The flow generated by the volume increase in the oxygen electrode is neglected here.

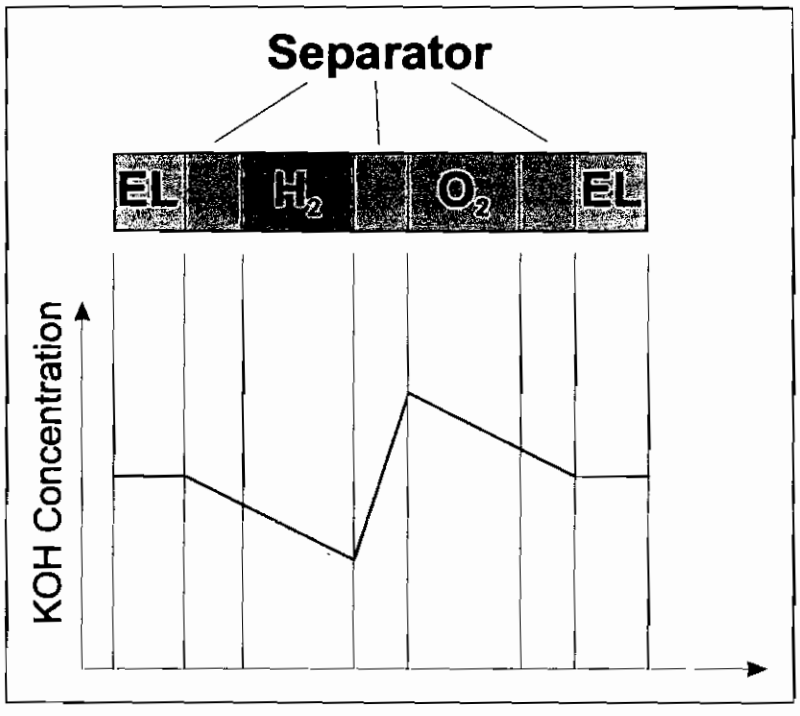

Figure 5-3: Progression of the concentration across a single cell

5.4.1 Calculated Matter Balance

A simulated representation of the experiment on the concentration measurement yields results very similar to the actual experiment. In the calculations the properties of the components were neglected, which thus appear to have no influence. However, it has to be considered that the concentration progression was measured in the electrolyte distributor. It is difficult to draw conclusions from this about the processes in the cell.

In Diagram 5-8 the calculated concentration progression is presented. The input parameters were chosen such that the calculated progression was closest to the

measured one. A volume measurement in this experiment could have improved the calculation considerably; however, this was not possible for the concentration measurement because of the modified cell construction.

As input parameter the initial amount of potassium hydroxide in the fuel cell could be modified. Furthermore, it was possible to change the matter transport between the two electrodes. The maximum amount of substance necessary to ensure the charge transport for a current of I = 1 A was the respective variable. Of this, a percentage of the matter transport could be provided. For the diagram below (Diagram 5-8) a starting volume of 16 cm^3 was chosen. The percentage for the transport of water towards the oxygen electrode was set to 85 %. The corresponding portion of KOH transported towards the hydrogen electrode was set to 98.9 %.

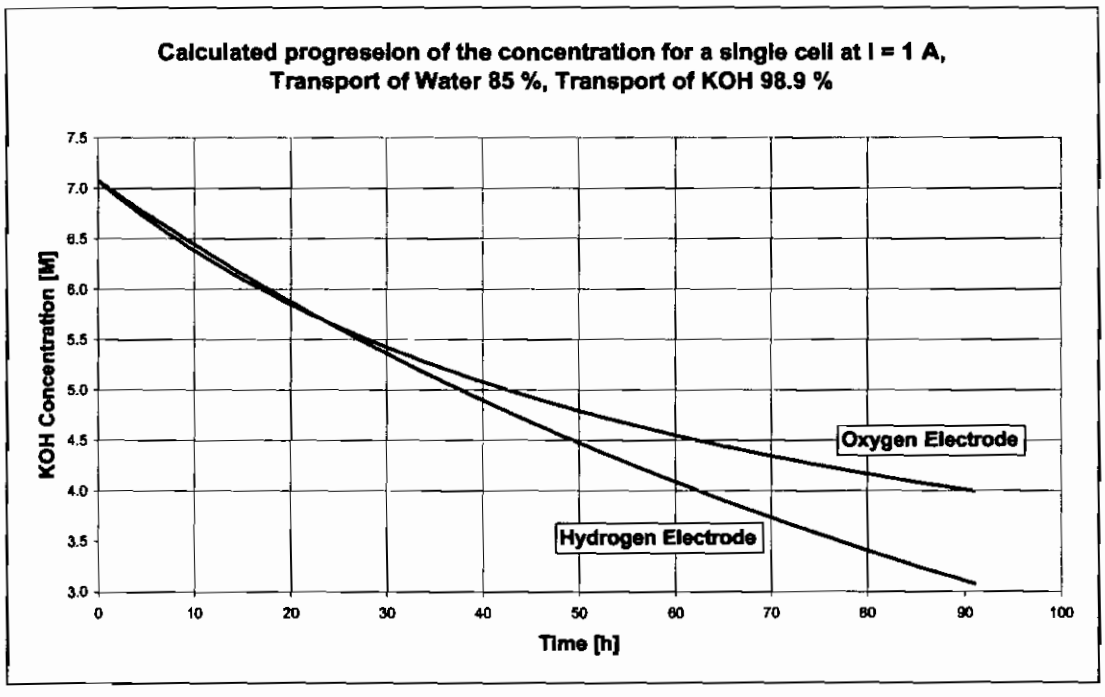

Diagram 5-8: Calculated progression of the concentration for a single cell at I = 1 A

It stands out at this simulation calculation that the concentration progression reacts very sensitive to the KOH transport. Deviations of the above value smaller than 1 % result in completely different concentration progressions. The water transport was significantly less sensitive and changes of several per cent did not have a significant effect.

6 Conclusions and Future Work

This research has shown that it is possible to run an alkaline fuel cell at a temperature of circa 5 °C. It was not necessary to change the standard electrode material of the hydrogen electrode or of the oxygen electrode to reach the power output of 5 W.

Furthermore, it could be shown that it is not necessary to have an electrolyte circulation for a small load current. The exchange of KOH and water is achieved by diffusion. The tests confirmed, that it is in principle possible to run an AFC under these conditions. In the future, long-time tests will be started. To accommodate this, it will necessary to change the design of the AFC housing. It is suggested to combine the fuel cell with the KOH storage tank.

An interesting result was the extraction of the reaction water via the oxygen electrode. In combination with the concentration measurements, it was possible to find out more about the internal transport of KOH and water. The diffusion measurement on the electrodes could show that the transport of KOH and especially OH^--ions does not take place by diffusion. Only the water transport is caused by diffusion. Different possible mechanisms for the transport of ions were represented. During this work it was not possible to identify the responsible mechanism for the behaviour observed in this research. Future work should concentrate on osmosis and electro-osmosis. The tests on the concentration measurement should be repeated. The tests should encompass different load currents. In all tests, the electrode potential should be measured, as this can yield information about the condition in the electrode.

At the end of the work, a test was carried out with a small electrolyser cell. The results are not presented in this thesis. This test showed, that the electrolyte moves in the direction of the cathode (the electrode where the OH^--ions were produced). This is the same result than in the fuel cell. Contrary to a fuel cell, it is possible to change the polarity of an electrolyser cell, which resulted in a reversed flow. The same test as with the fuel cell should be repeated with an electrolyser cell and the results compared with the results of the fuel cell. It appears possible to have a flow of electrolyte caused by the mechanism described above.

Appendix A

Helpful Tables and Diagrams

A.1 Amount of Substances

For the work with fuel cells and electrolysers it his helpful to have a diagram about the volume flow of gases and reaction water as function of the current.
The values are calculated using the Faraday equation.

Diagram A-1 shows the amount of substances for fuel cells and electrolysers as a function of current. The gas flows are denoted in standard litres per hour. The values are calculated for a single cell unit.

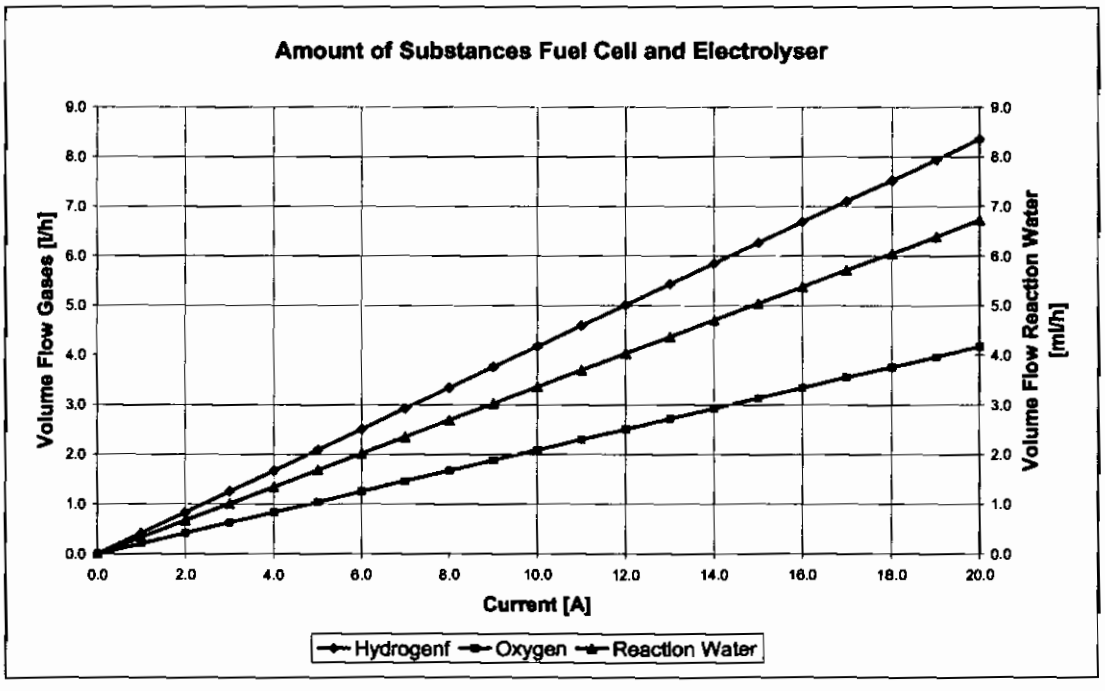

Diagram A-1: Amount of substances for an AFC or AEL

Table A-1 shows the amount of substances for fuel cells and electrolysers as a function of current. The gas flows are in standard litres per hour. The values are calculated for a single cell unit.

I	H_2	H_2	O_2	O_2	Water	Water
[A]	[l/h]	[g/h]	[l/h]	[g/h]	[ml/h]	[g/h]
0	0.0000	0.0000	0.0000	0.0000	0.0000	0.0000
1	0.4179	0.0376	0.2089	0.2985	0.3361	0.3361
2	0.8358	0.0752	0.4179	0.5969	0.6721	0.6721
3	1.2537	0.1128	0.6268	0.8954	1.0082	1.0082
4	1.6716	0.1504	0.8358	1.1938	1.3443	1.3443
5	2.0894	0.1880	1.0447	1.4923	1.6803	1.6803
6	2.5073	0.2256	1.2537	1.7908	2.0164	2.0164
7	2.9252	0.2632	1.4626	2.0892	2.3525	2.3525
8	3.3431	0.3009	1.6716	2.3877	2.6885	2.6885
9	3.7610	0.3385	1.8805	2.6862	3.0246	3.0246
10	4.1789	0.3761	2.0894	2.9846	3.3607	3.3607
11	4.5968	0.4137	2.2984	3.2831	3.6968	3.6968
12	5.0147	0.4513	2.5073	3.5815	4.0328	4.0328
13	5.4326	0.4889	2.7163	3.8800	4.3689	4.3689
14	5.8504	0.5265	2.9252	4.1785	4.7050	4.7050
15	6.2683	0.5641	3.1342	4.4769	5.0410	5.0410
16	6.6862	0.6017	3.3431	4.7754	5.3771	5.3771
17	7.1041	0.6393	3.5521	5.0739	5.7132	5.7132
18	7.5220	0.6769	3.7610	5.3723	6.0492	6.0492
19	7.9399	0.7145	3.9699	5.6708	6.3853	6.3853
20	8.3578	0.7521	4.1789	5.9692	6.7214	6.7214

Table A-1: Amount of substances for an AFC or AEL

A.2 Properties of KOH solution [A-1]

For the calculation of the concentration of KOH solution in an alkaline fuel cell the following tables are helpful.

Diagram A-2 shows the density of KOH solution as a function of the KOH concentration.

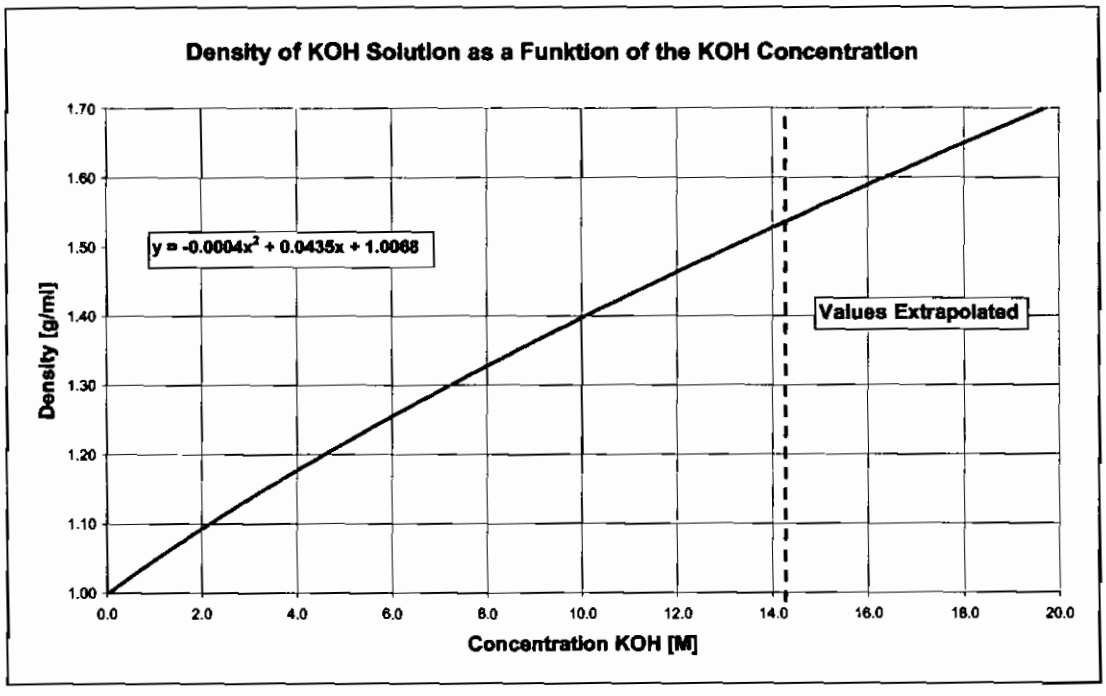

Diagram A-2: Density of KOH as a function of the concentration

Diagram A-3 shows the KOH concentration as a function of the density of a KOH solution.

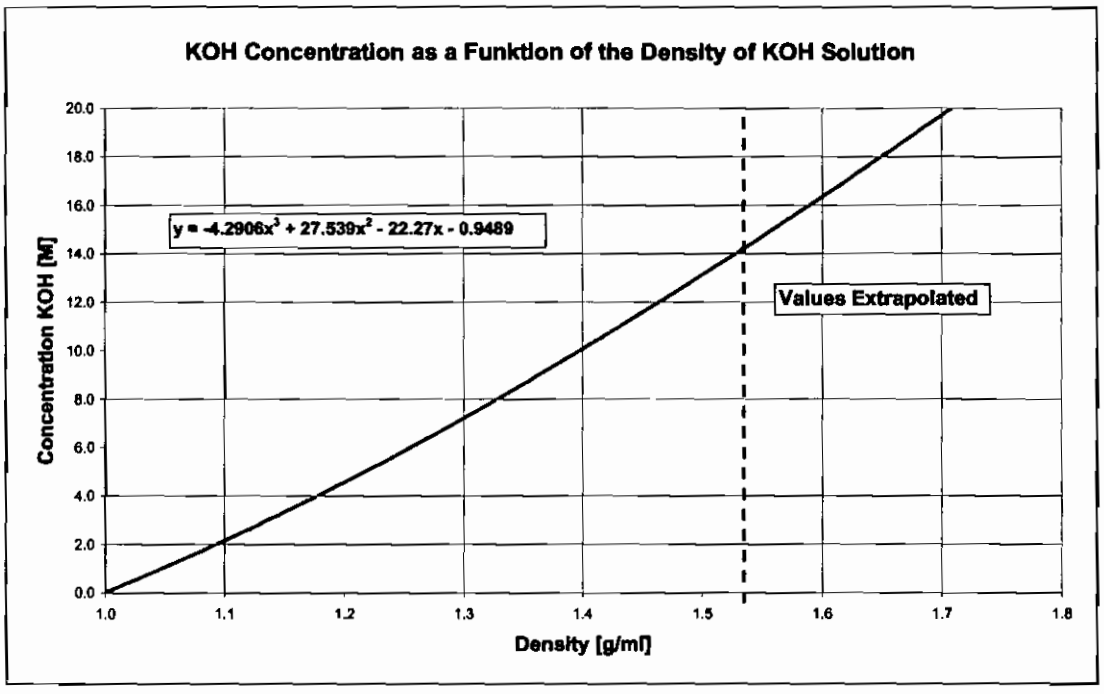

Diagram A-3: Concentration as a function of the density of KOH

Diagram A-4 shows the KOH concentration as a function of the KOH concentration in percent.

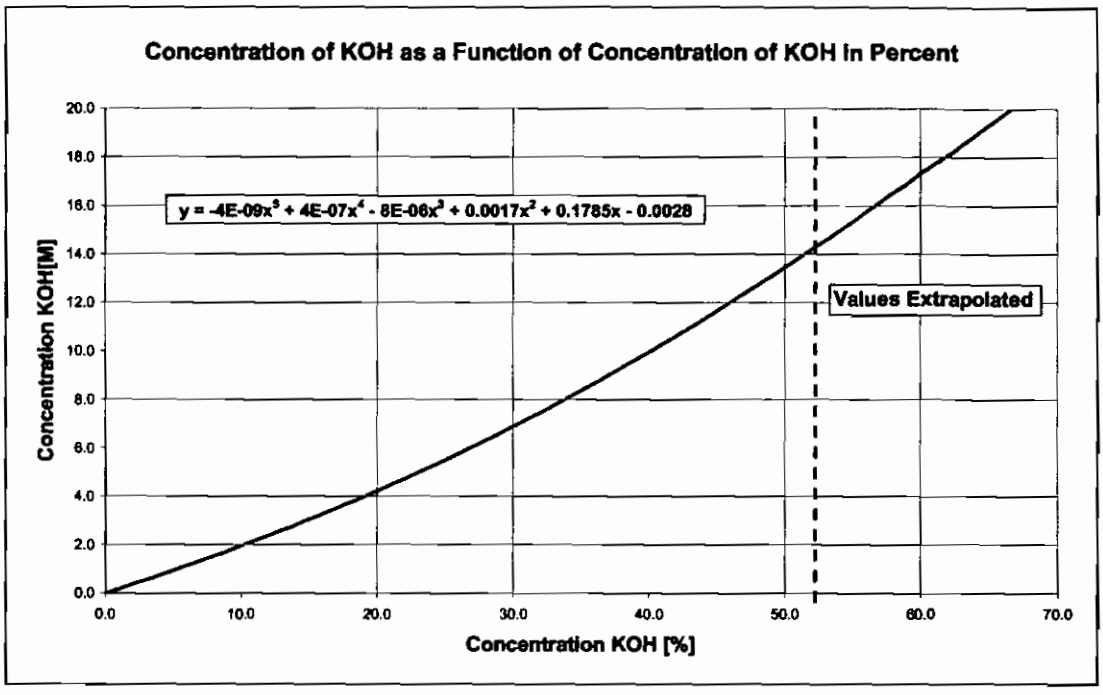

Diagram A-4: KOH concentration in M as a function of concentration in %

Diagram A-5 presents the concentration of water in a KOH solution as a function of the concentration of KOH.

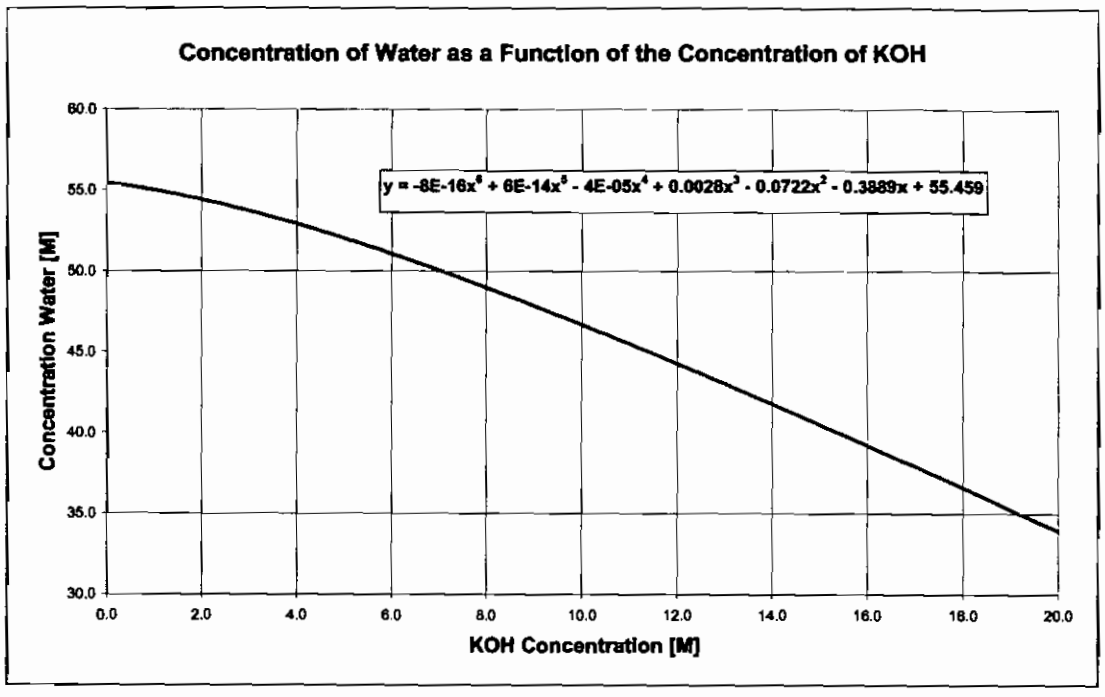

Diagram A-5: Concentration of water in KOH solution as a function of the concentration of KOH

Appendix B

Calculation of the KOH concentration of a running AFC

B.1 Calculation

In chapter 5.4.1 the results of a calculation about the KOH concentration in an AFC were presented. The concentration was calculated as a function of time at a constant current.

The calculation started with the Faraday equation, which was used to calculate the mass of reaction water and the mass of KOH. The each electrolyte compartments of the fuel cell was filled with circa 16 cm^3 of 7 M KOH solution. For each compartment the mass of water and the mass of KOH was calculated.

On the hydrogen electrode OH^--ions react with hydrogen and produce water. The mass of KOH—calculated using the Faraday equation—was subtracted from the start mass of KOH in the hydrogen electrolyte compartment. The mass of reaction water was added to the start mass of water. Additionally it was possible to calculate how much water was transported to the oxygen electrode and how much KOH was transported from the oxygen electrode to the hydrogen electrode. The mass transport was calculated in per cent of the maximum transported mass of KOH and reaction water.

At the oxygen electrode water reacts with oxygen and forms OH^--ions. The mass of water and the mass of KOH was also calculated for this. The values were calculated using the Faraday equation. The mass of produced KOH was added to the start mass of KOH. The required water was subtracted from the start mass of water. The mass of transported water and KOH was calculated in per cent of the maximum transported substances.

From the ratio of KOH and water it was possible to calculate the concentration and the volume at each compartment. Now it was possible to get the values for concentration and volume as a function of the time.

For example:

The concentration is to be calculated for a current of 1.0 A and for a runtime of 5 h. The transport of water from the hydrogen electrode to the oxygen electrode is set to 50 % of the mass. The transport of KOH from the oxygen electrode to the hydrogen electrode is set by 100 % of the mass.

1 cm^3 of 7.0 M KOH has a total mass of 1.295 g. It contains of 0.393 g KOH and 9.02 g water. At the beginning of the test each electrolyte compartment of the fuel cell contains a volume of 16 cm^3 of 7.0 M KOH, corresponding to 6.288 g KOH and 14.432 g water. This is a total mass of 20.720 g.

Now the mass of reaction water and KOH is calculated using the Faraday equation.

$$m_{H_2O} = \frac{I \cdot t}{z \cdot F} \cdot m_{mol} \qquad \text{(Gl.: 5-1)}$$

$$m_{H_2O} = \frac{1A \cdot 18000s}{2 \cdot 96485As} \cdot 18.0152\frac{g}{mol} = 3.361g$$

This value is multiplied by two because on the hydrogen electrode two molecules of water are formed and on the oxygen electrode one molecule is consumed. This behaviour is considered by the calculation.

Due to the water transport of 50 % only 3.361 g of reaction water are transported from the hydrogen electrode to the oxygen electrode. The water remains in the in the hydrogen electrode where it dilutes the KOH solution.

At the hydrogen electrode 3.361 g of water are added to the 14.432 g of water in the electrolyte compartment. At the oxygen electrode there is no net change of the mass of water. 3.361 g are added to the 14.432 g of water in the electrolyte compartment and in the same time they are subtracted because they react to KOH (OH^- ions, it is always used the mass of KOH because it can be supposed that each OH^--ion needs a K^+-ion).

Now starts the calculation of the KOH. Therefore also the Faraday equation is used.

$$m_{KOH} = \frac{1A \cdot 18000s}{2 \cdot 96485As} \cdot 56.1056\frac{g}{mol} = 10.467g$$

This mass also has to be multiplied by two because each molecule of hydrogen reacting with two OH^--ions and one molecule of water react with oxygen to two OH^--ions. This mass can now subtracted at the hydrogen electrode from the mass of KOH and at the oxygen electrode it can added to the mass of KOH. At the beginning it was said that the transport of KOH is set by 100 %. It is not necessary to subtract or add the mass because the whole mass of KOH which is produced at the oxygen electrode is consumed at the hydrogen electrode.

For the calculation of the concentration at the hydrogen side it means that after 5 h there is a mass of 16.112 g of water and of 6.288 g of KOH. Now the ratio of the mass of KOH and the mass of water can be calculated in per cent. The value is 28.06 %. That value can be used to calculated the KOH concentration in M. Therefore the equation in Diagram A-4 or the curve of the diagram can be used.

At the hydrogen side there is a concentration of 6.410 M. At the oxygen side there is a concentration of 7.0 M (There was no change of masses).

The total characteristic of the example above is shown in diagram B-1. It can be seen that the KOH concentration on the hydrogen side drops over the whole runtime. The KOH concentration on the oxygen side keeps constant. This characteristic cannot be reached in a real alkaline fuel cell because the gradient of KOH concentration will cause a transport of masses effected by diffusion.

The calculation should only be an example for the calculation. The values of the exchange of water and KOH can be adapted to the behaviour of a real AFC.

Diagram B-1 represents the calculation of the concentration in the fuel cell for a current of 1 A, an exchange of water from 50 % and an exchange of KOH of 100 %. The runtime is from 0 h to circa 90 h.

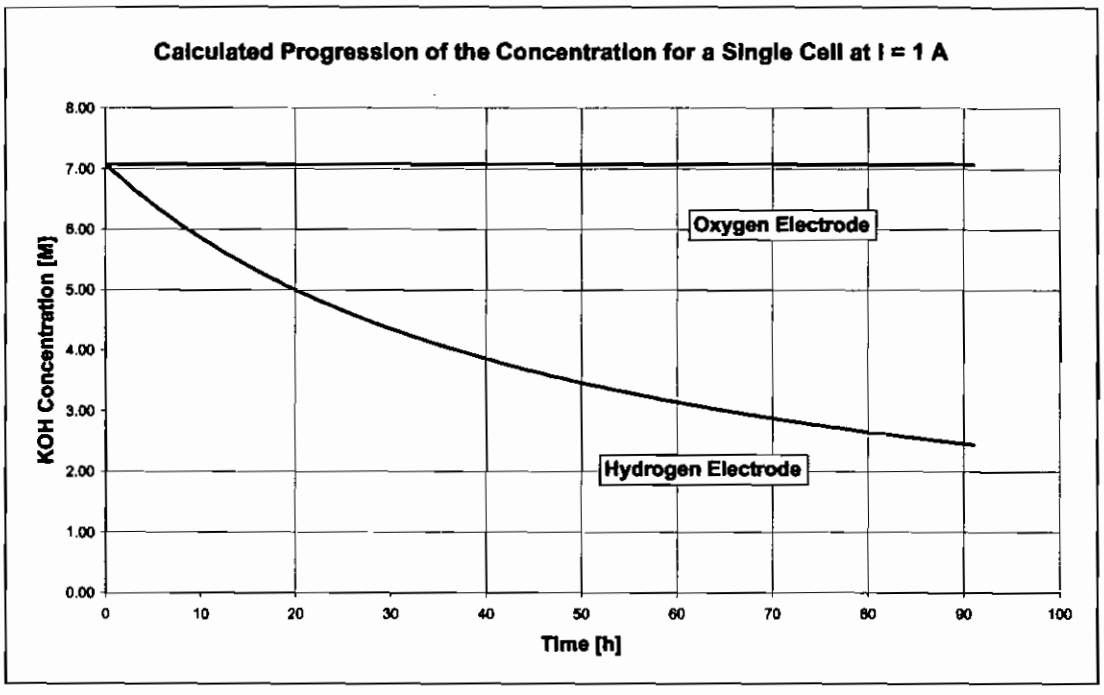

Diagram B-1: Calculated progression of the concentration for an AFC

References

2-1 Leibniz-Institut für Meereswissenschaften (Leibniz Institute of Marine Sciences), Kiel, www.ifm-geomar.de

2-2 Publication, Robert Grove,
Philosophical Magazine, Ser. 3, 1839, 14, 127

2-3 Nicolas Leonard Sadi Carnot (1796-1832),
„Betrachtungen über die bewegende Kraft des Feuers und die zur Entwicklung dieser Kraft geeigneten Maschinen",
„La force motrice de la chaleur" (The motive force of heat)

2-4 Josiah Willard Gibbs (1839-1903),
See also P.W. Atkins, Physikalische Chemie, VCH Verlagsgesellschaft mbH. Weinheim, 1987

2-5 Eduard Justi and August Winsel, Kalte Verbrennung (Cold Combustion), Steiner Verlag 1963

2-6 Wolf Vielstich, Brennstoffelemente, Verlag Chemie GmbH, Weinheim, 1965

2-7 Günter Cerbe und Hans-Joachim Hoffmann, Einführung in die Thermodynamik, Hanser Verlag 1996

2-8 Astris Energi Inc., Mississauga, Ontario, Canada

2-9 Siemens AG, Erlangen, Deutschland

2-10 Klaus Rühling, Untersuchungen an neuartigen PTFE-Gebundenen Raney-Nickel- und Silberelektroden, Diplomarbeit 1986

2-11 Jochen Grassegger, Aufbau eines Messstandes für Gasdiffusionselektroden in Halbzellenanordnung und Erprobung an Sauerstoffverzehrelektroden, Diplomarbeit 1993

2-12 Björn Weitzel, Prokaryotische Aktivität und Diversität an marinen Bio-Geo-Schnittstellen in der Tiefsee unter besonderer Berücksichtigung der Prozesse der Methanoxidation, Dissertation 2004

2-13 US Naval Research Lab, 4555 Overlook Ave., SW,
Washington, DC 20375

2-14 Steffen Schudt, Design and Development in the Field of Alkaline Fuel Cell Technology for Operation With Air, Master Thesis, 2006

2-15 Air Liquide Deutschland GmbH, Gaskatalog, Hans-Günther-Sohl-Straße 5, D-40235 Düsseldorf

2-16 August Winsel and Ralf Wendtland, Process of operating fuel cell, US-Pat. Nr. US000003597275, (1971)

2-17 Carl H. Hamann and Wolf Vielstich, Elektrochemie, Wiley-VCH, 1985

2-18 Uri Lachish, guma science, http://urila.tripod.com/

2-19 Varta AG, Brennstoffzellen-Handbuch, 1966

2-20 Karl Kordesch, Brennstoffbatterien, Springer-Verlag, Wien New York, 1984

2-21 Rudolf Holze, Leitfaden der Elektrochemie, Teubner Stuttgart Leipzig, 1998

2-22 Beijing Haoyun Industry Co., Ltd., District Beijing 102218 China

5-1 P.W. Atkins, Physikalische Chemie, VCH Verlagsgesellschaft mbH. Weinheim, 1987

5-2 Ionic Conductivity and Diffusion at Infinite Dilution, CRC Handbook of Chemistry and Physics, 77th Edition, Page 5-104, CRC Press, 1996

5-3 BioMax, Ausgabe 15, 2004, Max-Planck-Gesellschaft, München

5-4 CRC Handbook of Chemistry and Physics, 77th Edition, Page 5-104, CRC Press, 1996

5-5 GKN Sinter Metals Filters GmbH, Radevormwald, Deutschland

5-6 Wolf Vielstich, Brennstoffelemente, Verlag Chemie GmbH, Weinheim, 1965

5-7 Varta AG, Brennstoffzellen-Handbuch, 1966

5-8 Oliver Führer, Modellbildung fürdie Wasserentsorgung in alkalischen H2/O2-Brennstoffzellen nach dem EloFlux-Prinzip, Dissertation, Kassel, 1990

5-9 A. Winsel, Verfahrenstechnik poröser Elektroden, Chemie-Ingenieur-Technik, Jahrgang 43 Heft 4, Seite 191-195, 1971

A-1 Merck KGaA, LAB TOOLS- Tabellen für das Labor, Darmstadt

List of Figures

List of Diagrams

List of Tables